# The Receptor for Advanced Glycation End Products (RAGE) controls ductular reaction-mediated fibrosis during cholestasis

Dissertation

Faculty of Biosciences

Ruperto Carola University Heidelberg

Wai Ling Macrina Lam

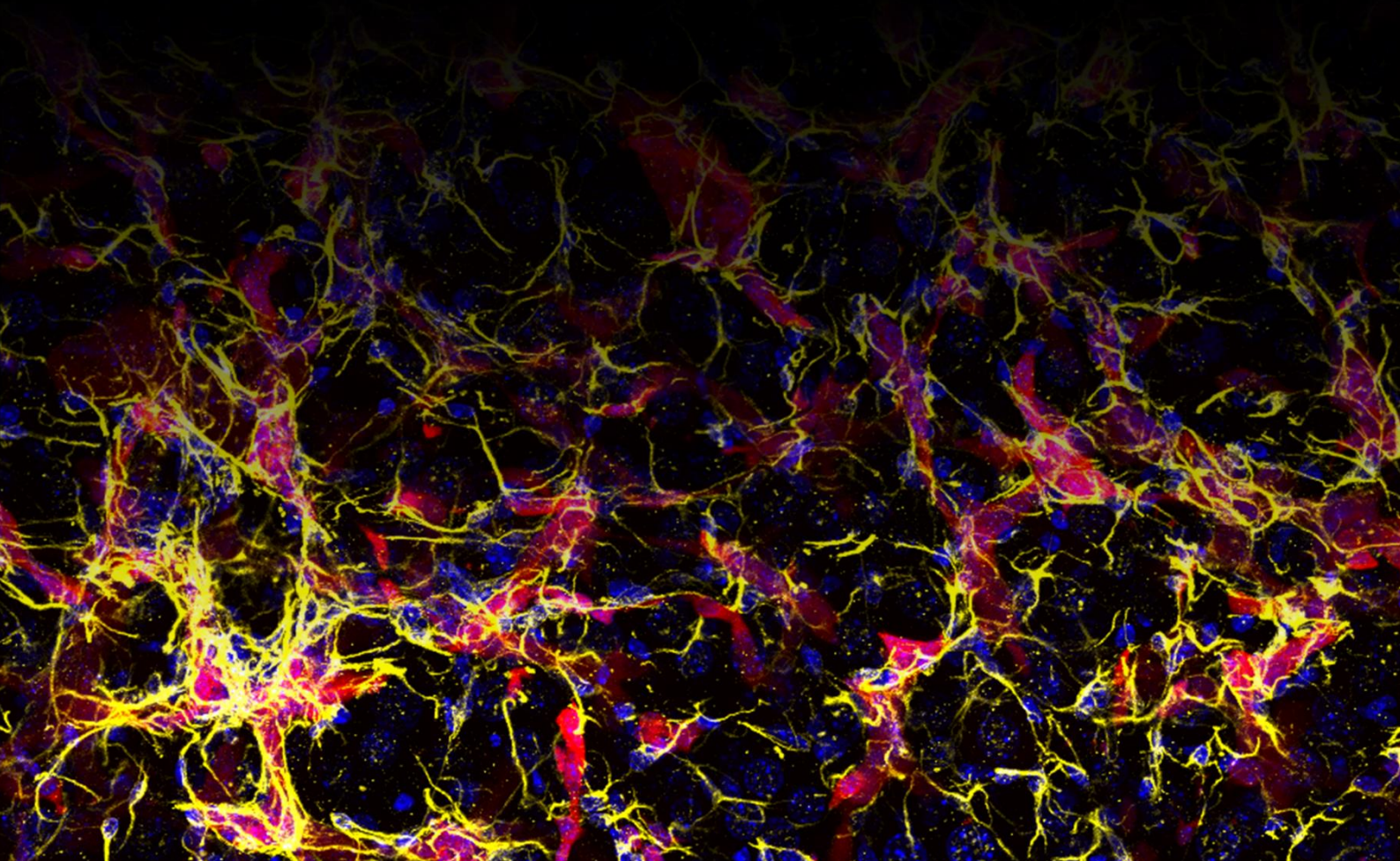

Inaugural dissertation

for

obtaining the doctoral degree

of the

Combined Faculty of Mathematics, Engineering and Natural Sciences

of the

Ruprecht – Karls – University

Heidelberg

Presented by

Wai Ling Macrina Lam, M.Phil.

Born in: Hong Kong SAR

Oral examination: 27th February, 2023

# The Receptor for Advanced Glycation End Products (RAGE) controls ductular reaction-mediated fibrosis during cholestasis

Referees: Prof. Dr. Peter Angel

Prof. Dr. Mathias Heikenwälder

*Dedicated to my parents and my grandma..*
*For your unconditional love.*

## Summary

Hepatic fibrosis is implicated in most etiologies of chronic liver diseases (CLD). It is a pathological process resembling a wound repair response, which is characterized by hepatic stellate cells (HSCs) activation and excessive production and deposition of extracellular matrix (ECM), which elicits substantial tissue scarring and impairment of liver function. Ductular reaction (DR) is a common clinical manifestation observed among most of the etiologies of CLD, but most prevalent in cholangiopathies, including cholestasis, primary biliary cholangitis and primary sclerosing cholangitis. It refers to the proliferative response of the biliary epithelial cells (BECs) that line the bile ducts in the biliary systems. DR is commonly associated with increased risk of fibrosis. On the contrary, DR is thought to serve as a regenerative mechanism to compensate for the anatomical or functional loss of the biliary system in the damaged liver. In view of the conflicting results from earlier studies, it remains elusive how DR and fibrogenic events are linked with each other.

The Receptor for Advanced Glycation End Products (RAGE) is an immunoglobulin and pattern recognition receptor that interacts with a variety of ligands, including the advanced glycation end products, HMGB1 and S100 proteins, which are released by damaged tissues and activated immune cells. In an environment with persistent stress, the accumulated RAGE ligands interact with RAGE and activates multiple pro-proliferation and inflammatory pathways, including Janus kinase (JAK)/ signal transducers and activators of transcript (STAT), mitogen-activated protein kinase (MAPK), phosphoinositide 3-kinase (PI3K)/AKT and nuclear factor-κB (NFκB) pathways, thus sustaining inflammatory responses. Apart from playing a pivotal role in modulating the tissue microenvironment, earlier studies have also demonstrated RAGE in acting as a critical direct or indirect mediator of BEC expansion and onset of fibrosis during chronic injury.

In this dissertation, the specific function of RAGE on BECs in DR and its potential association with fibrosis in the context of cholestasis was elucidated by both *in vivo* and *in vitro* approaches. To examine the role of BEC-specific RAGE activity under cholestatic condition *in vivo*, *Rage* was conditionally deleted in BECs in a biliary tracing reporter murine model *R26*$^{Tom}$*Hnf1bCreER*, followed by administration of choline-deficient ethionine-supplemented (CDE) diet for three weeks. In CDE-induced cholestatic condition, RAGE deficiency in BECs strongly impaired DR, alongside a substantial reduction of stellate cell activation and attenuation of bridging fibrosis. RNA-seq data of primary BECs isolated from CDE-challenged mice revealed a RAGE-dependent mechanistic

role of BECs in ECM remodeling and HSC activation. In line with the *in vivo* results, the *in vitro* analyses demonstrated an interplay between BECs and HSCs dependent on BEC-specific RAGE activity. To be more specific, it uncovered *Jag1* mRNA expression and secretory proteins were released by BEC in a RAGE-dependent manner. BEC-derived secretory JAG1 activates Notch signaling in HSCs in *trans*, and enhances the transformation of HSCs into a myofibroblastic-like status, thus establishes a pro-fibrotic milieu. All in all, my present study contributes to an increased understanding of the adverse consequence of DR in cholestasis-associated fibrosis and may guide future studies on new anti-fibrotic therapeutic strategies for unmet medical needs.

# Zusammenfassung

Die Leberfibrose ist für die meisten chronischen Lebererkrankungen (CLD) verantwortlich. Es handelt sich dabei um eine, der Wundheilung ähnelnde pathologische Reaktion, die durch eine Aktivierung der hepatischen Sternzellen (HSC) und eine übermäßige Produktion und Ablagerung von extrazellulärer Matrix gekennzeichnet ist, was zu einer erheblichen Vernarbung des Gewebes und einer Beeinträchtigung der Leberfunktion führt. Die duktuläre Reaktion (DR) ist eine häufige klinische Manifestation, die bei den meisten CLD-Ätiologien beobachtet wird, am häufigsten jedoch bei Cholangiopathien, einschließlich Cholestase, primär biliärer Cholangitis und primär sklerosierender Cholangitis. Sie beruht auf der proliferativen Reaktion der biliären Epithelzellen (BEC), die die Gallengänge im biliären System auskleiden. Die DR wird im Allgemeinen mit einem erhöhten Fibroserisiko in Verbindung gebracht. Im Gegensatz dazu wird angenommen, dass die DR als Regenerationsmechanismus dient, um den anatomischen oder funktionellen Verlust des biliären Systems in der geschädigten Leber zu kompensieren. Angesichts der widersprüchlichen Ergebnisse früherer Studien bleibt unklar, wie DR und fibrogene Ereignisse miteinander verknüpft sind.

Der "Receptor for Advanced Glycation End Products" (RAGE) ist ein Immunglobulin- und Mustererkennungsrezeptor, der mit einer Vielzahl von Liganden interagiert, darunter die "advanced glycation end products", HMGB1- und S100-Proteine, die von geschädigtem Gewebe und aktivierten Immunzellen freigesetzt werden. In einer Umgebung mit anhaltendem Stress interagieren die akkumulierten RAGE-Liganden mit RAGE und aktivieren mehrere proliferationsfördernde und entzündungsfördernde Signalwege, darunter Janus-Kinase (JAK)/Signaltransducers and Activators of Transcript (STAT), Mitogen-aktivierte Proteinkinase (MAPK), Phosphoinositid-3-Kinase (PI3K)/AKT und Nuclear Factor-κB (NFκB), wodurch Entzündungsreaktionen gefördert werden. Frühere Studien haben gezeigt, dass RAGE nicht nur eine zentrale Rolle bei der Regulierung der Mikroumgebung des Gewebes spielt, sondern auch ein entscheidender, direkter oder indirekter Vermittler der BEC-Expansion und des Auftretens von Fibrose bei chronischen Verletzungen ist.

In meiner Dissertation habe ich die spezifische Funktion von RAGE auf BECs in DR und seine mögliche Verbindung mit Fibrose im Zusammenhang mit Cholestase sowohl durch *in vivo* als auch durch *in vitro* Ansätze aufgeklärt. Um die Rolle der BEC-spezifischen RAGE-Aktivität unter cholestatischen Bedingungen *in vivo* zu untersuchen, wurde *Rage* in BECs in einem biliären Reporter-Mausmodell R26TomHnf1bCreER konditionell deletiert, gefolgt von der Verabreichung einer dreiwöchigen cholindefizienten, ethioninergänzten (CDE) Diät. Unter CDE-induzierten cholestatischen Bedingungen beeinträchtigte der RAGE-Verlust in BECs die DR stark, zusammen mit einer

erheblichen Verringerung der Sternzellenaktivierung und einer Abschwächung der überbrückenden Fibrose. RNA-seq-Daten von primären BECs, die aus CDE-belasteten Mäusen isoliert wurden, zeigten eine RAGE-abhängige mechanistische Rolle der BECs beim ECM-Umbau und der HSC-Aktivierung. In Übereinstimmung mit den *in vivo* Ergebnissen zeigten die *in vitro* Analysen ein Zusammenspiel zwischen BECs und HSCs, das von der BEC-spezifischen RAGE-Aktivität abhängig ist. Im speziellen wurde aufgedeckt, dass die JAG1-mRNA-Expression und sekretorische Proteine von BEC in RAGE-abhängiger Weise freigesetzt wurden. Das aus BEC stammende sekretorische *Jag1* aktiviert in *trans* die Notch-Signalübertragung in HSCs und fördert die Umwandlung von HSCs in myofibroblastenähnliche Zellen, wodurch ein pro-fibrotisches Milieu geschaffen wird. Zusammenfassend trägt diese Studie zu einem besseren Verständnis der negativen Folgen der DR bei cholestaseassoziierter Fibrose bei und kann zukünftige Studien zu neuen antifibrotischen therapeutischen Strategien für den bischer unzureichenden medizinischen Bedarf unterstützen.

# Table of Contents

# List of Figures

# List of Tables

# Abbreviations

| | |
|---|---|
| 2AAF | 2-acetylaminofluorene |
| AAV | Adeno-Associated Virus |
| ABCG5 | ATP Binding Cassette Subfamily G Member 5 |
| AGE | Advanced glycation end products |
| ALD | Alcoholic liver diseases |
| ALGS | Alagille syndrome |
| ALK5 | Activin receptor-like kinase 5 |
| ALP | Alkaline phosphatase |
| ALT | Alanine transaminase |
| ANGPT | Angiopoietin |
| ASBT | Apical Sodium Dependent Bile Acid Transporter |
| ASK1 | Apoptosis signal-regulating kinase 1 |
| AST | Aspartate transaminase |
| BA | Bile acid |
| BDL | Bile duct ligation |
| BEC | Biliary epithelial cell |
| BMP | Bone morphogenetic proteins |
| BSA | Bovine serum albumin |
| BSEP | Bile salt export pump |
| CCL | CC Chemokine ligand |
| $CCl_4$ | Carbon tetrachloride |
| CCN1 | Cellular Communication Network Factor 1 |
| Ccna2 | Cyclin A2 |
| Ccnd1 | Cyclin D1 |
| Ccne2 | Cyclin E2 |
| CDE | Choline-deficient ethionine |
| CLD | Chronic liver diseases |
| CLEC4F | C-Type Lectin Domain Family 4 Member F |
| CLF | Cholyl-lysyl-fluorescein |
| CM | Conditioned medium |
| COL1A1 | Collagen type I alpha 1 |
| COL3A1 | Collagen type III alpha 1 |
| CT | Cycle of threshold |
| CTGF | Connective tissue growth factor |
| CV | Central vein |
| DAB | 3,3'-diaminobenzidine |
| DAMP | Damage-associated molecular patterns |
| DDC | 3,5-diethoxycarbonyl-1,4-dihydrocollidine |
| DE | Differentially expressed |
| DEN | Diethylnitrosamine |
| DLL | Delta-like ligands |
| DMEM | Dulbecco's Modified Eagle Medium |
| DMN | Dimethylnitrosamine |
| DMSO | Dimethyl sulfoxide |
| DNA | Deoxyribonucleic acid |
| DPBS | Dulbecco's phosphate-buffered saline |
| DR | Ductular reaction |
| ECM | Extracellular matrix |
| EDTA | Ethylenediaminetetraacetic acid |
| EGF | Epidermal growth factor |
| EGFR | Epidermal growth factor receptor |

| | |
|---|---|
| EGTA | Ethylene glycol tetraacetic acid |
| ERK | Extracellular signal-regulated kinase |
| EV | Empty vector |
| FACS | Fluorescence-activated cell sorting |
| FAK | Focal adhesion kinase |
| FBS | Fetal bovine serum |
| FFPE | Formalin-Fixed Paraffin-Embedded |
| FGF | Fibroblast growth factors |
| FSC | Forward scatter |
| FXR | Farnesoid X receptor |
| GFP | Green fluorescent protein |
| GM-CSF | Granulocyte-macrophage colony-stimulating factor |
| GOI | Gene of interest |
| GOLM1 | Golgi Membrane Protein 1 |
| GPCR | G protein-coupled receptors |
| H&E | Hematoxylin and eosin |
| HBSS | Hanks' Balanced Salt Solution |
| HBV | Hepatitis B virus |
| HCC | Hepatocellular carcinoma |
| HCV | Hepatitis C virus |
| HDV | Hepatitis D virus |
| HEPES | N-2-hydroxyethylpiperazine-N-2-ethane sulfonic acid |
| HES | Hairy and Enhancer of split |
| HEY | Hairy/enhancer-of-split related with YRPW motif protein |
| HFD | High-fat diet |
| HGF | Hepatocyte growth factor |
| HMGB1 | High mobility group box 1 |
| HNF1B | Hepatocyte nuclear factor-1-beta |
| HPC | Hepatic progenitor cell |
| Hrs | Hours |
| HRP | Horseradish peroxidase |
| HSC | Hepatic stellate cell |
| i.v. | Intravenous |
| IBAT | Ileal bile acid transporter |
| ICC | Intrahepatic cholangiocarcinoma |
| IF | Immunofluorescence |
| IFN | Interferon |
| IGF | Insulin-like growth factor |
| IHC | Immunohistochemistry |
| IPA | Ingenuity Pathway Analysis |
| JAK | Janus Kinase |
| JNK | c-Jun N-terminal kinase |
| KEGG | Kyoto Encyclopedia of Genes and Genomes |
| KLB | Klotho Beta |
| KO | Knockout |
| LATS | Large tumor suppressor kinase |
| LGR | Leucine-rich repeat-containing G-protein coupled receptor |
| LOXL2 | Lysyl Oxidase Like 2 |
| LSEC | Liver sinusoidal endothelial cells |
| LTBP1 | Latent Transforming Growth Factor Beta Binding Protein 1 |
| MAPK | Mitogen-activated protein kinases |
| MCD | Methionine choline-deficient |
| MDR | Multidrug resistance protein |
| MEM | Minimum Essential Medium |
| mins | Minutes |
| MMP | Matrix metalloproteinases |

| | |
|---|---|
| MRP | Multidrug resistance-associated protein |
| NAD | Nicotinamide adenine dinucleotide |
| NADPH | Nicotinamide adenine dinucleotide phosphate |
| NAFLD | Non-alcoholic fatty liver disease |
| NASH | Nonalcoholic steatohepatitis |
| NCAM1 | Neural Cell Adhesion Molecule 1 |
| ND | Normal diet |
| NFκB | Nuclear factor-κB |
| NICD | Notch intracellular domain |
| NOX | NADPH oxidase |
| NPC | Non-parenchymal cell |
| OPN | Osteopontin |
| ORF | Open reading fram |
| p.adj. | *p*-adjusted value |
| PBC | Primary biliary cholangitis |
| PBS | Phosphate-buffered saline |
| PCR | Polymerase chain reaction |
| PDGF | Platelet-derived growth factor |
| PEI | Polyethylenimine |
| PFIC | Progressive familial intrahepatic cholestasis |
| PHx | Partial hepatectomy |
| PI3K | Phosphoinositide 3-kinases |
| PKC | Protein kinase C |
| PPAR | Peroxisome proliferator-activated receptors |
| PRR | Pattern recognition receptor |
| PSC | Primary sclerosing cholangitis |
| PV | Portal vein |
| RAGE | Receptor for Advanced Glycation Endproducts |
| REF | Reference gene |
| RNA | Ribonucleic acid |
| RNA-seq | RNA sequencing |
| ROS | Reactive oxygen species |
| RT | Reverse transcription |
| SAA1 | Serum Amyloid A1 |
| SCD1 | Stearoyl-CoA desaturase-1 |
| SDS | Sodium dodecyl sulfate |
| secs | Seconds |
| SOX9 | SRY-Box Transcription Factor 9 |
| SREBP | Sterol regulatory element-binding protein |
| SSC | Side scatter |
| STAT | Signal transducers and activators of transcript |
| TAA | Thioacetamide |
| TBIL | Total bilirubin |
| tdTom | tdTomato |
| TEAD | TEA Domain Transcription Factor |
| TERT | Telomerase reverse transcriptase |
| TGFB1 | Transforming growth factor beta 1 |
| TIMP | Tissue inhibitor of metalloproteinases |
| TIRAP | Toll-interleukin 1 receptor domain-containing adaptor protein |
| TK | Tyrosine kinase |
| TLR | Toll-like receptor |
| TMB | 3,3',5,5'-Tetramethylbenzidine |
| TNF | Tumor necrosis factor |
| TPA | 12-O-tetradecanoyl-phorbol-13-acetate |

# Chapter 1
## Introduction

## Section 1.1 Liver architecture and physiology

The liver is a central organ for organismal homeostasis and carries out vital cellular functions including metabolism, nutrients uptake and storage, maintenance of blood sugar level, removal of toxic substances and immunoregulation. The liver cells are categorized as parenchymal and non-parenchymal cell types. The parenchymal cell population comprises mainly of hepatocytes, which account for approximately 60-70% of total liver cells and make up to 90% of total liver mass. Another parenchymal cell type, cholangiocytes, also known as biliary epithelial cells (BECs), constitute only 3-5% of the total liver cell population. The non-parenchymal fraction comprises of small liver resident cells in the hepatic sinusoids, including hepatic stellate cells (HSCs), liver sinusoidal endothelial cells (LSECs), Kupffer cells and pit cells (also known as immunoreactive natural killer cells).

The portal triad, which consists of the portal vein, hepatic artery and bile duct, is located at the periphery of the hepatic lobule. Essentially, approximately 75% of the blood entering the liver is venous blood from small intestine, pancreas, spleen and stomach. The venous blood, which carries all the absorbed nutrients from other organs, converges and enters the liver via the portal vein to support cellular functions. The remaining 25% of blood supply enters the liver via the hepatic artery. Subsequently, the blood enters the sinusoids from the terminal branches of the portal vein and hepatic artery, and flows directionally towards the central vein. The blood circulation in each lobule forms the hepatic sinusoids, which are the vascular channels lined with non-parenchymal sinusoidal endothelial cells, thereby facilitating the exchange of nutrients between blood and hepatocytes.

The anatomical functional unit is the hexagonal hepatic lobule that comprises of the portal triad, hepatocytes arranged in linear cords lined by sinusoidal network, and the central vein (Figure 1-1). The distinct liver cell types are arranged in highly specialized patterns that form discrete functional areas referred as ‘liver zonation’. The architecture and cellular interactions between various cell types define the identity and microenvironment of the organ in distinct metabolic zones. These metabolic zones are compartmentalized into periportal (zone 1), mid-lobular (zone 2) and pericentral (zone 3) zones. As blood flow directionally from the portal triad towards the central vein via the sinusoids, the surrounding hepatocytes take up oxygen and nutrients from the blood progressively, which eventually create a gradient along the periportal-pericentral axis, thus shaping the tissue microenvironment for differential cellular functions. Specifically, cells in periportal zone 1 are supplied with blood abundant in oxygen and nutrients, thus zone 1 is mainly involved in cellular processes which are more energetically demanding, including

gluconeogenesis, β-oxidation, cholesterol biosynthesis, protein secretion and ureagenesis; mid-lobular zone 2 is mainly specialized in iron homeostasis and modulation of insulin growth factors; pericentral zone 3 receives blood with the least oxygen and nutrients levels, therefore it is engaged in metabolic processes that required the least energy, such as glycolysis, bile acid production and glutamine synthesis [1, 2].

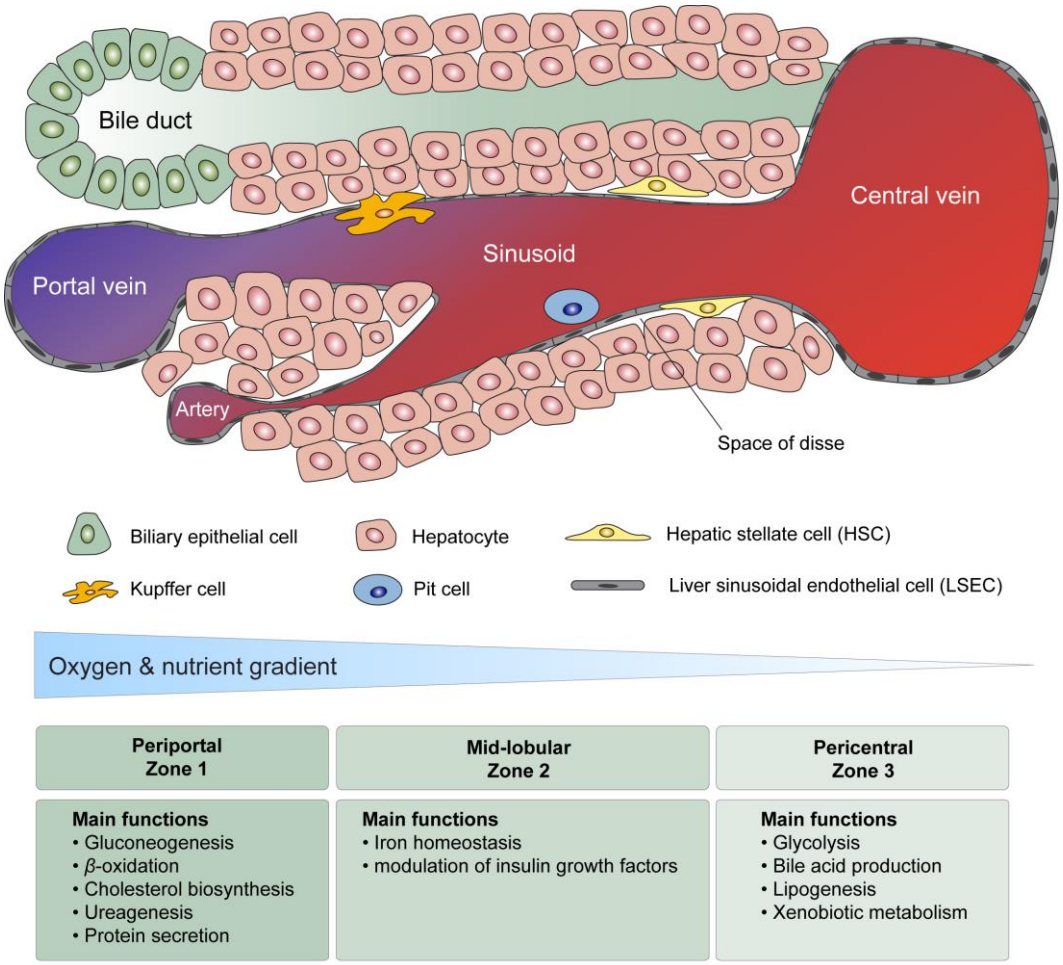


**Figure 1-1. Schematic diagram of the hepatic architecture**.

The liver lobule is comprised of the hepatic plates lined between the portal triad and the central vein. The portal triad consists of the bile duct, portal vein and hepatic artery. Venous blood circulate from the intestines converges with the arterial blood at the periportal zone, and travels directionally through the sinusoid towards the central vein. The surrounding hepatocytes take up oxygen and nutrients from the blood progressively, thus creating a gradient along the periportal-pericentral axis that support various fundamental cellular processes in three distinct metabolic zones. The liver sinusoidal endothelial cells (LSEC) form the lining of the sinusoids, where kupffer cell and pit cells reside. The hepatic stellate cells (HSC) are located in the perisinusoidal space called the space of disse. Bile canaliculi are formed between the hepatocytes. The bile is collected from hepatocytes flows directionally towards the bile duct at the portal vein. Adapted from [3].

The biliary system is composed of intrahepatic and extrahepatic ducts. It is a complex tubular structure essential for the transport of bile, which the hepatocytes produce to facilitate the digestion of lipids and bilirubin excretion.

The organization of the bile duct system is coupled with the apical-basal polarization of the hepatocytes. The hepatocytes are highly polarized, with the basolateral domain faces the sinusoids, and the apical membranes of neighboring hepatocytes are held together by tight junctions that form an intercellular space called bile canaliculi, where it collects the bile from the apical membrane of the hepatocytes. These bile canaliculi are interconnected and drain the bile produced from hepatocytes into the bile ducts lined by biliary epithelial cells (BECs). Concurrently, the BECs are the major cell type to secrete fluids and electrolytes and contribute to bile composition. The small bile ducts or ductules lined by BECs increase progressively in size into larger ducts, and eventually converges to form a common bile duct. The bile flows through the common bile duct and enters the intestine directly, or is stored and concentrated in the gall bladder. Bile is formed under an osmotic mechanism. It is crucial for physiological functions, including (1) facilitating lipid absorption and digestion, and (2) to eliminate waste from the body.

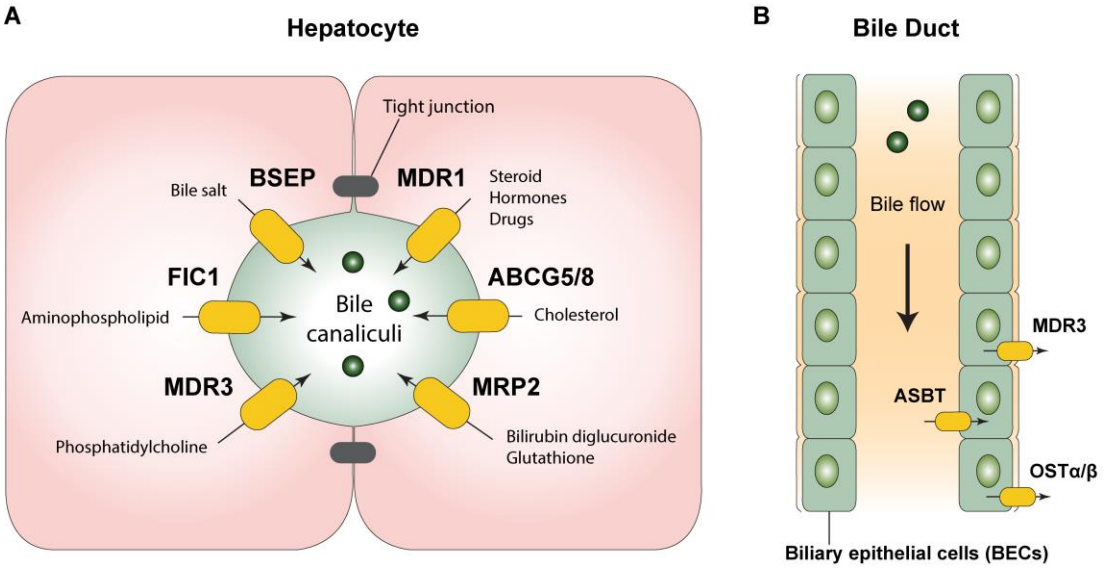


**Figure 1-2. Bile transport in hepatocytes and bile ducts**.

(A) The adjacent hepatocytes are held together by tight junctions. Between the apical membranes of the hepatocytes form the bile canaliculi, where the components of bile, including bile salt, steroid, cholesterol, bilirubin, phospholipids and others, are collected. These components of bile is actively transported into the bile canaliculi via different transporters. (B) The bile subsequently travel from the bile canaliculi into the bile duct, where it is lined by the biliary epithelial cells (BECs, also known as cholangiocytes). Bile acids are reabsorbed by cholangiocyte via the sodium-dependent transporter ASBT, and effluxed into the blood circulation via MDR3 and OSTα/β.

Bile is constituted mainly of conjugated bile salts, bilirubin, bile salts, phospholipids, amino acids and cholesterol. The formation of bile is an osmotic process driven by active transport of the abovementioned organic solutes mediated by transporters into the bile canaliculi, followed by the osmotic attraction of water. These active transporters on the apical membrane of

hepatocytes include BSEP, FIC1, MDR3, MDR1, ABCG5/8 and MRP2 are responsible for transporting different components to form bile. The bile components are transported into the bile canaliculi to form bile, followed by flowing into the bile duct line by BEC. The bile acids transporter ASBT expressing on the apical membrane of BECs is responsible for absorbing bile acids from the bile duct. Subsequently, the bile acids effluxes on the basolateral membrane of BECs via the transporters t-ASBT, MDR3, and the heteromeric Ostα/Ostβ transporters into the blood circulations (Figure 1-2).

## Section 1.2 Liver regeneration during homeostasis and injury

Homeostatic and injury-induced liver regeneration have unique mechanisms. Homeostatic maintenance of the liver occurs under normal physiological conditions in the absence of external injury, while injury-induced liver regeneration occurs to compensate for the impaired endogenous proliferation of the liver cells and to restore liver mass to the pre-injury state.

### 1.2.1 Homeostatic liver regeneration

The liver has a remarkable capacity to maintain its tissue mass. Hepatocytes are a unique population of differentiated cells as they encompass extensive proliferative capacity despite a slow turnover in normal liver. Hepatocytes are heterogeneous, and their spatial organization in the liver lobule is the key determinant to its contribution on cell proliferation and self-renewal processes. Numerous lineage tracing studies demonstrated that pre-existing hepatocytes can undergo self-renewal and replenish itself during normal homeostasis [4-8].

Partial hepatectomy (PHx) is a classic surgical procedure and is often utilized to explore the regenerative mechanism in liver under physiological conditions. The procedure involved the removal of two-third of the liver (three of the five liver lobes), and produces a relatively ‘clean’ regenerative environment without much tissue damage to the two residual lobes. Under physiological conditions, the normal adult liver is quiescent, with only 0.2% percent of hepatocytes proliferate. Following parenchymal loss from PHx, cell cycle genes including Cyclin D1 (*Ccnd1*), Cyclin A2 (*Ccna2*) and Cyclin E2 (*Ccne2*), and cyclin-dependent kinases are activated to promote hepatocyte proliferation during G1-to-S phase transition [9, 10]. The mature hepatocytes undergo rapid proliferation and DNA synthesis to restore hepatic mass and metabolic functions [9, 11]. In addition, hepatocytes produce abundant mitogenic growth factors that induce growth of the epithelial, vascular endothelial and immune cells, which help to coordinate liver regeneration and restore the hepatic architecture. These growth factors include but are not limited to, angiopoietin 1 and 2 (ANGPT1 and ANGPT2), vascular endothelial growth factor (VEGF), fibroblast growth factor 1 and 2 (FGF1 and FGF2), and transforming growth

factor-α (TGFα) for endothelial cells like LSECs and HSCs, and granulocyte-macrophage colony-stimulating factor (GM-CSF) for Kupffer cells [12].

Extensive lineage tracing studies have been employed to elucidate the mechanisms of liver development and growth in different zones in the liver lobule. Genetic lineage tracing studies demonstrated that pericentral Axin2-positive hepatocytes with a Wnt-rich anatomical niche [4], as well as the LGR4-positive hepatocytes or telomerase reverse transcriptase (TERT)-expressing hepatocytes that spread throughout the liver [5, 6] encompass superior proliferative capacity to regenerate the liver during homeostasis. In contrast, two recent lineage tracing studies employed unbiased long-term *in vivo* cell proliferation labelling strategy in the entire liver lobule and provided global insights into the homeostatic regenerative processes. To be more specific, one study utilized the *Rosa26-Rainbow Cre* mouse to track single-cell lineages of the hepatocytes randomly [7], while the other study employed a proliferation tracer (ProTracer) lineage tracing strategy with high-spatiotemporal resolution [8]. In both studies, the proliferation of hepatocytes was also found to be broadly distributed throughout the lobule rather than limited to a rare stem cell-like population, with mid-lobular zone 2 hepatocytes displaying a higher proliferation rate and contribute the most to liver regrowth during homeostasis.

### 1.2.2 Injury-induced liver regeneration

The liver has a notable tissue repair and detoxifying capacity, and several regenerative mechanisms are involved to guarantee adequate liver functions in response to acute and chronic insults. Intrinsic and extrinsic factors such as circulating growth factors and bile acids are important to support regeneration under abnormal conditions. Several mouse models have been used to model different etiologies of chronic liver diseases, including but not limited to the choline-deficient ethionine-supplemented (CDE) diet, 1,4-dihydro-2,4,6-trimethylpyridine-3,5-dicarboxylate (DDC) diet, and bile duct ligation (BDL) for cholestasis; hepatotoxin carbon tetrachloride ($CCl_4$) for fibrosis, 2-Acetylaminofluorene (2-AAF) for hepatocellular injury around the central vein. It was proven that hepatocytes can self-renew and replicate to restore liver mass. For instance in the $CCl_4$ hepatotoxin model, it was shown that the SRY-Box Transcription Factor 9 (SOX9)-expressing periportal hepatocytes were the preferential source for extensive proliferation and replenishment of the liver mass [13]; in DDC diet-induced cholestasis, hepatocytes expressing high level of TERT were crucial for hepatocellular regenerative response [6]. Nonetheless, many injury-induced liver regeneration studies gave rise to conflicting theories, including the ‘streaming liver’ which the hepatocytes would stream along the hepatic plates to repopulate [4], and the highly controversial ‘facultative stem cell’ concept [14].

The ‘facultative stem cells’ are also known as hepatic progenitor cells (HPCs). It was suggested that these progenitor cells arise from the biliary epithelial cell (BECs) lineage and have the bipotential to give rise to both hepatocytes and BECs itself. They are anatomically located in the canal of Hering – the junctional structure between the bile ducts and the bile canaliculi formed by adjacent hepatocytes, and are recognized only under injury conditions [14]. Recent single-cell RNA-sequencing studies revealed that HPCs are heterogeneous and encompass plasticity with a dynamic gene expression profile within its own population [15, 16]. Many genes and cytokines have been reported to have a regulatory role on HPC proliferation. It was demonstrated that FGF7 or Tumor necrosis factor-like weak inducer of apoptosis (TWEAK) are the inducers of HPCs proliferation during severe injury [17]. Several other reports proposed multiple growth factors and pathways to be responsible for liver parenchymal cell differentiation. For instance, developmental genes such as *WNT* [18], and hepatocyte growth factor (HGF)/MET axis [19] were shown to promote HPCs specification to hepatocytes; whereas epidermal growth factor (EGF)/EGF receptor (EGFR) and Notch signaling are important for promoting HPC differentiation to biliary cells or cholangiocytes during chronic liver injury [20-22]. Inflammatory cytokines such as tumor necrosis factor-alpha (TNFα), interferon-gamma (IFNγ), interleukin-6 (IL6) are also implicated in HPCs response during injury conditions [14]. Although PHx is a relatively ‘clean’ model with limited acute inflammation and necrosis, it is also regarded as an injury model in a broader definition. PHx challenges the entire blood flow as the presence of portal veins are reduced abundantly, which increases the portal vein pressure and generates shear stress in the sinusoids. Thereby, the circulation through the portal vein is channeled through a narrower path [12], resulting in secondary injury in the biliary tree with increased secretion of bile and bile acids [23]. The number of intrahepatic bile ducts per portal area and the size of the bile ductules would increase to allow sufficient bile excretion out of the liver. This is described as a biliary epithelial cell (BEC) proliferative response or termed as ductular reaction – a compensatory mechanism for the injury within the biliary tree.

Ductular reaction (DR) is histologically defined by a ductular-like phenotype and is characterized by the proliferation of the BECs and migration into the parenchyma upon chronic liver injuries. The development of DR is thought to serve as an escape mechanism to compensate for the anatomical and functional obstruction of the biliary tree from chronic injury. It is a phenotype encountered in most of the etiologies of human liver diseases, including biliary diseases, alcoholic and nonalcoholic fatty liver disease, chronic viral hepatitis, and hepatocellular carcinoma (HCC) [24]. Extensive lineage tracing studies have employed various murine disease models to investigate the pathophysiological role of BECs and DR. Nonetheless, the role and significance of BECs in regeneration remains controversial and not clearly understood.

Multiple animal studies have employed BEC lineage tracing with *Krt19-CreERT* mouse [25, 26] or *Hnf1b-CreER* mouse [27], or hepatocyte labeling with Adeno-associated virus vector serotype 8 (AAV8) approach [25] to investigate the regeneration of liver mass after DDC or CDE-mediated hepatic injury. Consistently, it was proven that pre-existing hepatocytes, but not BECs, contribute significantly to hepatocyte neogenesis upon diet-induced hepatic injury. Practically, the liver regenerates only from the self-replication of hepatocytes with little to no contributions from the BECs. Nevertheless, when hepatocytes undergo senescence or when their proliferation is inhibited, large-scale parenchymal injury would induce DR in support of liver regeneration. Tumor necrosis factor-like weak inducer of apoptosis (TWEAK) is known to be a macrophage-derived mitogen for BEC expansion and activates DR via the fibroblast growth factor-inducible 14 (Fn14) receptor [28, 29]. In the context of impaired hepatocyte replication, it was demonstrated that Fn14/TWEAK cytokine-receptor axis is required for DR-mediated liver regeneration [26]. Other studies demonstrated that the mammalian Hippo signaling pathway plays a significant regulatory role for BEC-mediated biliary growth and regeneration following DDC diet- or BDL-induced cholestatic injury [30-32].

## Section 1.3 Fibrosis in chronic liver diseases

The growing burden of chronic liver diseases (CLD) has become a widespread clinical problem. It is one of the leading causes of morbidity and mortality. The common risk factors of CLD include hepatitis B and C viral infections, toxic or drug-induced insults, excessive alcohol consumption, obesity, and metabolic, cholestatic or autoimmune diseases. Tissue damage from CLD leads to chronic inflammation. However, unresolved inflammation often leads to fibrosis and the advanced stage of fibrosis called cirrhosis.

Hepatic fibrosis is implicated in most etiologies of CLD but results in distinctive fibrosis patterns. Fibrosis generally results from two types of persistent hepatic injury: cholestatic and hepatotoxic injury. Cholestatic injury is commonly caused by the obstruction of bile flow due to bile duct paucity or inflammation in the biliary system [33]. During cholestasis, hepatic damage resulted from the accumulation of bile acids can lead to progressive liver diseases and potential liver failure [34], whereas hepatotoxic injury generally arises from viral infections, steatohepatitis or metabolic syndrome like non-alcoholic steatohepatitis.

Hepatic fibrosis is the consequence of persistent damages in liver parenchyma that leads to scarring of tissues, characterized by excessive production and deposition of extracellular matrix by the hepatic myofibroblasts. Multiple mesenchymal cells, such as hepatic stellate cells (HSCs), portal fibroblasts,

bone marrow-derived fibrocytes, were suggested as the major source that give rise to myofibroblasts during injury and fibrosis [35-37]. Among all, HSCs are well-recognized to be the predominant contributor to liver fibrosis with remarkable plasticity in metabolic regulation, inflammation, immunity and energy and nutrient homeostasis [35, 37, 38].

### 1.3.1 Initiation and perpetuation of hepatic stellate cell activation

In the normal healthy liver, HSCs are resident non-parenchymal pericytes found in the perisinusoidal space called the space of Disse and are recognized as Ito cells or vitamin A (retinol)-storing lipocytes. During CLDs, the quiescent HSCs (qHSCs) are transformed into an activated, myofibroblastic-like HSCs (aHSCs) via a two-step process. First, the qHSCs undergo an initiation step, which is provoked by oxidative stress signals, apoptotic bodies, and paracrine stimuli from neighboring cells. It involves a rapid change in transcriptional program, including upregulation of HSC initiation markers such as *KLF6* and *ANKRD1* [39], and enrichment of early response events such as activation of the Yes-associated protein (YAP) [40] and unfolded protein response (UPR) signaling [41]. Moreover, the stellate cells lose the lipid droplets containing retinoid and peroxisome proliferator-activated receptor gamma (PPARγ), which are the biomarker and master regulator of stellate cell activity respectively [42]. Furthermore, HSCs are sensitized to the stimulation by the surrounding cells in the tissue microenvironment, which promote HSC activation, survival and motility in the second step.

The second step of HSC activation is perpetuation, which involves the differentiation to their full capacity of their myofibroblastic phenotypes that exert proliferative, contractile, fibrogenic, chemotactic and immunomodulatory features [38, 43]. These activated HSC features are potentiated by a series of paracrine and autocrine events that help to perpetuate injury and fibrosis [38]. For instance, chemokine serum amyloid A1 (SAA1) [44] and cellular fibronectin [45] serve as chemo-attractants that recruit HSCs towards the hepatic injury loci. At the site of injury, HSCs are activated by transforming growth factor-beta (TGFβ), epidermal growth factor (EGF) and platelet-derived growth factor (PDGF) secreted by platelets [46, 47], as well as TGFβ [48], PDGF [49] and connective tissue growth factor (CTGF) [50] secreted by Kupffer cells. Other immune cells like macrophages also exerts pro-inflammatory cytokines like TNFα, interleukin (IL)-1β, IL-6, C-C motif chemokine ligand 2 (CCL2) and 5 (CCL5) that either promote survival or activation of HSCs [51-53].

HSCs have a central role in regulating ECM remodeling in the tissue microenvironment. Following activation, HSCs produce excessive collagen, thus, altering the matrix composition and contributing to tissue scarring [35, 37, 54]. It was also demonstrated that HSCs express a wide range of matrix

metalloproteinases (MMPs) and tissue inhibitors of the metalloproteinase (TIMPs), which are important mediators of ECM turnover. MMPs are a family of enzyme that can degrade ECM, whereas TIMPs are a family of enzyme that is responsible for regulating the proteolytic activities of MMPs [55]. The dysregulation between MMPs and TIMPs are implicated in increased matrix stiffness and contributes to the development of fibrosis. For instance, the activities of MMP-9 and TIMP1 were modulated dependent on tissue stiffness via mechanotransduction. In scarred tissue, the stiffness of tissue provide a mechanical network that promotes TIMP-1 activity and inhibits the proteolytic activity of MMP-9, thereby attenuating the degradation of ECM, and providing a positive mechanosensitive feedback network that promote fibrosis [56].

### 1.3.2 Cholestatic injury-associated fibrosis

Cholangiopathies are the biliary diseases associated with dysfunctional BECs in both intrahepatic and extrahepatic biliary trees, leading to obstructed bile flow and parenchymal damages, followed by biliary fibrosis and end-stage liver diseases. Cholangiopathies are classified in two categories: (1) primary biliary diseases due to genetic predisposition or mutation that directly target the bile ducts and (2) secondary biliary diseases when the bile ducts degrade as a consequence of other chronic pathological processes [57]. The most common chronic biliary diseases are primary biliary cholangitis (PBC) and primary sclerosing cholangitis (PSC). They are both chronic cholestatic diseases caused by the scarring of the bile ducts due to inflammation, leading to subsequent blockade of the bile flow. Other common primary biliary diseases include progressive familial intrahepatic cholestasis (PFIC) and Alagille syndrome (ALGS), which are rare genetic diseases in children and infants [34, 58].

Chronic biliary diseases commonly result from impaired bile secretion or biliary phospholipid secretion [59]. Under cholestatic conditions, hepatocytes lose tight junctions that leads to leaky junctions and collapse of bile canaliculi. Consequently, bile acids continue to accumulate in the liver, causing oxidative stress and hepatotoxicity, subsequently leading to cell death or senescence. In the bile ducts, the obstructed bile flow leads to tissue remodeling in the interlobular bile ducts. This pathophysiology in the ducts is termed as ductular reaction characterized by increasing ductules branching, such that the transport of bile is optimized to compensate for the obstructed bile flow. The patients are at high risk of developing periportal fibrosis. Biliary fibrosis often develop in the concurrent proliferation of the reactive bile ductules and periductular myofibroblasts at the portal-parenchymal interface [60, 61], suggesting an extensive paracrine crosstalk between the BECs and fibroblasts, and led to the hypothesis that ductular reaction is the ‘pacemaker of portal fibrosis’ in the context of biliary diseases [62]. These BECs expressed an increased amount

of cytokines, chemokines, such as TNFα, IL-1, IL-6, IL-8, IFNγ, and growth factors including HGF, VEGF, CTGF, IGF1 and others, which are crucial for the activation of HSC, and serve as paracrine signals to stimulate their proliferation and migration [62]. Elevated bile acid levels during biliary diseases also serve as activators of several signaling pathways that promote fibrosis. For instance, bile acids can bind to the epidermal growth factor receptor (EGFR) on HSCs and activate HSC proliferation via the protein kinase C/p70S6K-dependent pathway [63]. In other studies using BDL or DDC-diet cholestasis-associated mouse models, it was demonstrated that the nuclear receptor Farnesoid X Receptor (FXR) is a key regulator for intrahepatic bile acids, and the genetic loss of FXR results in decreased bile acids concentration, and reduced liver injury and fibrosis [64, 65], suggesting that bile acids mediate cholestasis-associated fibrosis via the FXR in autocrine or paracrine manner.

### 1.3.3 Hepatotoxic injury-associated fibrosis

#### 1.3.3.1 Viral infection-induced fibrosis

The major cause of CLD and liver fibrosis arise from hepatitis virus infection, including hepatitis B (HBV), hepatitis C (HCV) and hepatitis D virus (HDV) infection. HBV infection involved the integration of the DNA virus into the host genome and results in the production of viral HBx protein that induces chromosomal instability and the activation of the oncogenic genes, such as RAS, RAF, MAPK, ERK and JNK. Furthermore, HBV-induced oxidative stress could also lead to activation of stellate cells, resulting in hepatic injuries and fibrosis [66, 67]. Unlike HBV, HCV is an RNA virus that does not integrate into the host genome. Instead, the virus enters the hepatocytes by endocytosis mediated by cell surface proteins and translates and replicates in the host cells [67, 68]. Chronic HCV infection is positively associated with increased pro-inflammatory cytokines and chemokines, such as IL-1β and IL-18, from hepatocytes and immune cells. The constant production of the pro-inflammatory cytokine helps to propagate inflammatory response and activate HSCs. Additionally, HCV induces an increased expression of profibrogenic factors, such as transforming growth factor beta 1 (TGFβ1), and modulates HSCs activation by upregulating fibrotic genes such as Collagen type I alpha 1 (*Col1a1*) and Collagen type III alpha 1 (*Col3a1*), and downregulating the fibrolytic matrix metalloproteinase in favor of extracellular matrix degradation, thereby promoting a fibrogenic microenvironment [69]. Similarly, HDV is also an RNA virus that does not integrate into the host genome but requires the HBV surface antigens for its replication and infection on the host cells, meaning HDV often infects the host in the presence of HBV. Therefore, patients with HBV/HDV co-infection are often associated with severe fibrosis and increased risk of cirrhosis when compared to HBV infection alone [70]. Among all chronic viral hepatitis, the pattern of fibrosis results from portal-to-central vein bridging

necrosis, thus creating a derangement of the vascular connection with the portal system, and causing early portal hypertension [60, 61].

#### 1.3.3.2 Alcoholic liver disease (ALD) and non-alcoholic fatty liver disease (NAFLD)-induced fibrosis

Alcoholic liver disease (ALD) is caused by the excessive consumption of alcohol, whereas non-alcoholic fatty liver disease (NAFLD) is the consequence of obesity and insulin resistance. ALD and NAFLD progress with a common well-recognized pattern, beginning with accumulation of triglycerides in the hepatocytes that leads to hepatic steatosis, followed by inflammation and hepatocyte ballooning that result in steatohepatitis. Persistent injury in the liver eventually leads to progressive fibrosis and cirrhosis [71].

During ALD progression, persistent alcohol intake activates Kupffer cells in an autocrine manner and promotes hepatic inflammation. Eventually, alcohol, the metabolic intermediate acetaldehyde, and hepatic inflammation-induced ROS can promote fibrosis by directly activating HSCs or stimulating immune cells to produce pro-fibrogenic mediators [71, 72]. Alcohol can also accelerate fibrosis by inhibiting the anti-fibrotic effects of natural killer cells on activated HSCs [73]. In NAFLD, the increased level of fatty acids and inflammation caused by non-alcoholic steatohepatitis cause endoplasmic reticulum (ER) stress, Jun N-terminal kinase (JNK) activation, ROS production and mitochondrial dysfunction, and eventually cell death in hepatocytes. Damage-associated molecular patterns (DAMPs), such as high-mobility group box 1 (HMGB1) protein (see 1.4.1.2 below), are released by dying hepatocytes and function as danger signaling molecules to the neighboring cells. The effector cells including Kupffer cells and stellate cells respond to DAMPs stimuli via the cell surface toll-like receptors (TLR), thereby promoting the transdifferentiation of HSCs into collagen-producing myofibroblasts [74, 75]. In addition, it was also shown that increased cholesterol intake from diet causes free cholesterol accumulation in HSCs, and sensitize HSCs to TGFβ stimulation, thereby promoting liver fibrosis [76]. Although having distinctive pathogenesis, the fibrosis pattern in both ALD and NAFLD appears to be pericellular and perisinusoidal and is described as a ‘chicken-wire’ pattern. Histologically, the extracellular matrix is concentrated around the sinusoids and surrounds a group of hepatocytes in zone 3 that progressively becomes pan-lobular [60].

### Section 1.4 Receptor for Advanced Glycation End-Products (RAGE)-dependent signaling in liver pathogenesis

RAGE is a multifunctional receptor that is known to play key roles in inflammation and diseases. It is a transmembrane protein belonging to the immunoglobulin superfamily of cell surface receptor [77] and the family of cell

adhesion molecules [78]. It is also recognized as a pattern recognition receptor that engages a broad repertoire of inflammation-associated ligands, such as advance glycation end products (AGEs), amyloid-β (Aβ) peptide and damage-associated molecular pattern (DAMP) molecules, including high mobility group box-1 (HMGB1) and S100 protein family, and is crucial for modulating inflammation and immunity in various diseases [79] (Figure 1-3). RAGE is encoded in the locus of class III region of the major histocompatibility complex on chromosome 6. It is comprised of three extracellular immunoglobulin-like domains (one V-type domain and two C-type domains), a transmembrane domain, and a cytoplasmic tail. The V domain has two *N*-glycosylation sites and is responsible for extracellular ligand binding; whereas the cytoplasmic tail is responsible for engaging intracellular signaling [80].

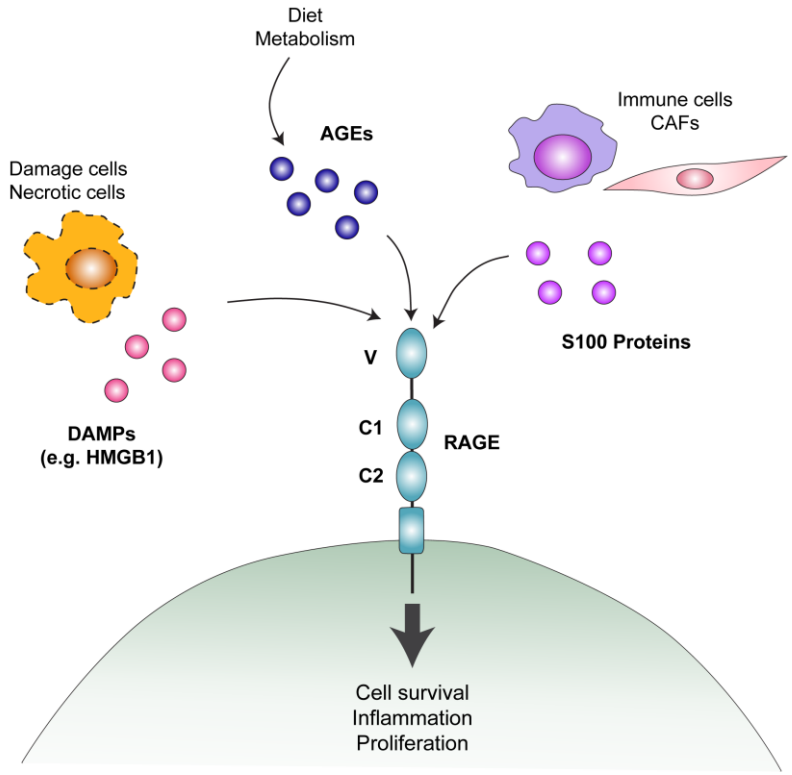


**Figure 1-3. Overview of RAGE structure and its ligands**.

RAGE comprises of the extracellular domain (V, C1 and C2 domains), a transmembrane domain and a cytoplasmic domain. It is recognized as a pattern recognition receptor that binds to various molecules upon tissue damage and during inflammation. RAGE interacts with the damage-associated molecular patterns (DAMPs) such as HMGB1 that are released by damaged cells or necrotic cells, advanced glycation end-products (AGEs) from diet or metabolism, or S100 protein family from activated immune cells. The interaction of RAGE with its ligands trigger a series of signal transduction cascades that are involved in cell survival, proliferation and inflammatory response.

RAGE is expressed in multiple isoforms. The three dominant isoforms are identified as full-length RAGE (fl-RAGE), soluble RAGE (sRAGE) and dominant negative RAGE (dnRAGE) [81]. These isoforms are produced by alternative

mRNA splicing or proteolytic cleavage of the full-length RAGE. Under normal physiological conditions, the expression of RAGE is extremely low or undetectable in most differentiated cells and immune cells, but it is strongly expressed in type I and type II alveolar cells in the lung. However, the protein expression of RAGE is elevated significantly during various pathological conditions, such as diabetes, Alzheimer's disease, cardiovascular disease and cancers [82].

### 1.4.1 RAGE ligands in chronic injury

#### 1.4.1.1 Advanced Glycation End Products (AGEs)

The RAGE ligands, AGEs, are a heterogeneous group of molecules formed by non-oxidative and oxidative reactions of sugars and their adducts to proteins and lipids. These molecules are normally produced and accumulated during aging, but also at an accelerated rate in various diseases, such as diabetes, neurodegenerative diseases or cancers [83]. Increased intake of fructose and high fat diet containing saturated fatty acids are also the major source of the formation of AGEs [84]. It was suggested that AGEs-RAGE axis is implicated in liver diseases, including NASH, fibrosis, cirrhosis and hepatocarcinogenesis [85-87]. The circulating AGEs level has been shown to be a biomarker for evaluating liver function. For instance, the plasma *N*-carboxy-methyllysine, a form of AGE structure, was shown to be elevated in patients with cirrhosis and is positively correlated with the severity of the disease [86]. Similarly, the serum level of glyceraldehyde-derived AGEs were also found to be elevated in NASH patients [87]. In the perspective on AGE-RAGE pathogenesis, it was proposed that AGE-RAGE is involved in the development and metabolic responses of insulin resistance [88, 89], which is a common risk factor for diabetes, obesity and, thus, NASH. Other studies also suggested the pathogenic role of AGE-RAGE axis in other liver diseases. For instance, administration of AGEs could potentiate RAGE expression and augments liver fibrosis using the BDL cholestatic injury model [90]. AGE-RAGE axis may also prime pro-inflammatory response in endothelial cells, thereby amplifying the outcome of chronic inflammation-associated diseases [91].

#### 1.4.1.2 High-mobility group box 1 (HMGB1)

The high-mobility group box 1 (HMGB1), is a DAMP molecule that has a high binding affinity to RAGE. It is aberrantly expressed during injury and promotes the onset of inflammation and oncogenic events. It is well-established that HMGB1 can interact with inflammation-associated receptors, such as RAGE and TLR, and coordinate numerous cellular responses, including immunoregulation, cell growth, chemotaxis and tissue repair [92]. During chronic hepatitis, chromatin-associated HMGB1 is released from the nucleus

into the cytoplasm followed by release into the extracellular milieu [93, 94]. It was suggested that HMGB1 plays a pathogenic role in downregulating *Foxp3* and inhibit the regulatory T cells, thus promoting liver failure [95]. In addition, employing DDC diet-induced chronic injury model, classical diethylnitrosamine (DEN)/$CCl_4$ or autophagy-deficient HCC models, it was suggested that HMGB1-RAGE axis is the main driver of DR and hepatocarcinogenesis [96, 97]. Clinically, in the perspective of liver fibrosis, it was shown that HMGB1 protein expression positively correlates with the fibrotic stage in patients with chronic HCV, primary biliary cirrhosis and alcoholic steatohepatitis [98]. Interestingly, it was suggested that extracellular HMGB1 activates PI3K/AKT or ERK pathways via RAGE on HSC and induces collagen type I synthesis, thereby promoting fibrosis [98, 99].

#### 1.4.1.3 S100 protein family

The S100 protein family is a class of molecules of 21 members that also interact mainly with RAGE. They are involved in numerous cellular functions, including cell growth, differentiation and energy metabolism [100]. In pathological conditions, they serve as danger signals in regulating immune responses and inflammation via interacting with RAGE [101]. RAGE have been shown to bind to several S100 proteins, including S100A7, S100A12, S100A8/A9 and S100B, leading to activation of NF-κB and induction of pro-inflammatory cytokines that recruits neutrophils, monocytes, and macrophages [101-103]. Specifically in liver pathogenesis, it was demonstrated that co-expression of S100A8 and S100A9 promotes HCC malignancy and progression, in part due to the induction of ROS production, as well as protecting HCC cells against apoptosis [104, 105]. More recently, it was demonstrated that the S100B proteins and RAGE expression are upregulated, and S100B-RAGE axis is associated with the proliferation of BECs in BDL-induced cholestatic injury and promoting the activation of HSCs in support of biliary fibrosis [106].

### 1.4.2 The role of RAGE signaling during liver injury

RAGE signaling plays an essential role in modulating the tissue microenvironment, and its activation is required for perpetuating inflammation in various diseases [107, 108]. In the context of acute stress, RAGE ligands are transiently synthesized and released, which eventually induce an innate immune response by activating immune cells via RAGE. In contrast, in an environment with persistent stress, the accumulation of RAGE ligands would trigger and sustain series of inflammatory response and leads to pathogenesis [109]. Upon interaction with its ligands, RAGE is phosphorylated by PKCζ, followed by recruitment of adaptor proteins such as toll-interleukin 1 receptor domain-containing adaptor protein (TIRAP), MYD88, or mammalian diaphanous-1 (MDia1) [110]. Subsequently, the engagement of RAGE and its

ligands triggers and activates multiple signaling pathways, including Janus kinase (JAK)/signal transducers and activators of transcript (STAT), mitogen-activated protein kinase (MAPK), and phosphoinositide 3-kinase (PI3K)/AKT [82]. These pathways predominantly results in the activation of the transcription factors, including activator protein 1 (AP-1), STAT and the nuclear factor-κB (NFκB), which play critical role in proliferation and pro-inflammatory responses [110], and creating a tissue microenvironment that favors neoplastic transformation and malignant progression. More importantly, in the hepatotoxic CDE diet-induced injury model and the inflammation-associated *Mdr2*$^{-/-}$ HCC model, RAGE was identified as a critical mediator of DR, onset of liver fibrosis and HCC formation [111].

### 1.4.3 Beneficial role of RAGE inhibition

Targeting RAGE-ligand interaction may represent a feasible approach to block RAGE-dependent signal cascade. RAGE antagonists or small molecule inhibitors were suggested to be able to alleviate RAGE-mediated inflammation in various diseases. These inhibitors can block RAGE-ligand interaction by blocking the extracellular domain of RAGE or inhibit the downstream signal transduction by binding to the intracellular domain of RAGE. A phase 2b study of Azeliragon (TTP488), an orally bioavailable small molecule inhibitor of RAGE, suggested that Azeliragon may slow cognitive decline in patients with mild Alzheimer's disease [112]. Although the investigation of this inhibitor was later on terminated in a phase 3 clinical trial as it failed to meet the co-primary endpoint, it was shown that there were some improvements in cognition in a subcategory of patients who had diabetes [113].

Despite the failure of the clinical trials on Azeliragon, several other RAGE inhibitors, neutralizing antibodies, or its own antagonist soluble isoform sRAGE, were investigated and have shown effectiveness in inhibiting RAGE in various pre-clinical models. For instance, FPS-ZM1 is a small molecule inhibitor that was suggested to be able to block the ligand binding site of RAGE. By inhibiting Aβ-induced cellular stress in brain cells and tissues both *in vitro* and *in vivo*, it was proposed that FPS-ZM1 can effectively control the progression of Aβ-mediated brain disorder like Alzheimer's diseases [114, 115]. Additionally, several studies demonstrated that anti-RAGE neutralizing antibodies have a beneficial effect in preclinical models of melanoma, atherosclerosis, and sepsis [116-118]. Most interestingly, in liver diseases studies, it was commonly suggested that sRAGE has a protective capacity for liver diseases. The soluble isoform, sRAGE, is a decoy receptor that lack the transmembrane and cytoplasmic domain. The serum level of sRAGE is suggested to be the prognostic biomarker for liver diseases, as it was found to be negatively correlated with the severity of liver diseases [119, 120]. Therapeutically, sRAGE has the capacity to compete with wildtype RAGE for ligand binding, thus

inhibiting the transduction of the signal. In a preclinical model of NASH, administration of sRAGE to the high-fat-diet-treated mice was shown to improve insulin sensitivity and reduced inflammation, suggesting that sRAGE protects the liver against high-fat-diet-induced obesity and insulin resistance [88]. In the acetaminophen-induced liver injury mouse model, animals treated with sRAGE were shown to have improved survival rate with decreased hepatic necrosis [121]. Nevertheless, although these potential RAGE-targeting agents showed beneficial effects in preclinical models, they have not yet progressed beyond preclinical testing. Thus, the clinical applications on RAGE inhibition would require further comprehensive knowledge on the intracellular and intercellular regulatory network.

## Section 1.5 Aims and objectives

Liver disease progression is complex and multifactorial. In the past decades, enormous effort has been made to search for reliable biomarkers to detect liver diseases and cancer at an early stage. Despite significant advancement in our understanding of the underlying mechanisms driving liver fibrosis, there are currently no FDA- or EMA-approved anti-fibrotic treatments available. Therefore, it is of vital importance to further investigate and understand the complex mechanism that regulates the fibrotic niche.

The progression and the degree of fibrosis correlates with ductular reaction (DR) in most of the etiologies of human liver diseases [24, 122-125]. Although numerous studies reported that BECs proliferation contribute to liver regeneration upon injury [126-129]; growing evidence have shown that BECs can contribute to fibrosis [130, 131] and formation of HCC [132-134]. Recent study with advanced multidimensional imaging has further shed light on the fundamental role of BECs, and revealed that these BEC-lined duct-like structure functions as an escape route for accumulative bile during cholestasis [135]. Interestingly, previous study revealed that RAGE is a major regulator to modulate DR, the onset of fibrosis and HCC formation in the context of chronic cholestatic injury [111]. Nonetheless, it remains controversial whether RAGE-mediated DR is beneficial or detrimental to the liver in the context of fibrosis.

In hopes of seeking appropriate therapeutic strategies to repair chronic liver diseases, it is crucial to understand the association between DR and fibrosis deeply and comprehensively. In this dissertation, I aimed to elucidate the role of RAGE in the context of cholestasis-associated liver injury and fibrosis by addressing the following objectives:

(1) Characterization of RAGE in biliary epithelial cells (BECs)
(2) Defining the role of BEC-specific RAGE expression on cholestasis-induced liver inflammation, DR, and fibrosis

(3) Identification of RAGE-dependent genetic programs in BECs during cholestasis by utilizing transcriptome sequencing
(4) Delineate whether DR-associated fibrosis is RAGE-dependent and define its underlying mechanism

# Chapter 2

## Materials and Methods

## Section 2.1 Materials

### 2.1.1 Chemicals and reagents

| | |
|---|---|
| 2-mercaptoethanol | Sigma-Aldrich, Taufkirchen |
| 16% Formaldehyde solution (w/v), Methanol-free | Thermo Fischer Scientific, USA |
| Acetic acid | Fischer Chemical, Switzerland |
| Agarose | Carl Roth, Karlsruhe |
| ALLin™ Red Taq Mastermix | highQu GmbH, Germany |
| Absolute Ethanol | Sigma-Aldrich, Taufkirchen |
| Bovine Serum Albumin (BSA) | Sigma-Aldrich, Taufkirchen |
| Bradford MX | Expedeon, UK |
| Calcium chloride ($CaCl_2$) | Merck, Darmstadt |
| Citric acid | AppliChem, Darmstadt |
| Collagenase Type IV | Sigma-Aldrich, Taufkirchen |
| Ethylenediamine-tetraacetic acid (EDTA) | Carl Roth, Karlsruhe |
| Ethylene glycol tetraacetic acid (EGTA) | Sigma-Aldrich, Taufkirchen |
| Eosin 1% | Morphisto, Offenbach |
| Eukitt® Mounting Medium | ORSAtec, Germany |
| dNTPs mix (25 mM) | Thermo Fischer Scientific, USA |
| Dako Fluorescence Mounting Medium | Agilent Technologies, USA |
| Deoxyribosnuclease I Type II (DNase I) | Sigma-Aldrich, Taufkirchen |
| Dimethylsulfoxide (DMSO) | Biomol, Hamburg |
| DNA Ladders (6X) | New England Biolabs, USA |
| DNA Loading Dye (6X) | Thermo Fischer Scientific, USA |
| FuGENE HD transfection reagent | Promega, USA |
| Glucose | Sigma-Aldrich, Taufkirchen |
| Hank's Balanced Salt solution (HBSS) | Thermo Scientific, USA |
| Hematoxylin acidic after MAYER | Morphisto, Offenbach |
| Heparin Sodium Salt | Sigma-Aldrich, Taufkirchen |
| HEPES | Sigma-Aldrich, Taufkirchen |
| Hydrochloric acid (HCl) | VWR Chemical, France |
| Hydrogen peroxide 30% | Carl Roth, Karlsruhe |
| Isopropanol (2-Propanol) | Sigma-Aldrich, Taufkirchen |
| Normal Goat Serum | Vector Laboratories, USA |
| Magnesium sulfate ($MgSO_4$) | Sigma-Aldrich, Taufkirchen |
| Methanol | Merck, Darmstadt |
| Oil Red O | Thermo Fischer Scientific, USA |
| Oligo $(dT)_{18}$ primers | Thermo Fischer Scientific, USA |
| Percoll® | Sigma-Aldrich, Taufkirchen |
| Picro-sirius Red | Morphisto, Offenbach |
| Polybrene transfection reagent | Merck, Darmstadt |
| Polyethylenimine (PEI) | Sigma-Aldrich, Taufkirchen |
| Potassium chloride (KCl) | Carl Roth, Karlsruhe |
| Potassium dihydrogen phosphate ($KH_2PO_4$) | Carl Roth, Karlsruhe |
| *Power* SYBR™ Green PCR Master Mix | Thermo Fischer Scientific, Lithuania |
| Pronase | Roche, Mannheim |
| Propylene glycol | Sigma-Aldrich, Taufkirchen |
| Proteinase K | Sigma-Aldrich, Taufkirchen |
| Random Hexamer Primer | Thermo Fischer Scientific, USA |
| Reaction Buffer for RT (5X) | Thermo Fischer Scientific, USA |
| RevertAid Reverse Transcriptase | Thermo Fischer Scientific, USA |

| | |
|---|---|
| RiboLock RNase inhibitor | Thermo Fischer Scientific, USA |
| RNase-Free DNase Set | Qiagen, Hilden |
| ROTI® Histofix 4% formaldehyde | Carl Roth, Karlsruhe |
| Sodium chloride (NaCl) | Fischer Chemical, Switzerland |
| Sodium citrate tribasic dihydrate | Fluka, Buchs |
| Sodium dihydrogen phosphate ($NaH_2PO_4$) | Carl Roth, Karlsruhe |
| Sodium hydrogen carbonate ($NaHCO_3$) | Merck, Darmstadt |
| Sodium hydroxide (NaOH) | VWR Chemical, France |
| Sucrose | Sigma-Aldrich, Taufkirchen |
| Superfrost Plus Adhesive Microscope Slides | Thermo Fischer Scientific, USA |
| Tissue-Tek O.C.T. Compound | Sakura, Netherlands |
| Tris-hydrochloride (Tris-HCl) | Carl Roth, Karlsruhe |
| Triton X-100 | AppliChem, Darmstadt |
| HISTO-COMP Paraffin | Vogel MedTec, Fernwald |
| Xylene | VWR Chemical, France |

### 2.1.2 Buffers

| Buffer | Composition |
|---|---|
| Antigen retrieval citrate buffer | 1.8 mM citric acid<br>8.2 mM sodium citrate<br>pH 6.0 |
| Antigen retrieval TE buffer | 10 mM Tris-HCl<br>1 mM EDTA<br>pH 9.0 |
| Blocking buffer for IHC | 0.5% Goat serum in 1X PBS |
| FACS buffer | 2% (v/v) BSA<br>5 mM EDTA<br>1X PBS |
| PBS (1X) | 137 mM NaCl<br>2.7 mM KCl<br>10 mM $Na_2HPO_4$<br>1.8 mM $KH_2PO_4$<br>pH 7.4 |
| Liver perfusion buffer I | 120 mM NaCl<br>240 mM $NaHCO_3$<br>20 mM Glucose<br>5 mM HEPES<br>4.8 mM KCl<br>1.2 mM $MgSO_4$<br>1.2 mM $KH_2PO_4$<br>0.5 mM EGTA<br>2% (v/v) Heparin 5000 U/ml<br>pH 7.4 |
| Liver perfusion buffer II | 67 mM NaCl<br>6.7 mM KCl<br>20 mM $CaCl_2$<br>100.7 mM HEPES<br>0.1% (w/v) Collagenase type IV<br>pH 7.6 |

| Buffer | Composition |
|---|---|
| Non-parenchymal cell isolation digestion buffer | HBSS buffer<br>0.1% (w/v) Collagenase type IV<br>0.1% (w/v) Pronase<br>1% (w/v) DNase I |
| Non-parenchymal cell isolation wash buffer | William's E medium<br>10% FBS<br>1% L-Glutamine |
| TNB blocking buffer for *in situ* hybridization | 0.1 M Tris-HCl, pH 7.5<br>0.15 M NaCl<br>0.5% Blocking Reagent (provided in TSA biotin kit) |

### 2.1.3 Cell culture supplements

| | |
|---|---|
| Dimethylsulfoxide (DMSO) | Sigma-Aldrich, Taufkirchen |
| Dulbecco's Modified Eagle's Medium (DMEM) – high glucose | Sigma-Aldrich, Taufkirchen |
| Epidermal Growth Factor, Mouse Natural (Culture Grade) (EGF) | Corning, Kaiserslautern |
| Dulbecco's Phosphate Buffered Saline (DPBS) | Sigma-Aldrich, Taufkirchen |
| Fetal Bovine Serum (FBS) | Sigma-Aldrich, Taufkirchen |
| Gibco™ Advanced DMEM/F12 Basal Medium | Thermo Fischer Scientific, USA |
| Gibco™ B-27 Supplement (50X), minus Vitamin A | Thermo Fischer Scientific, USA |
| Gibco™ GlutaMAX Supplement | Thermo Fischer Scientific, USA |
| Gibco™ L-Glutamine | Thermo Fischer Scientific, USA |
| Gibco™ N-2 Supplement (100X) | Thermo Fischer Scientific, USA |
| Gibco™ TrypLE Express Enzyme (1X) | Thermo Fischer Scientific, USA |
| Gibco™ Williams' Medium E | Thermo Fischer Scientific, USA |
| HEPES Solution Bioxtra, 1M, pH 7.0-7.6 | Sigma-Aldrich, Taufkirchen |
| Insulin-like Growth Factor-II, Human (IGF2) | Sigma-Aldrich, Taufkirchen |
| Insulin, Human | Sigma-Aldrich, Taufkirchen |
| *N*-Acetyl-L-Cysteine | Sigma-Aldrich, Taufkirchen |
| Nicotinamide | Sigma-Aldrich, Taufkirchen |
| Matrigel® Growth Factor Reduced Basement Membrane Matrix | Corning, USA |
| Opti-MEM Reduced Serum Medium | Thermo Fischer Scientific, USA |
| Recombinant Human FGF-10 | PeproTech, Hamburg |
| Recombinant Human Noggin | PeproTech, Hamburg |
| Recombinant Murine EGF | PeproTech, Hamburg |
| Recombinant Murine HGF | PeproTech, Hamburg |
| Penicillin/Streptomycin Solution | Sigma-Aldrich, Taufkirchen |
| SB 431542 | PeproTech, Hamburg |
| Trypsin 2.5% in PBS | PAN-Biotech, Aidenbach |
| Y-27632 Dihydrochloride | Sigma-Aldrich, Taufkirchen |

### 2.1.4 Cell Culture Media

| Media | Compositions |
|---|---|
| BEC freezing medium | William's E growth medium<br>5% (v/v) FBS<br>10% (v/v) DMSO |
| DMEM full medium | DMEM high glucose medium<br>10% (v/v) FBS<br>2 mM L-Glutamine<br>1% (v/v) penicillin/streptomycin |
| HEK293T freezing medium | 90% (v/v) FBS<br>10% (v/v) DMSO |
| MIM1-4HSC freezing medium | 90% (v/v) FBS<br>10% (v/v) DMSO |
| William's E growth medium | William's E medium<br>5% (v/v) FBS<br>30 ng/ml IGF2<br>20 ng/ml EGF<br>10 µg/ml Insulin<br>2 mM L-glutamine<br>1% (v/v) penicillin/streptomycin |

### 2.1.5 Cell lines

| Cell lines | Cell types | Species | References |
|---|---|---|---|
| HEK293T | Immortalized | Human | American Type Culture Collection (ATCC) |
| BEC RAGE WT | Primary | Mouse | Isolated by Aurora De Ponti |
| BEC RAGE KO | Primary | Mouse | Established by myself for this study |
| MIM1-4HSC | Immortalized | Mouse | [136] |
| MIM1-4HSC-mCherry | Immortalized | Mouse | Established by myself for this study |

### 2.1.6 Consumables

| | |
|---|---|
| Abbocath-T 24 G ¾ cannula | Megro, Germany |
| AGANI™ Needle 25G x 5/8" | Terumo Deutschland, Germany |
| Cell Culture Plate (60 mm / 10 cm) | Greiner Bio-One, Germany |
| CELLSTAR® Cell Culture Flask, 75 $cm^2$ | Greiner Bio-One, Germany |
| Conical Centrifuge Tubes 15 ml | Corning, USA |
| Conical Centrifuge Tubes 50 ml | Corning, USA |
| Cryogenic vials | Starlab, UK |
| Disposable Reagent Reservoir | Dominique Dutscher SAS, France |
| ELISA plate 96 well clear | Sarstedt, Nümbrecht |
| Filter pipette tips (10 µl / 20 µl / 200 µl) | Kisker, Steinfurt |
| Filter pipette tips (1000 µl) | Nerbe Plus, Winsen |
| Glass bottom plate 24 well | Cellvis, USA |
| LABSOLUTE® Adhesive Microscopic slides | Th. Geyer, Renningen, Germany |

| | |
|---|---|
| Medifix® Infusion system | B. Braun Melsungen AG, Melsungen |
| MicroAmp® fast optical 96 well reaction plate | Applied Biosystems, USA |
| MicroAmp® optical adhesive covers | Applied Biosystems, Singapore |
| Millex-GS Syringe Filter Unit, 0.22 µm | Merck Millipore, Ireland |
| Embedding cassette Histosette | Simport, Netherlands |
| Embedding cassette Mega Cassette | Sakura, Netherlands |
| Eppendorf tubes | Sarstedt, Germany |
| FACS tube | Corning, USA |
| FEATHER® Disposable Scapel | Feather Safety Razor, Japan |
| FEATHER® Microtome Blade C35 Type | Feather Safety Razor, Japan |
| Fuji Dri-Chem Slide ALP | Fujifilm Europe, Germany |
| Fuji Dri-Chem Slide GOT/ AST | Fujifilm Europe, Germany |
| Fuji Dri-Chem Slide GPT/ ALT | Fujifilm Europe, Germany |
| Fuji Dri-Chem Slide TBIL | Fujifilm Europe, Germany |
| Pasteur capillary pipettes | WU, Mainz |
| PCR reaction tubes | Nerbe Plus, Winsen |
| Pipette tips (10 µl / 20 µl / 200 µl / 1000µl) | Nerbe Plus, Winsen |
| Serological pipet (5 ml / 10ml / 25ml) | Corning, USA |
| Syringes 1 ml Injekt-F | B. Braun Melsungen AG, Melsungen |
| Thermo Scientific™ SuperFrost™ Plus Microscope Slides | Fischer Scientific, Schwerte |
| Tissue Culture Plate Flat Bottom (6 well / 24 well) | Corning, USA |
| Tissue-Tek® Cryomold® standard 25 x 20 x 5 mm | Sakura Finetak, Netherlands |
| 70 µm Cell Strainer | Greiner Bio-One, Germany |

### 2.1.7 Equipments

| | |
|---|---|
| Axio Scan.Z1 Slidescanner | Zeiss, Oberkochen |
| BD LSRFortessa™ Cell analyzer | BD Biosciences, Heidelberg |
| BD FACSAria™ I | BD Biosciences, Heidelberg |
| BD FACSAria™ II | BD Biosciences, Heidelberg |
| CLARIOstar microplate reader | BMG LABTECH, Ortenberg |
| Counting Chambers Neubauer | Glaswarenfabrik Karl Hecht, Sondheim vor der Rhön |
| Drying cabinet | Heraeus, Hanau |
| Electrophoresis chamber for SDS-PAGE | Bio-Rad Laboratories, Munich |
| Embedding machine Tissue-Tek TEC | Sakura, USA |
| Fujifilm DRI-CHEM NX500i Serum Analyzer | Fujifilm Europe GmbH, Germany |
| Heracell™ 240i $CO_2$ Incubator | Thermo Fischer Scientific, USA |
| Heraeus Biofuge Fresco | Heraeus, Hanau |
| Heraeus MEGAFUGE16 Centrifuge | Thermo Fischer Scientific, USA |
| Magnetic stirrer/ heat plate IKA® BH basic2 | IKA, Staufen |
| Magnetic stirrer/ heat plate MR 2000 | Heideloph, Schwabach |
| Microplate Reader Clariostar | BMG Labtech, Ortenberg |
| Mr. Frosty™ Freezing Container | Thermo Fischer Scientific, USA |
| NanoDrop Spectrophotometer UV-VIS ND-1000 | PeqLab Biotechnology, Erlangen |
| Olympus IX51 Light Microscope | Olympus, Japan |
| Peristaltic Pump Reglo Digital MS-2/12 | Ismatec, Zürich |
| pH meter 765 Calimatic | Knick, Berlin |

| | |
|---|---|
| Pipette Pipetman P10/ P20/ P200/ P1000 | Gilson, USA |
| Pipetboy Acu | Integra Biosciences, Switzerland |
| Leica CM3050 S Cryostat | Leica Biosystems, Wetzlar |
| Rotational vacuum concentrator | Martin Christ Gefriertrocknungsanlagen, Osterode am Harz |
| StepOnePlus™ Real-Time PCR System | Applied Biosystems, UK |
| Slide Staining Tray | Pyramid Innovation, UK |
| Thermocycler PTC-200 | MJ Research, USA |
| Thermocycler MJ Mini | Bio-Rad Laboratories, Munich |
| Thermomixer 5437 | Eppendorf, Hamburg |
| Vacuum Infiltration Processor | Sakura, USA |
| Vortex | Bender&Hobein/IKA, Staufen |
| Z2 Coulter Particle Count and Size Analyzer | Beckman Coulter, USA |
| Zeiss LSM 710 ConfoCor 3 | Carl Zeiss Microscopy, Jena |

### 2.1.8 Mouse strains

| Mouse strains | Descriptions | Origins |
|---|---|---|
| C57BL/6 | Wildtype | Charles River |
| *Ager +/fl* | Exons 2 to 7 of Ager are flanked by loxP followed by the promoterless EGFP ORF in one allele | P. Angel, DKFZ [111] |
| *Ager fl/fl* | Exons 2 to 7 of Ager are flanked by loxP followed by the promoterless EGFP ORF in both alleles | P. Angel, DKFZ; originally from B. Arnold, DKFZ |
| *R26$^{Tom}$ Hnf1b-CreER* | The Cre recombinase is regulated by BEC-specific Hnf1b promoter; a loxP-flanked STOP cassette is inserted in the ubiquitously expressed Gt(ROSA)26Sor locus | F. Geisler, TUM |
| *R26$^{Tom}$ Hnf1b-CreER Ager$^{+/fl}$* | *R26$^{Tom}$ Hnf1b-CreER* crossed with *Ager$^{+/fl}$* | P. Angel, DKFZ |
| *R26$^{Tom}$ Hnf1b-CreER Ager$^{fl/fl}$* | *R26$^{Tom}$ Hnf1b-CreER* crossed with *Ager$^{fl/fl}$* | P. Angel, DKFZ |

### 2.1.9 Mouse diet and chemical substances

| Substances | Descriptions | Manufacturers |
|---|---|---|
| Choline-deficient diet | Choline-deficient chow diet | Research Diet Inc, USA |
| DL-Ethionine | Chemical substance dissolved in drinking water | Sigma-Aldrich, Taufkirchen |
| KETASET | Ketamine hydrochloride used in anesthesia cocktail mix | Zoetis, Spain |
| Rompun® 2% | Xylazine hydrochloride used in anesthesia cocktail mix | Bayer Animal Health GmbH, Leverkusen |

| Substances | Descriptions | Manufacturers |
|---|---|---|
| Tamoxifen | Chemical substance to induce Cre recombinase activation | Sigma-Aldrich, Taufkirchem |
| Sunflower Seed oil | Vehicle to dissolve tamoxifen | Sigma-Aldrich, Taufkirchem |

### 2.1.10 Oligonucleotides used for genotyping

| Gene names | Strands | Sequences (5' to 3') | Amplicon sizes (bp) |
|---|---|---|---|
| *Rage* exon 5/7 | Forward | AGCTGGCACTTAGATGGGAAACTT | 500 |
| | Reverse | TGGGCAGAGATGGCACAGGT | |
| *Rage* exon 6/8 | Forward | CCCCACCCAAGGAGGAAC | 950 |
| | Reverse | TCAGGGAGGAGCAGCACAG | |
| *eGFP* | Forward | CAGGAGCGCACCATCTTCTT | 300 |
| | Reverse | TGGGGGTGTTCTGCTGGTAG | |
| *CreERT2* control | Forward | CAATGGTAGGCTCACTCTGG | 300 |
| | Reverse | AACACACACTGGCAGGACTG | |
| *CreERT2* 347/349 | Forward | CCTGGAAAATGCTTCTGT | 400 |
| | Reverse | CAGGGTGTTATAAGCAATCCC | |
| *tdTomato* control | Forward | AAGGGAGCTGCAGTGGAGTA | 200 |
| | Reverse | CCGAAAATCTGTGGGAAGTC | |
| *tdTomato* | Forward | CTGTTCCTGTACGGCATGG | 300 |
| | Reverse | GGCATTAAAGCAGCGTATCC | |

### 2.1.11 Mouse qPCR primers

| Gene names | Strands | Sequences (5' to 3') |
|---|---|---|
| *Acta2* | Forward | GTCCCAGACATCAGGGAGTAA |
| | Reverse | TCGGATACTTCAGCGTCAGGA |
| *Ck19* | Forward | CTGAAGTCATCTGCAGCCAG |
| | Reverse | AGACCATCGAGGACTTGCG |
| *Col1a1* | Forward | GCTCCTCTTAGGGGCCACT |
| | Reverse | CCACGTCTCACCATTGGGG |
| *Col1a2* | Forward | GTAACTTCGTGCCTAGCAACA |
| | Reverse | CCTTTGTCAGAATACTGAGCAGC |
| *Col4a1* | Forward | CTGGCACAAAAGGGACGAG |
| | Reverse | ACGTGGCCGAGAATTTCACC |

| Gene names | Strands | Sequences (5' to 3') |
|---|---|---|
| *Col16a1* | Forward | GAGAGCGAGGATACACTGGC |
| | Reverse | CTGGCCTTGAAATCCCTGG |
| *Col18a1* | Forward | GTGCCCATCGTCAACCTGAA |
| | Reverse | GACATCTCTGCCGTCAAAAGAA |
| *Ctgf* | Forward | AGAACTGTGTACGGAGCGTG |
| | Reverse | GTGCACCATCTTTGGCAGTG |
| *Gapdh* | Forward | TGAAGCAGGCATCTGAGGG |
| | Reverse | CGAAGGTGGAAGAGTGGGA |
| *Hprt* | Forward | CTGGTTAAGCAGTACAGCCC |
| | Reverse | CAAAAGTCTGGGGACGCAGC |
| *Hes1* | Forward | CAACACGACACCGGACAAAC |
| | Reverse | GGAATGCCGGGAGCTATCTT |
| *Hey1* | Forward | TGAGCTGAGAAGGCTGGTAC |
| | Reverse | ACCCCAAACTCCGATAGTCC |
| *Hey2* | Forward | TGAGAAGACTAGTGCCAACAGC |
| | Reverse | TGGGCATCAAAGTAGCCTTTA |
| *Jag1* | Forward | CCTCGGGTCAGTTTGAGCTG |
| | Reverse | CCTTGAGGCACACTTTGAAGTA |
| *Rage* | Forward | ACAGGCGAGGGAAGGAGGTC |
| | Reverse | TTTGCCATCGGGAATCAGAAG |
| *Tgfb1* | Forward | CTCCCGTGGCTTCTAGTGC |
| | Reverse | GCCTTAGTTTGGACAGGATCTG |
| *Timp1* | Forward | GCAACTCGGACCTGGTCATAA |
| | Reverse | CGGCCCGTGATGAGAAACT |

### 2.1.12 Plasmids

| Plasmids | Origins |
|---|---|
| psPAX2 (2nd generation) | Addgene |
| pUltra-Hot (3rd generation) | Addgene |
| pCMV-VSV-G (2nd generation) | Addgene |
| pMXpie-EV | P. Angel Lab |
| pMXpie-Cre | P. Angel Lab |

### 2.1.13 Ready-to-use commercial kits

| | |
|---|---|
| DAB Peroxidase Substrate kit | Vector Laboratories, USA |
| Invitrogen™ Rat Jagged 1 ELISA Kit | Thermo Fischer Scientific, USA |
| RNAscope™ 2.5 HD Brown Kit | Advanced Cell Diagnostics, USA |

| | |
|---|---|
| RNeasy Mini Kit | Qiagen, Hilden |
| Total Bile Acid Assay Kit | Diazyme Europe GmbH, Germany |
| TSA Biotin System | Perkin Elmer, USA |
| VECTASTAIN® Elite® ABC HRP Kit | Vector Laboratories, USA |
| BD Cytofix/Cytoperm™ Fixation/Permeabilization Solution Kit | BD Biosciences, Heidelberg |

### 2.1.14 Recombinant proteins

| | |
|---|---|
| Recombinant mouse Jagged2 Fc chimera protein, CF | Bio-Techne, Wiesbaden |
| Recombinant rat Jagged1 Fc chimera protein, CF | Bio-Techne, Wiesbaden |
| Recombinant human TGF-beta 1 Protein | Bio-Techne, Wiesbaden |

### 2.1.15 Primary antibodies

| Primary antibodies | Species | Concentration/ Dilution (Application) | Sources | Catalog no. |
|---|---|---|---|---|
| A6 | Rat | 2 µg/ml (IHC, IF) | DSHB | AB_2618041 |
| TROMA-III CK19 | Rat | 1 µg/ml (IHC) | DSHB | AB_2133570 |
| CD11b | Rabbit | 1:5000 (IHC) | Abcam | ab13357 |
| CD44 | Rat | 1:1000 (IHC) | Abcam | ab112178 |
| CLEC4F | Goat | 1:1000 (IHC) | R&D | AF2784-SP |
| F4/80 | Rat | 1:250 (IHC) | Linaris | T-2006 |
| HES1 | Rat | 1:50 (IHC, TSA amplified) | MBL international Corporation | D134-3 |
| HNF1B | Rabbit | 1:500 (IHC) | Proteintech | 12533-1-AP |
| mCherry | Rabbit | 1:500 (IHC) | Abcam | ab167453 |
| CK19 | Rabbit | 1:300 (IF) | Abcam | ab133496 |
| Desmin | Rabbit | 1:150 (IF) | Abcam | ab15200 |
| GFP | Chicken | 1:1000 (IF) | Abcam | ab13970 |
| VCAM-1 | Goat | 1:500 (IHC) | R&D | AF643 |
| Vimentin | Rabbit | 1:500 (IF) | Abcam | ab92547 |
| αSMA | Rabbit | 1:100 (ICC) | Abcam | ab5694 |
| BODIPY™ 493/503 | N/A | 5 µM (ICC) | Invitrogen | D3922 |
| αSMA-eFluor660 | Mouse | 1:50 (FACS) | eBioscience | 50-9760-82 |
| LIVE/DEAD™ Fixable Aqua Dead cell stain (405 nm) | N/A | 1:1000 (FACS) | Invitrogen | L34957 |

### 2.1.16 Secondary antibodies

| Secondary antibodies | Dilution | Sources | Catalog no. |
|---|---|---|---|
| Biotinylated Goat α-rabbit IgG | 1:500 | Vector Laboratories | BA-1000 |
| Biotinylated Goat α-rat IgG | 1:500 | Vector Laboratories | BA-9400 |
| Goat α-rabbit Alexa 647 | 1:500 | Invitrogen | A21244 |
| Goat α-rat Alexa 647 | 1:500 | Invitrogen | A21247 |
| Goat α-chicken Alexa 647 | 1:500 | Invitrogen | A21449 |
| Hoechst 33342 | 1:1000 | Biomol | CDX-B0030 |

### 2.1.17 Softwares

| | |
|---|---|
| BD FACSDiva™ Software | Becton Dickinson Biosciences, Heidelberg |
| FlowJo v10 | Tree Star, USA |
| GraphPad Prism 7.03 | GraphPad Software, USA |
| Image J | National Institues of Health, USA |
| Primer-BLAST | National Institues of Health, USA |
| MaxQuant version 1.6.14.0 | Max Planck Institute for Biochemistry, Germany |
| StepOne Software v2.3 | Life Technologies, Darmstadt |
| ZEN 2.3 (Blue edition) | Zeiss, Oberkochen |

## Section 2.2 Methods

### 2.2.1 Animal Experiments

#### 2.2.1.1 Housing and breeding

All mice were maintained under specific pathogen free conditions in individually ventilated cage with controlled temperature of 21˚C, humidity of 50-60% and light cycles of 12 hours at the DKFZ animal facilities. Food and water were provided by *ad libitum* access. All animal experiments were approved by the responsible authority for animal experiments (Regierungspräsidium Karlsruhe, Germany) and performed in conformity with the German Law for Animal Protection.

##### 2.2.1.1.1 Generation of BEC-specific conditional *Rage* knockout mouse strains

The Cre-*loxP* system was employed extensively in this study for targeted gene deletions. The biliary lineage tracing reporter mouse model (*R26*$^{Tom}$ *Hnf1b-CreER*) described previously [27] was utilized to trace tamoxifen-inducible Cre recombinase activity in *Hnf1b*-positive cells. In this transgenic model, the ubiquitously expressed *Rosa26* locus was modified by the insertion of a strong and ubiquitously expressed *CAG* promoter, followed by the 'lox-stop-lox' cassette placed upstream of the *tdTomato* fluorescent gene sequence [137]. Upon Cre activation in *Hnf1b*-positive duct cells, the stop cassettes in the *Rosa26* locus is deleted, followed by the transcription of *tdTomato* fluorescent gene.

A transgenic RAGE/EGFP reporter mouse was utilized for *Rage* deletion [138]. The main domains of *Rage* (encoded in exons 2 to 7) were flanked by two *loxP* sites in the same orientation followed by the promoterless EGFP open reading frame (ORF). Upon Cre recombinase activate, the exons 2 to 7 of *Rage* are deleted, thus, the thymidine kinase (TK) promoter is moved to the start site of the EGFP ORF and promotes EGFP transcription [138].

*Rage* was targeted for either heterozygous or homozygous deletion in BECs. To target deletion of *Rage* specifically and conditionally in BEC, the tamoxifen-inducible *Hnf1b*-Cre td-tomato reporter mouse (*R26*$^{Tom}$ *Hnf1b-CreER*) mouse strain was crossed with RAGE/EGFP reporter mice that carry either heterozygous and homozygous floxed alleles for *Rage* (*Rage*$^{+/fl}$ or *Rage*$^{fl/fl}$).

Tamoxifen was dissolved in warm absolute Ethanol/sunflower seed oil mixture (1:9) and vortexed vigorously to achieve a homogenous mixture at a final concentration of 20 mg/ml. To induce Cre activation and delete *Rage*

conditionally, the tamoxifen solution was injected intraperitoneally to 4- to 5-week-old mouse mice at 100 mg/kg body weight every third day for three doses in total.

#### 2.2.1.1.2 Choline-deficient ethionine-supplemented (CDE) diet model

The CDE diet was employed to investigate the effect of BEC-specific *Rage* activity on diet-induced cholestasis and its influence on ductular reaction and fibrosis.

The mice with the following genotypes were used as the control group: *R26*$^{Tom}$*Rage*$^{+/+}$, *R26*$^{Tom}$ *Hnf1b-CreER Rage*$^{+/fl}$ and *R26*$^{Tom}$ *Hnf1b-CreER Rage*$^{fl/fl}$. The mice with the following genotypes were used as the experimental group: *R26*$^{Tom}$*Rage*$^{+/+}$, *R26*$^{Tom}$ *Hnf1b-CreER Rage*$^{+/fl}$ and *R26*$^{Tom}$ *Hnf1b-CreER Rage*$^{fl/fl}$.

After tamoxifen injection, the mice were maintained for two weeks of wash-out period prior to the start of the injury model. The control mice were fed with normal chow diet and drinking water. To induce chronic liver injury and cholestasis, the experimental mice were fed with choline-deficient (CD) diet and 0.165% DL-ethionine in drinking water by *ad libitum* access for three weeks. The stability of ethionine in water was assessed by natural remanent magnetization (NRM) stability test. The ethionine-containing drinking water was replaced freshly once a week. The health status of the mice was monitored, and the weight was measured daily. Mice were sacrificed at the end of the three-week CDE treatment. The mice were housed in the DKFZ S2 animal facility headed by Dr. Karin Müller-Decker. The experiment was performed under the license number G250/16.

### 2.2.1.2 Genotyping

#### 2.2.1.2.1 Genomic DNA extraction

The tail or ear punch biopsy was obtained and used for genotyping prior to the start of the animal experiments. To extract DNA from tail biopsy or ear punch biopsy, 600 µl or 200 µl of 50 mM sodium hydroxide was added to the sample and incubated at 95˚C for 10 minutes with shaking. The extract was neutralized by 75 µl or 25 µl of 1M Tris-HCl (pH 8.0) and mixed well.

#### 2.2.1.2.2 Polymerase chain reaction (PCR)

The genomic DNA extracted from the tail or ear punch biopsy was used for PCR to detect the presence of the targeted genomic sequences. The component of the PCR reaction mix includes 1.5 µl gDNA template, 10 µl of 2X PCR ALLin$^{TM}$ Red Taq Mastermix (HighQu GmbH), 0.3 µl of 10 µM forward

primer, 0.3 µl of 10 µM reverse primer and 7.9 µl distilled water. The oligonucleotides used were listed in 2.1.10. The PCR cycling conditions for the corresponding oligonucleotides pairs were described in Table 2-1, Table 2-2 and Table 2-3.

**Table 2-1. PCR cycling conditions for oligo pairs *Rage* 5/7, *Rage* 6/8 and *eGFP*.**

| Steps | Procedure | Temperature | Durations | Cycles |
|---|---|---|---|---|
| 1 | Initial denaturation | 94˚C | 5 mins | 1 |
| 2 | Denaturation | 94˚C | 30 secs | 30 |
| 3 | Annealing | 60˚C | 30 secs | |
| 4 | Elongation | 72˚C | 30 secs | |
| 5 | Final elongation | 72˚C | 5 mins | 1x |

**Table 2-2. PCR cycling conditions for oligo pair *CreERT2*.**

| Steps | Procedure | Temperature | Durations | Cycles |
|---|---|---|---|---|
| 1 | Initial denaturation | 94˚C | 6 mins | 1 |
| 2 | Denaturation | 94˚C | 1 min | 40 |
| 3 | Annealing | 60˚C | 30 secs | |
| 4 | Elongation | 72˚C | 30 secs | |
| 5 | Final elongation | 72˚C | 7 mins | 1 |

**Table 2-3. PCR cycling conditions for oligo pairs *tdTomato*.**

| Steps | Procedure | Temperature | Durations | Cycles |
|---|---|---|---|---|
| 1 | Initial denaturation | 95˚C | 3 mins | 1 |
| 2 | Denaturation | 95˚C | 45 secs | 40 |
| 3 | Annealing | 58˚C | 1 min | |
| 4 | Elongation | 72˚C | 1 min 30 secs | |
| 5 | Final elongation | 72˚C | 5 mins | 1 |

#### 2.2.1.2.3 DNA gel electrophoresis

After the PCR, 5 µl of 20 mg/ml Proteinase K and 5 µl of 6X DNA ladder was added to the PCR reaction mix and mixed well. The PCR products were run on 1% to 1.8% agarose gel at 100-120V for 30 minutes.

#### 2.2.1.3 Mouse sample processing

##### 2.2.1.3.1 Necropsy and sample collection

At the end point of each respective animal experiment, mice were weighed on a scale and body weight was measured. The mice were anesthetized with the anesthesia cocktail comprising 100 mg/kg KETASET (Ketamine hydrochloride) and 10 mg/kg Rompun® 2% (Xylazine hydrochloride) by intraperitoneal injection.

Whole blood was drawn from the mice by final heart puncture using 1 ml syringes with 25-gauge needle. The needle was removed, and the blood was dispensed into the Eppendorf tube gently. The blood was let sit at room temperature and coagulate for 30 minutes, followed by centrifugation at 6000 rpm for 10 minutes. The supernatant was transferred to new Eppendorf tube, snap frozen in liquid nitrogen and stored at -80˚C until biochemical serum analysis described in 2.2.1.3.2.

The abdomen cavity of the mouse was opened, and the liver was exposed and incised under deep anesthesia. The liver and spleen were excised and weighed on a scale. The liver-to-body weight and spleen-to-body weight ratio were calculated. In preparation for liver histological and immunohistochemistry analyses, the medial lobe was incised and fixed in 4% formaldehyde overnight for subsequent paraffin embedding described in 2.2.1.3.3; the left lobe was halved, and the lower part of left lobe was fixed in 4% formaldehyde for two to three hours for subsequent cryoprotection and cryo-embedding described in 2.2.1.3.4. For subsequent RNA or protein analysis, the remaining half of the left lobe, the right lateral lobe, caudate lobe and papillary process were cut into small pieces and transferred to Eppendorf tube for snap freezing in liquid nitrogen. The tip of the tail was collected for re-genotyping.

##### 2.2.1.3.2 Biochemical serum analysis

The serum biochemical parameters of the liver enzymes including alanine aminotransferase (ALT), aspartate transaminase (AST), alkaline phosphatase (ALP) and total bilirubin (TBIL) were measured using commercial biochemical sensor ships by Fujifilm DRI-CHEM NX500i serum analyzer.

The serum total bile acids was analyzed by total bile acids assay kit with microplate reader according to the manufacturer’s instruction. In brief, 4 µl of standard or mouse serum sample was mixed with 90 µl of reagent 1 containing Thio-NAD and incubated for 3 minutes at 37˚C. Thereafter, 30 µl of reagent 2 containing 3-α-hydroxysteroid dehydrogenase (3-α-HSD) and excess NADH was added to each sample. In the presence of Thio-NAD and excess NADH, the enzyme 3-α-HSD converts bile acids in the sample to 3-keto steroids and

Thio-NADH. The absorbance was measured by a microplate reader at 405 nm every min for 5 minutes. The rate of formation of Thio-NADH is determined by the change of the absorbance value.

#### 2.2.1.3.3 Tissue preservation by formalin-fixed paraffin-embedded (FFPE)

After fixation by 4% formaldehyde overnight as described above in 2.2.1.3.1, the liver tissues were transferred tissue cassettes and incubated in 70% ethanol for mild shaking until further sample processing. The liver samples were dehydrated and infiltrated with wax using the Vacuum Infiltration Processor with the fully automated program described in Table 2-4 below. To embed the liver sample in paraffin, the sample was removed from the tissue cassette and placed into the metal mold filled with pre-warmed paraffin. The tissue-containing metal mold was transferred to a 4˚C cooling plate to cool down the paraffin until it was completely solidified. The preserved FFPE tissue blocks were stored at room temperature until sectioning.

The FFPE liver samples were sectioned at 5 µm thick using the Leica CM3050 S Cryostat and placed in 40˚C water bath for flattening out. The cut sections were then transferred to adhesive microscopic slides and dried in a 42˚C drying cabinet overnight. The sections were stored at room temperature until immunohistochemistry staining.

**Table 2-4. Automated tissue processor program.**

| Steps | Reagents | Temperature | Durations | Cycles |
|---|---|---|---|---|
| 1 | 70% Ethanol | 35˚C | 60 mins | 1 |
| 2 | 80% Ethanol | 35˚C | 90 mins | 1 |
| 3 | 90% Ethanol | 35˚C | 90 mins | 2 |
| 4 | 96% Ethanol | 35˚C | 90 mins | 2 |
| 5 | 100% Isopropanol | 35˚C | 90 mins | 2 |
| 6 | Xylene | 40˚C | 120 mins | 2 |
| 7 | Paraffin | 58˚C | 120 mins | 4 |

#### 2.2.1.3.4 Tissue preservation by cryo-protection and embedding

After fixation by 4% formaldehyde for 2-3 hours as described above in 2.2.1.3.1, the liver tissue was rinsed once with 1X PBS and incubated in 10% sucrose/PBS solution on a tube rotator overnight or until it sank. This step was repeated by incubating the tissue in 20% sucrose/PBS solution, then in 30% sucrose/PBS solution. Subsequently, the tissue was placed in a Cryomold filled

with O.C.T. compound and frozen on dry ice slowly. The embedded tissues were stored at -80˚C until sectioning. The cryo-embedded tissues were sectioned at 5 µm thick at the chamber temperature of around -20˚C to -25˚C using a Leica CM3050S Cryostat. The sectioned tissues were transferred to Superfrost Plus adhesive microscope slides and dry at room temperature for 5-10 minutes. The sectioned tissues were stored at -80˚C until further used for immunofluorescence staining.

### 2.2.2 Histological analyses

#### 2.2.2.1 Hematoxylin and Eosin (H&E) staining

FFPE liver tissues were deparaffinized, rehydrated in ethanol with decreasing concentration, followed by cell nuclei staining with hematoxylin and counterstaining of cell cytoplasm with 1% eosin. The excess stain was washed off in tap water, dehydrated in increasing alcohol concentration and mounted in xylene-based mounting medium. The detailed protocol is described in Table 2-5 below. The H&E staining was either performed in Angel lab at DKFZ or at the Pathology Institute of the University Hospital Heidelberg.

**Table 2-5. Hematoxylin and eosin staining.**

| Steps | Procedures | Reagents | Durations |
|---|---|---|---|
| 1 | Deparaffinization | Xylene | 10 mins |
| 2 | | Xylene | 10 mins |
| 3 | Rehydration | 96% Ethanol | 2 mins |
| 4 | | 80% Ethanol | 2 mins |
| 5 | | 70% Ethanol | 2 mins |
| 6 | | 60% Ethanol | 2 mins |
| 7 | | Distilled $H_2O$ | 2 mins |
| 8 | Staining | Hematoxylin | 30 secs |
| 9 | | Running tap water | 8 mins |
| 10 | | 0.1% Eosin | 1 min |
| 11 | | Distilled $H_2O$ | rinse |
| 12 | Dehydration | 80% Ethanol | 1 min |
| 13 | | 96% Ethanol | 2 mins |
| 14 | | 96% Ethanol | 2 mins |
| 15 | | 100% Isopropanol | 2 mins |
| 16 | | Xylene | 5 mins |
| 17 | | Xylene | 5 mins |

#### 2.2.2.2 Picro-sirius Red staining

FFPE liver tissues were deparaffinized, rehydrated in ethanol with decreasing concentration. The cell nuclei were stained with Weigert's hematoxylin and the collagen fibers were stained with picro-sirius red. The excess stain was washed off by acetic acid. The stained tissues were dehydrated in increasing alcohol concentration and mounted in xylene-based mounting medium. The detailed protocol is described in Table 2-6 below. The H&E staining was either performed in Angel lab at DKFZ or at the Pathology Institute of the University Hospital Heidelberg.

**Table 2-6. Picro-sirius red staining.**

| Steps | Procedures | Reagents | Durations |
|---|---|---|---|
| 1 | Deparaffinization | Xylene | 10 mins |
| 2 | | Xylene | 10 mins |
| 3 | Rehydration | 96% Ethanol | 2 mins |
| 4 | | 80% Ethanol | 2 mins |
| 5 | | 70% Ethanol | 2 mins |
| 6 | | 60% Ethanol | 2 mins |
| 7 | | Distilled $H_2O$ | 2 mins |
| 8 | Staining | Weiger's hematoxylin | 8 mins |
| 9 | | Running tap water | 8 mins |
| 10 | | Picro-sirius red | 1 hour |
| 11 | | 70% acetic acid | rinse |
| 12 | | 70% acetic acid | 1 min |
| 13 | Dehydration | 80% Ethanol | 1 min |
| 14 | | 96% Ethanol | 2 mins |
| 15 | | 96% Ethanol | 2 mins |
| 16 | | 100% Isopropanol | 2 mins |
| 17 | | Xylene | 5 mins |
| 18 | | Xylene | 5 mins |

#### 2.2.2.3 Immunohistochemistry (IHC) staining

FFPE liver tissues were deparaffinized, rehydrated in ethanol of decreasing concentration as described in Table 2-5 (steps 1-7). Thereafter, heat-mediated antigen retrieval was performed to unmask the epitope for immunostaining. Depending on the primary antibodies used, the sections were immersed in the respective boiling citrate buffer (pH 6.0) for 15 minutes or TE buffer (pH 9.0) for 25 minutes and let cooled down for further 20 minutes at room temperature.

For normal IHC staining, the tissue sections were rinsed with PBS for 5 minutes, followed by blocking of endogenous hydrogen peroxidase activity by 3% $H_2O_2$ in methanol in dark for 10 minutes at room temperature. The sections were washed in PBS for 10 minutes, followed by incubation with blocking buffer containing 0.1% BSA and 5% animal serum (of the species where the secondary antibody was raised in) in PBS for 1 hour at room temperature. Then, the sections were incubated with primary antibody diluted in blocking buffer overnight at 4˚C. On the next day, the sections were washed 3 times in PBS for 10 minutes each at room temperature. The sections were incubated with the

biotinylated secondary antibodies diluted 1:500 in blocking buffer for 1 hour at room temperature. In the meantime, the VECTASTAIN® avidin-biotin complex (ABC) solution was prepared according to manufacturer's instruction and let stand for 30 minutes at room temperature. After being incubated with secondary antibodies, the sections were washed in PBS for 10 minutes at room temperature for three times, followed by incubation with ABC solution for 30 minutes. Subsequently, the sections were washed in PBS for 10 minutes at room temperature for three times prior to chromogenic detection.

For IHC staining with TSA amplification, TSA Biotin System was used according to manufacturer's instruction. After antigen retrieval, tissue sections were rinsed with PBS for 5 minutes. The endogenous hydrogen peroxidase activity was blocked by 3% $H_2O_2$ in PBS in dark for 10 minutes. The sections were washed in PBS for 10 minutes, followed by incubation with the TNB blocking buffer for 30 minutes, then with primary antibody diluted in TNB blocking buffer overnight at 4˚C. On the next day, the sections were washed three times in PBS for 10 minutes each, then incubated with the appropriate biotinylated secondary antibody diluted in TNB buffer for 1 hour. After washing for three times in PBS for 10 minutes each, the sections were then incubated with HRP-conjugated streptavidin (1:100 dilution in TNB buffer) for 30 minutes and washed in PBS for 10 minutes for three times again. Subsequently, the sections were incubated in Biotin Tyramide working solution (1:50 dilution of Biotin Tyramide stock solution in 1X amplification diluent) for 10 minutes. The sections were washed again in PBS for 10 minutes for three times, followed by incubation with HRP-conjugated streptavidin (1:100 dilution in TNB buffer) for another 30 minutes. Finally, the sections were washed three times for 10 minutes with PBS prior to the chromogenic detection.

To visualize the staining by chromogenic detection method, the stained sections was developed with DAB (3,3'-diaminobenzidine) Peroxidase Substrate Kit according to manufacturer's instruction. The detection reaction was stopped by immersing the sections in tap water and washed for 5 minutes, followed by counterstaining by hematoxylin for 30 seconds. The sections were washed with running tap water for 8 minutes and dehydrated in increasing alcohol concentration as described in Table 2-5 (step 12-17) and mounted in xylene-based mounting medium.

#### 2.2.2.4 *In situ* hybridization

*In situ* hybridization for the detection of *Rage* RNA expression on FFPE liver tissue was performed using RNAscope 2.5 HD Brown kit according to manufacturer's instructions. RNAscope probe targeting Mus musculus *Rage* transcript variant 1 at exon 2-7 (Probe Mm-Rage-O3, Catalog no. 882411) was designed by ACD.

#### 2.2.2.5 Immunofluorescence (IF) staining on tissues

Cryo-embedded liver tissues were air dried and equilibrated to room temperature, then washed once with PBS for 10 minutes. For staining that requires permeabilization, the sections were incubated in 0.5% Triton-X in PBS for 1 hour prior to blocking. After that, the sections were then incubated in blocking buffer containing 0.1% BSA and 5% animal serum (of the species where the secondary antibody was raised in) in PBS for 1 hour at room temperature. The sections were then incubated with primary antibodies diluted in blocking buffer overnight at 4˚C. On the next day, the sections were washed three times with PBS for 10 minutes each, then incubated with appropriate fluorophore-conjugated secondary antibody for 1 hour at room temperature. Subsequently, the sections were washed three times with PBS for 10 minutes each, followed by nuclei staining with Hoechst 33342 diluted in blocking buffer for 15 minutes. The sections were washed once with PBS for 10 minutes and mounted in Dako fluorescence mounting medium.

#### 2.2.2.6 Oil red O staining

Cryo-embedded liver tissues were air dried, then incubated in propylene glycol for 2 minutes, followed by incubated in Oil red O solution for 6 minutes. Subsequently, the sections were differentiated in 85% propylene glycol for 1 min, then rinsed in water twice. The sections were counterstained in hematoxylin for 1 min and the excessive stain were rinsed off with water for three times. The sections were mounted in aqueous mounting medium.

#### 2.2.2.7 Histopathological evaluation

The histopathological evaluation was conducted by the certified veterinary pathologist, Dr. Tanja Poth at the Pathology Institute of the University Hospital Heidelberg. H&E and Picro-sirius Red stained slides were evaluated using a general non-alcoholic fatty liver disease (NAFLD) scoring system described previously [139-141] and adapted for this study. Histological features including steatosis, inflammation and ductular reaction were evaluated based on H&E staining; fibrosis was evaluated based on Picro-sirius Red staining. The histological features of lobular inflammation were graded based on the number of inflammatory foci per 400X field while portal inflammation was graded based on severity as described previously [139, 141]. Three features of steatosis, including macrovesicular steatosis (large lipid droplet present in hepatocytes), microvesicular steatosis (small lipid droplets present in hepatocytes) and hepatocellular hypertrophy, were graded based on the percentage of the total area affected: 0 (<5%), 1 (5-33%), 2 (34-66%) and 3 (>66%).

### 2.2.3 Isolation of primary BECs from animals for RNA-sequencing

The isolation of BECs was performed on CDE-diet treated *Rage* heterozygous and knockout mice with the following genotype: *R26$^{Tom}$ Hnf1b-CreER Rage$^{+/\Delta BEC}$* and *R26$^{Tom}$ Hnf1b-CreER Rage$^{\Delta BEC}$*.

#### 2.2.3.1 Liver perfusion

The animals were first anesthetized with the anesthesia cocktail comprising 100 mg/kg KETASET (Ketamine hydrochloride) and 10 mg/kg Rompun® 2% (Xylazine hydrochloride) by intraperitoneal injection. Livers were perfused with an adapted two-step collagenase protocol as described [103, 142]. Prior to perfusion, the perfusion buffers and PBS were pre-warmed in a 42˚C water bath. The silicone tubing with diameter 2.4 mm was mounted onto the peristaltic pump and immersed into the perfusion buffers on one end.

The abdominal cavity of the mouse was opened to expose the vena portae. The catheter Abbocath-T 24 G ¾ cannula was inserted into the portal vein and fixed with a clamp. The silicon tube was connected to the catheter and the peristaltic pump was switched on immediately. The liver perfusion buffer I was perfused into the liver using with pump velocity at 2 ml/min for 10 minutes. Immediately after the perfusion started, a small incision was made on the vena cava to increase blood pressure and permit sufficient outflow during perfusion. The perfusion was continued with perfusion buffer II with pump velocity at 4 ml/min for further 10 minutes. Warm PBS was poured onto the opened abdominal cavity of the mouse occasionally during perfusion to maintain the body temperature and the moisture of the internal organs. After perfusion, the gall bladder was removed, and the liver was resected for subsequent cell isolation. The perfusion procedure was assisted by Marvin Wäsch and Lena Postawa.

#### 2.2.3.2 Isolation of non-parenchymal cells

Following perfusion, the resected livers was transferred to a sterile 60 mm cell culture dish containing ice-cold wash buffer on ice. The following steps were performed in a sterile primary cell culture hood. The liver capsules were peel-opened by forceps gently to release perfused cells. The liver capsule was discarded, while the cell-containing wash buffer was transferred to a 50 ml tube and centrifuged at 300 x *g* for 7 min at 4°C. The supernatant was discarded, and the cell pellet was suspended in 12 ml digestion buffer. The resuspended cells in digestion buffer were incubated at 37°C for 1 hour on a rotating incubator at 50 rpm. After digestion, 12 ml of cold wash buffer was added to digested cells, mixed by inverting the tube up and down, and filtered through a 70 µm cell strainer. The filtered cell suspension was centrifuged at 40 x *g* for 5 min at 4°C. The cell pellet was discarded, and the supernatant was transferred

to a new tube. Equal volume of cold wash buffer was added, followed by centrifugation at 300 x *g* for 7 min at 4°C. In the meantime, the 20%/50% Percoll gradient was prepared. First, 15 ml of 20% Percoll and 15 ml of 50% Percoll in PBS were prepared in a 50 ml tube separately. Then, the 20% Percoll/PBS was transferred with a 25 ml serological pipette and slowly applied onto the 50% Percoll/PBS. After the centrifugation, the supernatant was discarded, and cold wash buffer was added to resuspend the cell pellet. The subsequent cell suspension was gently transferred to the top of the 20%/50% Percoll in PBS and centrifuged at 1400 x *g* for 20 min at 4°C without centrifuge brake. The layer of non-parenchymal cells (NPCs) was visible close to the 20%/50% interphase. Debris and fat in the top layer were removed and the NPC layer was collected with pipet and transferred to cold wash buffer gently. The cells were washed in wash buffer by inverting up and down gently, and centrifuged at 300 x *g* for 12 min at 4°C. The supernatant was removed, and the cell pellet was resuspended in 600 µl of 1% BSA in PBS and kept on ice until fluorescence-activated cell sorting (FACS) was performed.

#### 2.2.3.3 Fluorescence-activated cell sorting (FACS) for BECs isolation

Following the isolation of NPCs, the cell suspension was taken for FACS to isolate tdTomato positive BECs. Cell sorting was gated for tdTomato and GFP expression. The tdTomato positive cells were sorted from CDE-challenged *R26$^{Tom}$ Hnf1b-CreER Rage$^{+/\Delta BEC}$* animals while tdTomato- and GFP-double-positive cells from CDE-challenged *R26$^{Tom}$ Hnf1b-CreER Rage$^{\Delta BEC}$* animals were sorted directly into RNA lysis buffer of RNeasy Mini Kit for subsequent RNA isolation as described in 2.2.9.1. Total RNA was concentrated by a rotational vacuum concentrator. The sorting of BECs for FACS was assisted by Florian Blum, Klaus Hexel and Tobias Rubner by using FACSAria Cell Sorter.

### 2.2.4 Bulk RNA sequencing and data analysis

The RNA-seq data processing and analysis was performed by Dr. Giesela Gabernet at the Quantitative Biology Center (QBiC) of the University of Tübingen. Total RNA samples were sequenced using Illumina HiSeq 4000 sequencing system (paired-end 100bp) at DKFZ Genomics & Proteomics Core Facility. The Nextflow-based nf-core RNA-Seq pipeline (https://github.com/nf-core/rnaseq) was used for the bioinformatics analysis. An aggregation of the bioinformatics workflow analysis was conducted by MultiQC v1.7 [143]. FASTQC was used to determine quality of the FASTQ files. Subsequently, adapter trimming was conducted with Trim Galore v0.6.4 (https://www.bioinformatics.babraham.ac.uk/projects/trim_galore/). STAR v2.6.1d aligner [144] was used to map the reads that passed the quality control to the reference genome. The evaluation of the RNA-seq experiment was

performed with RSeQC v3.0.1 [145] and read counting of the features (e.g. genes) with featureCounts v1.6.4 [146].

For differential expression analysis, the raw read count table resulting from featureCounts is processed with the R package DESeq2 v1.22.1 [147]. The comparison was made between the gene expression data of the RAGE knockout BECs from *Rage*$^{\Delta BEC}$ mice and RAGE control from *Rage*$^{+/\Delta BEC}$ mice. The adjusted *p*-value was calculated in the DESeq2 package with the Benjamini-Hochberg method. Genes were considered differentially expressed (DE) when the adjusted *p*-value was lower than 0.05 (*p.adj.* < 0.05).

Graphs were also produced in the RStudio v1.1.456 with R version 3.5.1 mainly using the R package ggplot2 v3.2.1. Volcano plot displayed the DE genes in log2 fold change against their adjusted *p*-value in form of -log10. KEGG and REACTOME pathway analyses were performed with the gProfiler2 tool. The sample similarity heatmap in form of regularized logarithm (rlog) normalized gene counts was created using the edgeR v3.26.5 R.

### 2.2.5 Cell culture

#### 2.2.5.1 Maintenance of cell line

All cell lines were maintained in a 37˚C incubator with 5% $CO_2$. Primary BECs were isolated by Aurora De Ponti from a CDE-diet-treated transgenic RAGE/EGFP reporter mouse (*Rage*$^{fl/fl}$) mouse and was established according to the method previously described [148]. Immortalized hepatic stellate cell MIM1-4HSC was a gift from Prof. Wolfgang Mikulits [136]. BEC line was cultured in William's E medium supplemented with 5% (v/v) FBS, 30 ng/ml IGF2, 20 ng/ml EGF, 10 µg/ml insulin, 2 mM glutamine and 1% (v/v) penicillin/streptomycin. MIM1-4HSC and HEK293T were cultured in DMEM-high glucose medium supplemented with 10% (v/v) FBS, 2 mM L-glutamine and 1% (v/v) penicillin/streptomycin.

Cell lines were propagated using the corresponding cell growth medium. The cells were frozen down with the corresponding freezing medium as described in 2.1.4 and stored in a liquid nitrogen tank. Mycoplasma test was performed regularly to ensure contamination-free culturing condition.

#### 2.2.5.2 Generation of *Rage* knockout BEC line

To generate *Rage* wildtype (WT) or *Rage* knockout (KO) BEC line, primary BECs isolated from *Rage*$^{fl/fl}$ mouse were transiently transfected with pMXpie plasmids that either carry an empty vector (EV) or Cre recombinase (Cre) using FuGENE HD transfection reagent according to manufacturer's instruction (Figure 2-1). In brief, 1 x $10^5$ BECs were seeded onto a 6 well plate and

incubated in the incubator overnight. The medium was refreshed on the next day. Prior to the transfection, the transfection reaction mix was prepared with DNA to transfectant ratio at 1:4. Then, 6 µg of either pMXpie-EV or pMXpie-Cre plasmid was mixed with 270 µl OptiMEM, followed by mixing with 24 µl FuGENE HD transfection reagent. The transfection reagent mix was let stand at room temperature for 15 minutes, then was added directly into the 6 well plate containing the BECs in growth medium.

At 48-hour post-transfection, the growth medium was refreshed and incubated until confluent. Subsequently, the transfected cells were trypsinized and resuspended in 1% BSA in PBS. The cell suspension was subjected to FACS by FACSAria I cell sorter. BECs transfected with pMXpie-EV were bulk-sorted, whereas BECs transfected with pMXpie-Cre were sorted for GFP, which is linked to the deletion of the *Rage* locus. During sorting, the cells were sorted into 1% BSA/PBS. Following sorting, the cells were centrifuged at 1500 rpm for 5 minutes. The cell pellet was resuspended in William's E growth medium and re-seeded onto 6 well plate until confluent. The cell sorting was repeated for further two times to ensure a thorough selection for GFP-positive *Rage* KO BECs. The sorted cells were expanded and sub-cultured in William's E growth medium on 10 cm cell culture plate for subsequent experiment.

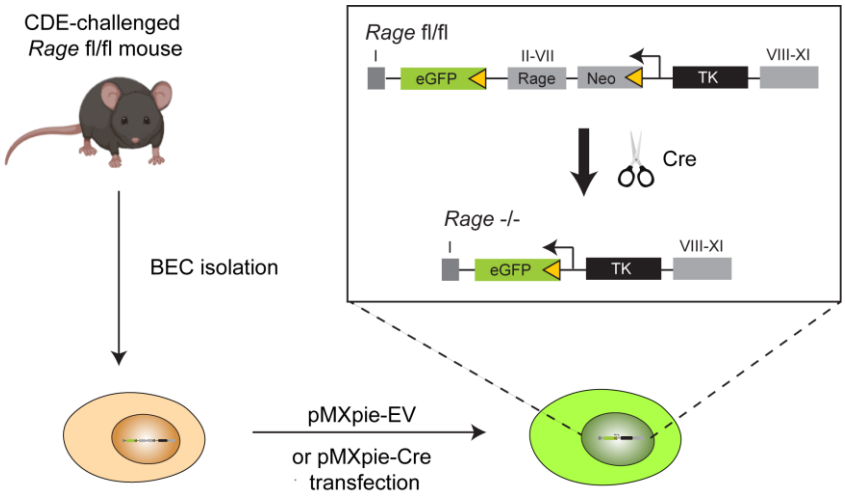


**Figure 2-1. Establishment of the *Rage* knockout BEC line**.

Primary BECs were isolated from CDE diet-treated *Rage*$^{fl/fl}$ mouse and sub-cultured on 2D cell culture format. The BECs were either transfected with pMXpie plasmid carrying a cassette with empty vector (EV) or Cre recombinase (Cre). In BECs transfected with pMXpie-Cre recombinase, exons 2 to 7 of the *Rage* locus were excised, thereby moving the TK promoter towards the eGFP open reading frame for transcription. The *Rage* knockout BECs can be distinguished from the wildtype BECs based on GFP expression.

### 2.2.5.3 Organoid Culture

To initiate an organoid culture, $1\times10^5$ BECs were resuspended in ice-cold Matrigel matrix and seeded as droplets in 24 well plate. The cell-containing matrigel droplet was allowed to solidify at 37˚C before overlaying with organoid expansion medium supplemented with 25 ng/ml Noggin and 10% Wnt3a-conditioned medium [149] (a kind gift from Christof Niehrs, DKFZ Heidelberg) and cultured for at least four days. The organoid expansion medium contains Advanced DMEM/F12 basal medium supplemented with 2 mM GlutaMAX, 1% penicillin-streptomycin, 10% R-Spondin1-conditioned medium, 1% N-2, 1% B27, 1.25 mM *N*-Acetyl-*L*-Cystein, 10 mM Nicotinamide, 50 ng/ml EGF, 100 ng/ml FGF-10, 50 ng/ml HGF, 6 µM SB431542 ALK inhibitor and Y-27632 ROCK inhibitor. After four days of organoid initiation, the culture medium was replaced by organoid expansion medium. After seven days of culturing, the initiated organoid culture was passaged by mechanically disruption and split at 1:3 ratio once a week.

### 2.2.5.4 Generation of mCherry-labelled stellate cells

Viral transduction was performed for stable expression of mCherry in MIM1-4HSC hepatic stellate cells. The procedure was performed in the DKFZ S2 cell culture facility. To produce lentivirus, 2.5 x $10^6$ HEK293T virus-packaging cells was seeded in DMEM full medium on 10 cm cell culture plate and incubated in a 37˚C incubator overnight. On the next day, the medium was refreshed two hours prior to transfection. The transfection reaction mix was prepared according to Table 2-7. The DNA mixture contained 8 µg DNA in total, which comprises of pUltra-Hot plasmid that carries the 3$^{rd}$ generation lentiviral vector for the expression of mCherry, 2$^{nd}$ generation packaging plasmid psPAX2 and 2$^{nd}$ generation VSVG-expressing envelope plasmid pCMV-VSV-G at 4:2:1 ratio. The plasmid mix was diluted by OptiMEM, followed by mixing with polyethylenimine (PEI) as the transfecting reagent with a DNA-to-PEI ratio at 1:3. The transfection mix was let stand at room temperature for 20 minutes, then added onto the medium with HEK293T cell dropwise.

**Table 2-7. Transfection mixtures for lentivirus production in HEK293T cell.**

| Reagents | Quantity used per reaction |
|---|---|
| pUltra-Hot | 4.56 µg |
| psPAX2 | 2.28 µg |
| pCMV-VSV-g | 1.14 µg |
| PEI | 24 µl |
| OptiMEM | 174.93 µl |

At 24-hour post-transfection, the medium for HEK293T cells was refreshed. At 48-hour post-transfection, the virus-containing medium was harvested, filtered through the 0.45 µm filter and stored at 4˚C. The HEK293T packaging cells was replaced with new DMEM full medium and incubated for further 24 hours. The medium was harvested as aforementioned and stored at 4˚C until further use.

To perform viral transduction, 1.5 x $10^5$ MIM1-4HSC was seeded per well in the 6 well plate. On the next day, the medium was aspirated and 1 ml of lentivirus-containing medium from HEK293T cells was transferred to the well, followed by addition of 1.5 µl of 12.5 µg/ml polybrene transfection reagent and mixed by gently swirling the plate. On the third day, the medium was replaced by fresh DMEM full medium. On the fourth day, the cells were washed twice with PBS to remove virus, then replaced by DMEM full medium again. The transduced MIM1-4HSC was expanded and sub-cultured in DMEM full medium on 10 cm cell culture plate for subsequent experiment.

#### 2.2.5.5 Co-culture assays

##### 2.2.5.5.1 Indirect co-culture assay of BECs and HSCs

To produce conditioned medium from *Rage* WT and *Rage* KO BECs, the cells were seed in T75 cell culture flask at a concentration of 3 x $10^6$ cells in 10 ml William's E growth medium and incubated at a 37˚C incubator with 5% $CO_2$ for 48 hours. The medium was collected and transferred to a 15 ml tube and spun at 1500 rpm for 5 minutes at room temperature. The supernatant was collected, filtered through a 0.22 µm filter and stored at -20˚C until further use.

MIM1-4HSC was seeded at a concentration of 2.5 x $10^5$ cells in 1.5 ml DMEM full medium per well in a 6 well plate or 1.5 x $10^5$ cells in 500 µl DMEM full medium per well in a 24 well glass bottom plate and incubated at a 37˚C incubator with 5% $CO_2$ overnight. On the next day, the cells were refreshed with new DMEM full medium for control or treated with conditioned medium from *Rage* WT and *Rage* KO BECs. The cells were incubated for further 48 hours for RNA isolation and subsequent qPCR analysis described in 2.2.9, or 96 hours for IF staining described in 2.2.6.

##### 2.2.5.5.2 Direct co-culture assay of BECs and HSCs

*Rage* WT BECs, *Rage* KO BECs and MIM1-4HSC-mCherry (MIM1-4HSC-mch) cells were trypsinized and the respective concentration was determined using a hemocytometer. To seed the BECs and MIM1-4HSC-mch in 1:1 ratio at a total concentration of 2.5 x $10^5$ cells per well on a 6 well plate, the desired amounted of cells were pooled into the 15 ml tube and spun down at 1500 rpm for 5 minutes. The supernatant was discarded, while the cell pellet was resuspended in 1.5 ml of William's E full medium and transferred onto the 6 well

plate. The cells were incubated for 96 hours and subjected for flow cytometry analysis described in 2.2.7.

### 2.2.6 Immunofluorescence (IF) staining on cells

The medium was aspirated the cells. Immediately after, the cells were fixed with 2% paraformaldehyde diluted in PBS for 20 minutes, followed by washing with PBS four times. The cells were permeabilized with 0.2% Triton-X in 1% BSA/PBS for 30 minutes, followed by blocking with 10% animal serum (of the species where the secondary antibody was raised in) in permeabilization buffer for one hour. Cells were incubated with primary antibodies diluted in blocking buffer overnight at 4˚C in a humidified environment. On the next day, the cells were washed with PBS for four times, followed by incubation with secondary antibodies diluted in blocking buffer for one hour at room temperature. The secondary antibody was removed. Thereafter, the cells were stained with Hoechst 33342 nuclear stain in blocking buffer for 15 minutes. The cells were washed with PBS for four times and immersed in PBS for subsequent image acquisition.

### 2.2.7 Flow cytometry analysis

The cells were trypsinized and resuspended in 500 µl of PBS, followed by addition of 0.5 µl of LIVE/DEAD™ Fixable Aqua Dead Cell Stain to stain the dead cells. The cells were mixed well and incubated on ice for 30 minutes in dark. Thereafter, the cells were washed with 0.5 ml PBS and centrifuged at 7000 rpm for 5 minutes. The supernatant was discarded. To permeabilize the cells, the cell pellet was resuspended in 100 µl of BD Cytofix/Cytoperm™ buffer and incubated at room temperature for 20 minutes. Thereafter, 1 ml of 1X BD Perm/Wash buffer was added on top. The cells were washed by inverting up and down for five times and centrifuged at 7000 rpm for 5 minutes. The supernatant was discarded, and the cell pellet was resuspend in 100 µl of BD Cytoperm Permeabilization Buffer Plus and incubated on ice for 10 minutes, followed by addition of 1 ml of 1X BD Perm/Wash buffer on top. The cells were washed by inverting up and down for five times and centrifuged at 7000 rpm for 5 minutes. The cell pellet was resuspended with 50 µl of αSMA-eFluor 660 antibody diluted 1:50 in 1X BD Perm/Wash buffer and incubated for 30 minutes at room temperature. The cells were washed with 1 ml of 1X BD Perm/Wash buffer and centrifuged 7000 rpm for 5 minutes. The cell pellet was resuspended in 300 µl of FACS buffer and subjected to flow cytometry analysis using BD LSRFortessa$^{TM}$ cell analyzer and FlowJo v10 Software.

### 2.2.8 Mass spectrometry

Protein concentration of William's E growth medium and BEC *Rage* WT and *Rage* KO conditioned medium were measured by Bradford assay. The subsequent procedures for protein sample preparation and mass spectrometry analysis described below were performed at DKFZ Genomics and Proteomics Core Facility.

Protein samples were fractionated by SDS-PAGE followed by In-gel digestion. Resulting peptides were loaded on a cartridge trap column, packed with Acclaim PepMap300 C18, 5 µm, 300Å wide pore (Thermo Scientific) and separated via a gradient from 3% to 40% ACN on a nanoEase MZ Peptide analytical column (300Å, 1.7µm, 75µm x 200 mm, Waters) using a 60min MS-method. Eluting peptides was analyzed by an online-coupled Orbitrap Exploris 480 mass spectrometer. Data analysis was carried out by MaxQuant (version 1.6.14.0). Match between runs option was enabled to transfer peptide identifications across Raw files based on accurate retention time and *m*/*z*. Quantification was done using a label-free quantification approach based on the MaxLFQ algorithm [150].

### 2.2.9 Quantitative real-time PCR analysis

#### 2.2.9.1 RNA isolation

For cell culture samples, the cells were washed once with 1X PBS, followed by cell lysis with buffer RLT. For mouse tissues, livers were harvested, cut into pieces and snap frozen until RNA isolation. Tissues were lysed by buffer RLT supplemented with 1% of 2-mercaptoethanol and grinded in an eppendorf tube on ice. The tissues were homogenized using a syringe with 25-gauge needle. Total RNA was isolated using the RNeasy Mini Kit along with the recommended on-column DNase digestion protocol using RNase-Free DNase Set according to manufacturer's instructions. The isolated RNA was eluted in 30-50 µl RNase-free water and stored at -80˚C until further use.

#### 2.2.9.2 Determining RNA yield and quality

The concentration and the quality of the isolated RNA was measured and determined by NanoDrop Spectrophotometer UV-VIS ND-1000. The purity of the RNA is indicated by the 260/280 and 260/230 absorbance ratio. A 260/280 ratio of approximately 2.0 and a 260/230 ratio of 2.0-2.2 of the RNA was regarded as appropriate quality with neglectable contaminants.

### 2.2.9.3 cDNA synthesis by reverse transcription

Double stranded cDNA was synthesized from 1 µg of isolated RNA by reverse transcription. The RNA was diluted to 100 ng/µl in 10 µl RNase free water and mixed with reaction mix 1 described in Table 2-8. The mixture was heated at 65˚C for 5 minutes in a thermocycler to denature the RNA template. The mixture was put promptly on ice, followed by the addition of reaction mix 2 described in Table 2-8. Reverse transcription (RT) was performed using a thermocycler with the program described in Table 2-9. Assuming the reverse transcription is at optimal efficiency, the cDNA is obtained at a concentration of 100 ng/µl. The cDNA was stored at -80˚C until further use.

**Table 2-8. Reaction mixtures for reverse transcription.**

| Mixtures | Components | Quantity |
|---|---|---|
| Reaction mix 1 | Oligo $(dT)_{18}$ primer | 0.25 µl |
| | Random Hexamer Primer | 0.25 µl |
| | RNase-free water | 3.5 µl |
| Reaction mix 2 | 5X reaction buffer for RT | 4 µl |
| | 25 mM dNTPs | 0.5 µl |
| | RiboLock RNase inhibitor | 0.5 µl |
| | RevertAid Reverse Transcriptase | 1 µl |

**Table 2-9. Reverse transcription thermocycler program.**

| Steps | Temperature | Durations |
|---|---|---|
| Reverse transcription | 42˚C | 1 hr |
| Termination | 72˚C | 10 mins |
| Cooling | 10˚C | Indefinite |

### 2.2.9.4 Quantitative real-time PCR (qRT-PCR)

The relative target gene expression was determined by qRT-PCR. Following reverse transcription, the cDNA was diluted to 1 ng/µl with RNase-free water. A total of 3 ng cDNA was used as input template. The reaction mix was prepared according to Table 2-10. The forward and reverse primer sequences are listed in 2.1.11. qRT-PCR was performed using StepOnePlus™ Real-Time PCR System with the program according to Table 2-11. Each sample was run in triplicates.

To calculate the relative expression of the gene of interest, the cycle of threshold (CT) of the gene of interest (GOI) and reference gene (REF) was considered. The amplification efficiencies of the primers were set to 2, assuming that the PCR product is doubled every cycle. The formula used for relative gene expression is described below:

$$Relative\ expression = \frac{Efficiency\ (GOI)^{\Delta CT[Control(GOI)-sample(GOI)]}}{Efficiency(REF)^{\Delta CT[Control(REF)-sample(REF)]}} = 2^{-\Delta\Delta CT}$$

**Table 2-10. Reaction mixtures for qRT-PCR.**

| Components | Quantity used per reaction |
|---|---|
| Diluted cDNA template (1 ng/µl) | 3 µl |
| 2X Power SYBR™ Green Master Mix | 6 µl |
| Forward primer (5 µM) | 0.3 µl |
| Reverse primer (5 µM) | 0.3 µl |
| Distilled water | 2.4 µl |

**Table 2-11. qRT-PCR thermocycling program.**

| Stages | Temperature | Durations | Cycles |
|---|---|---|---|
| Holding | 95˚C | 10 mins | 1 |
| Cycling | 95˚C | 15 secs | 40 |
| | 60˚C | 1 min | |
| Melting curve | 95˚C | 15 secs | 1 |
| | 60˚C | 1 min | |
| | +0.3˚C (until reaching 95˚C) | 15 secs | |
| | 95˚C | 15 secs | |

### 2.2.10 Enzyme-linked immunosorbent assay (ELISA)

The concentration of JAG1 soluble proteins in BEC plain growth medium and the conditioned medium collected from BEC *Rage* WT or *Rage* KO cells were measured by Rat Jagged 1 ELISA kit according to the manufacturer's instruction. In brief, the samples were diluted 1:30 in 1X assay diluent and incubated at room temperature for 2.5 hours, followed by washing for four times with 1X wash buffer thoroughly. Subsequently, the biotin conjugate was added into each well and incubated at room temperature for 1 hour with gentle shaking. The solution was discarded, and the plate was washed four times with

1X wash buffer again. Then, the streptavidin-HRP solution was added to each well and incubated at room temperature for 45 minutes with gentle shaking. The washing step was repeated, followed by addition of TMB substrate, and incubation at room temperature in the dark for 30 minutes with gentle shaking. Lastly, the stop solution was added to each well and mixed by gentle tapping. The absorbance of each sample was read at 450 nm with the CLARIOstar microplate reader.

### 2.2.11 Image acquisition and analysis

The images of the H&E, Picro-sirius Red, *in situ* hybridization or IF staining on liver sections were acquired at the magnification of 10X, 20X or 40X using Zeiss Axioscan.Z1. Raw images were adjusted for brightness and contrast using Zen Blue software (Zeiss). To quantify the percentage of the area of the collagen stained by Picro-sirius Red stain, raw images in .czi format were transformed to Big TIFF file format for subsequent analysis. To quantify the percentage of area of CK19, A6 and GFP staining, raw IF images in .czi format were transformed into OME TIFF file format. The transformed images were quantified using ImageJ macros written by Damir Krunic (DKFZ Light Microscopy Unit).

The images of the IF staining on cells were acquired at a magnification of 63X using Zeiss LSM 710 ConfoCor 3. The Plan-Apochromat 63X/1.4 oil DIC microscope objective and laser line UV diode, Argon 488 nm and Helium-neon laser 633 nm were used. *Z*-stack images were acquired and was processed by applying maximum intensity projection in the Zen Blue Software to obtain a stacked 2D images. The stacked images were analyzed using ImageJ macro written by Damir Krunic (DKFZ Light Microscopy Unit). The number of nucleus (size 2000-infinity pixel) and BODIPY-stained foci (size 2-infinity pixel) of each image was quantified). The average number of foci per cell was calculated per image.

### 2.2.12 Statistical tests

Data were presented as mean value ± standard deviation (*s.d.*). Two-tailed *t*-test was used for two groups and two-way ANOVA Turkey's multiple comparisons test was used for multiple groups of statistical comparison. Statistical tests were performed with GraphPad Prism 7.03. A $p$-value < 0.05 with 95% confidence interval was considered to be statistically significant (*$p$ < 0.05, **$p$ < 0.01, ***$p$ < 0.001, ****$p$ < 0.0001).

# Chapter 3

## Results

## Section 3.1 Characterization of biliary epithelial cells (BECs) *in vitro*

### 3.1.1 *Rage* is highly expressed in activated BECs

To investigate the ductular reaction (DR) in a liver disease mouse model, I have utilized the well-established choline-deficient ethionine-supplemented (CDE) diet that resembles the cholestatic setting in human liver disease. In this diet-induced cholestasis model, C57BL/6 mice were exposed to either normal diet or CDE diet for three weeks. Biliary epithelial cells (BEC) are known to be the major cell type that give rise and form a ductular network. Hence, I utilized BEC-specific markers including A6 and Cytokeratin19 (CK19) for immunohistochemistry (IHC) staining to investigate the impact of CDE diet on DR. As expected, A6- and CK19-positive BECs were restricted and located in the biliary compartment of the portal vein under normal physiological condition, whereas they expanded abundantly and infiltrated into the liver parenchyma upon CDE-diet induced injury (Figure 3-1A).

To characterize BECs on the gene expression level, primary hepatocytes and BECs were isolated from CDE-challenged mice followed by RNA isolation and qPCR analysis to examine the mRNA expression of indicative marker genes between these two major liver cell types. When compared to primary hepatocytes, BEC express an extremely low level of hepatoblast- or hepatocyte-specific markers, including alpha-fetoprotein (*Afp*) and albumin (*Alb*), whereas they express a high level of stem cell marker *Cd44* and cholangiocyte-lineage markers including Cytokeratin 7 (*Ck7*) and Cytokeratin 19 (*Ck19*). These results demonstrate that BECs belongs to the cholangiocyte-lineage and encompass stem cell markers (Figure 3-1B). Most importantly, the expression of *Rage* in BEC is approximately 16-fold higher as compared to hepatocytes, signifying that *Rage* is abundantly expressed in BECs under cholestatic conditions. This aligns with previous suggestions that RAGE may be a master regulator on BEC specifically and mediates BEC expansion in chronic liver disease states [111].

In view of the controversial discussion that BEC represents the facultative liver stem cell during liver injury, I hypothesized that the stemness properties of the BECs to perpetuate its lineage is also affected by the expression of *Rage* on BECs. To investigate the function of RAGE in mounting stemness characteristics of BECs *in vitro*, I established both a *Rage* wildtype (WT) and *Rage* knockout (KO) BEC cell line using the isolated primary BECs from CDE-challenged mice as described in 2.2.5.2. The deletion of *Rage* in BECs was confirmed by flow cytometry and qPCR analyses (Figure 3-2A & B).

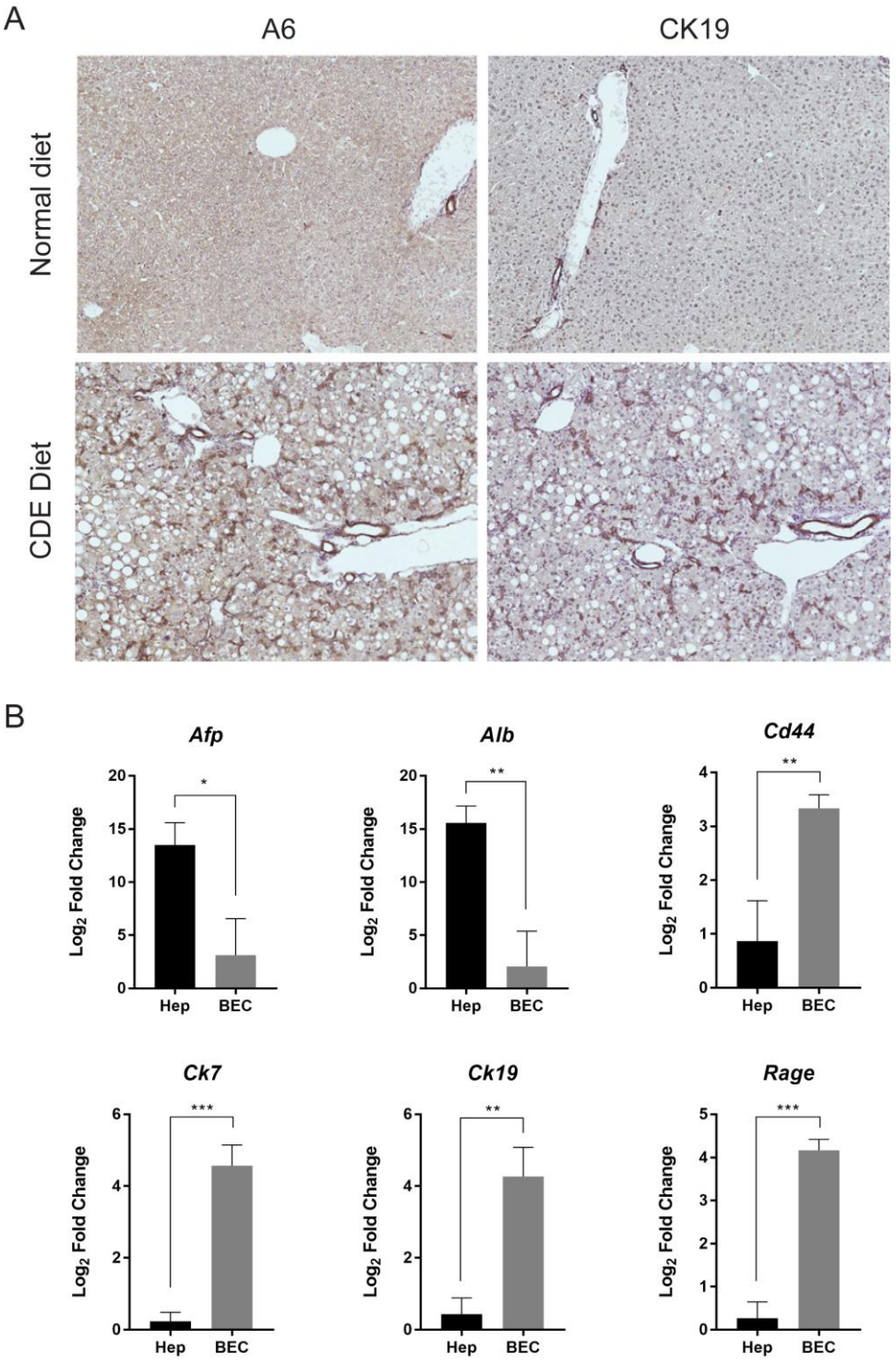


**Figure 3-1. RAGE is enriched in BECs in CDE-challenged mice**.

(A) IHC staining of BEC-specific markers A6 and CK19 in C57BL/6 wildtype mice fed with normal diet or CDE diet for 3 weeks. (B) Relative mRNA expression (in $log_2$ fold change) of hepatoblast or hepatocyte markers *Afp* and *Alb*; stem cell marker *Cd44*; cholangiocyte markers *Ck7* and *Ck19*; and *Rage* in primary hepatocytes and BECs isolated from CDE diet-challenged mice. Hep, hepatocytes.

Next, the organoid forming assay was performed as described in 2.2.5.3to examine whether the deletion of *Rage* affects the stemness property of BECs (Figure 3-2C). In brief, monolayer adherent BECs were trypsinized into single

cell suspension and resuspended in Matrigel matrix that mimic a 3-dimensional tissue growing environment. Interestingly, shortly after initiating the organoids for eight days, *Rage* WT BECs were already able to form larger pure organoids composed of a single layer of epithelial cells with large lumen. In contrast, *Rage* KO BECs were only able to form sphere clusters or smaller organotypic structures (Figure 3-2C). This suggested that ablation of *Rage* in BECs attenuates its proliferation, thus organoid formation ability. In other words, this suggests that RAGE is playing a regulatory role in BEC expanding capacity.

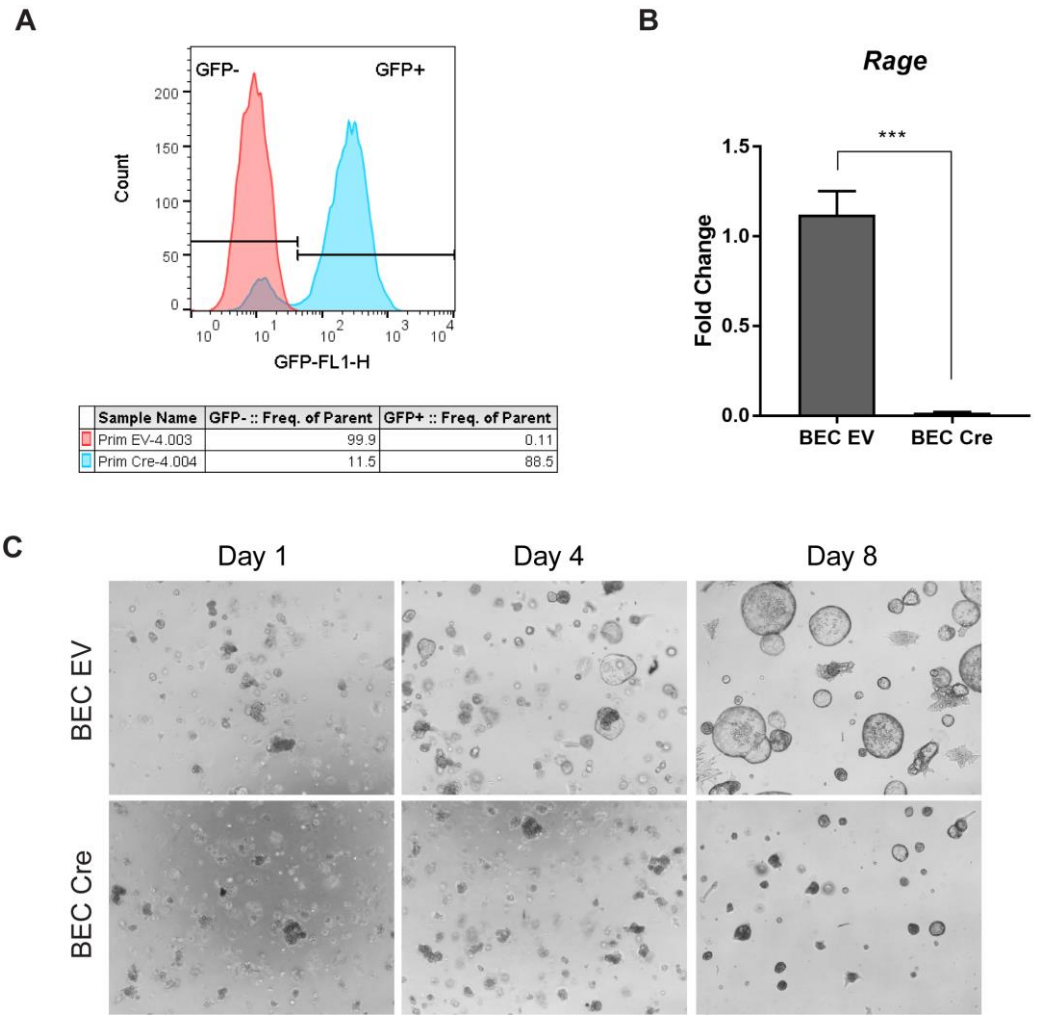


**Figure 3-2. RAGE regulates stemness capacity of activated BECs**.

(A) Flow cytometry analysis of GFP expression and (B) qPCR analysis of *Rage* mRNA expression of FACS-sorted BECs transfected with pMXpie-empty vector (EV) or –Cre recombinase. (C) Bright field images of organoid culture of BEC *Rage* WT and KO cells expanded for 8 days at passage 1. BEC EV, BEC *Rage* WT cell; BEC KO, BEC *Rage* KO cell.

### 3.1.2 Establishment of targeted deletion of *Rage* in BECs *in vivo*

As demonstrated in the previous section, RAGE is involved in controlling the expanding capacity of BEC in *in vitro* organoid culture. Next, I sought to further

investigate its functional role in BECs more specifically and in particular in cholestatic settings *in vivo*. Therefore, the Cre-*loxP* gene targeting system was employed to perform gene deletion of *Rage* conditionally in Hnf1b-positive BECs in a cholestasis mouse model. In brief, the *R26*$^{Tom}$*Hnf1b-Cre* mouse was crossed with the RAGE/EGFP report mouse to generate a BEC-specific *Rage* knockout mouse (Figure 3-3A). In this mouse line, the activity of Cre recombination in BECs can be traced by tdTomato (tdTom) expression whereas the deletion of *Rage* can be confirmed by GFP expression. Upon tamoxifen-induced Cre activation, the mice were fed with three weeks of normal diet as a control group, or three weeks of CDE diet to induce cholestasis (Figure 3-3B).

To confirm *Rage* deletion in BECs, co-IF analysis of tdTom and GFP was performed. Among the CDE diet-treated mice, *R26*$^{Tom}$ *Rage*$^{+/+}$ (*Rage*$^{WT}$) mice showed neither tdTom fluorescence nor GFP expression. As expected, *R26*$^{Tom}$*Hnf1b-CreER Rage*$^{+/fl}$ (*Rage*$^{+/\Delta BEC}$) showed tdTom fluorescence upon tamoxifen-mediated Cre activation. No GFP expression was observed due to the fact that targeting only one allele of the *Rage* locus is not sufficient to yield GFP levels that are above detection threshold. In *R26*$^{Tom}$*Hnf1b-CreER Rage*$^{fl/fl}$ (*Rage*$^{\Delta BEC}$) mice, both tdTom and GFP are expressed and co-localized as shown by the co-IF images (Figure 3-3C). Approximately 60% of the tdTom cells displayed GFP expression, confirming that *Rage* is knocked out in the majority of HNF1B-specific BEC cells (Figure 3-3D).

Furthermore, the liver tissues from mice were consecutively sectioned, and subjected for subsequent IHC analysis of HNF1B and tdTom and *in situ* hybridization of *Rage* (Figure 3-4). In this IHC analysis, a polyclonal anti-mCherry antibody was utilized to detect tdTomato expression. As both mCherry and tdTomato are the derivatives of dsRed protein, anti-mCherry antibody is sufficient to detect the tdTomato signal. Additionally, as a specific anti-RAGE antibody is not available, *in situ* hybridization of *Rage* is used for detecting the presence and expression of *Rage* on tissue sections.

In normal diet treated mice, the HNF1B-positive BECs reside exclusively next to the portal vein. Upon CDE-induced injury, these cells expanded into the parenchyma as shown by HNF1B staining. tdTomato was expressed in the *Rage*$^{WT}$ in neither normal, nor CDE condition since Cre was not present in the WT mouse. *Rage* was demonstrated to be expressed mainly in the HNF1B-positive BECs but not in the hepatocytes as shown by analysis of the consecutively cut tissue sections. CDE-challenged *Rage*$^{+/\Delta BEC}$ demonstrated an intermediate level of HNF1B-positive cells in the injured liver parenchyma. IHC staining of tdTom and *in situ* hybridization of *Rage* on consecutive tissue sections demonstrated that *Rage* is still expressed in the tdTom-labelled HNF1B cells. In CDE-challenged *Rage*$^{\Delta BEC}$ mice, *Rage* was completely abolished in HNF1B- and tdTom-positive BECs.

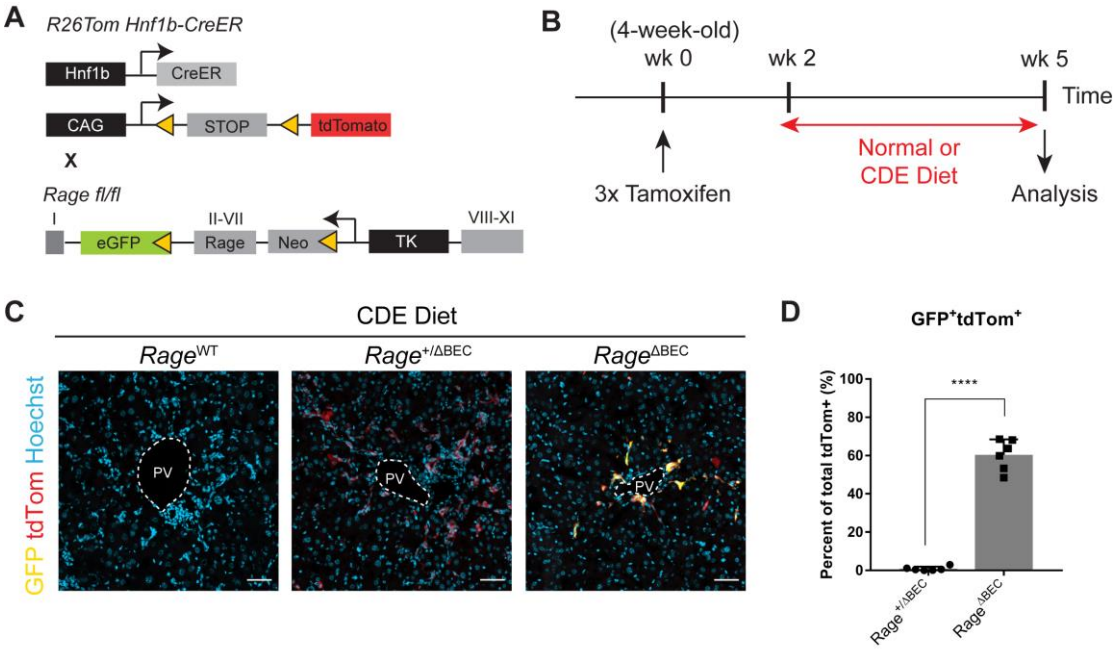


**Figure 3-3. Conditional deletion of *Rage* in BECs in the CDE-diet-induced injury model of cholestasis**.

Schematic diagram of generating a BEC-specific conditional *Rage* knockout mouse line. *R26TomHnf1b-CreER* reporter mice was crossed with *Rage*$^{fl/fl}$ mice that carries an eGFP reporter. (B) Schematic diagram of the experimental time line: tamoxifen was injected every third day into 4-week-old mice followed by a two-week wash-out period, and subsequently administered with three weeks of CDE-diet treatment. (C) Representative co-IF images of tdTomato (tdTom) and GFP staining to confirm with the genetic deletion of *Rage* in BEC in CDE-challenged mice. (D) Quantification of the percentage of GFP-positive cells out of total tdTom-positive cells. Data are shown in mean± *s.d*. Scale bar, 50 μm.

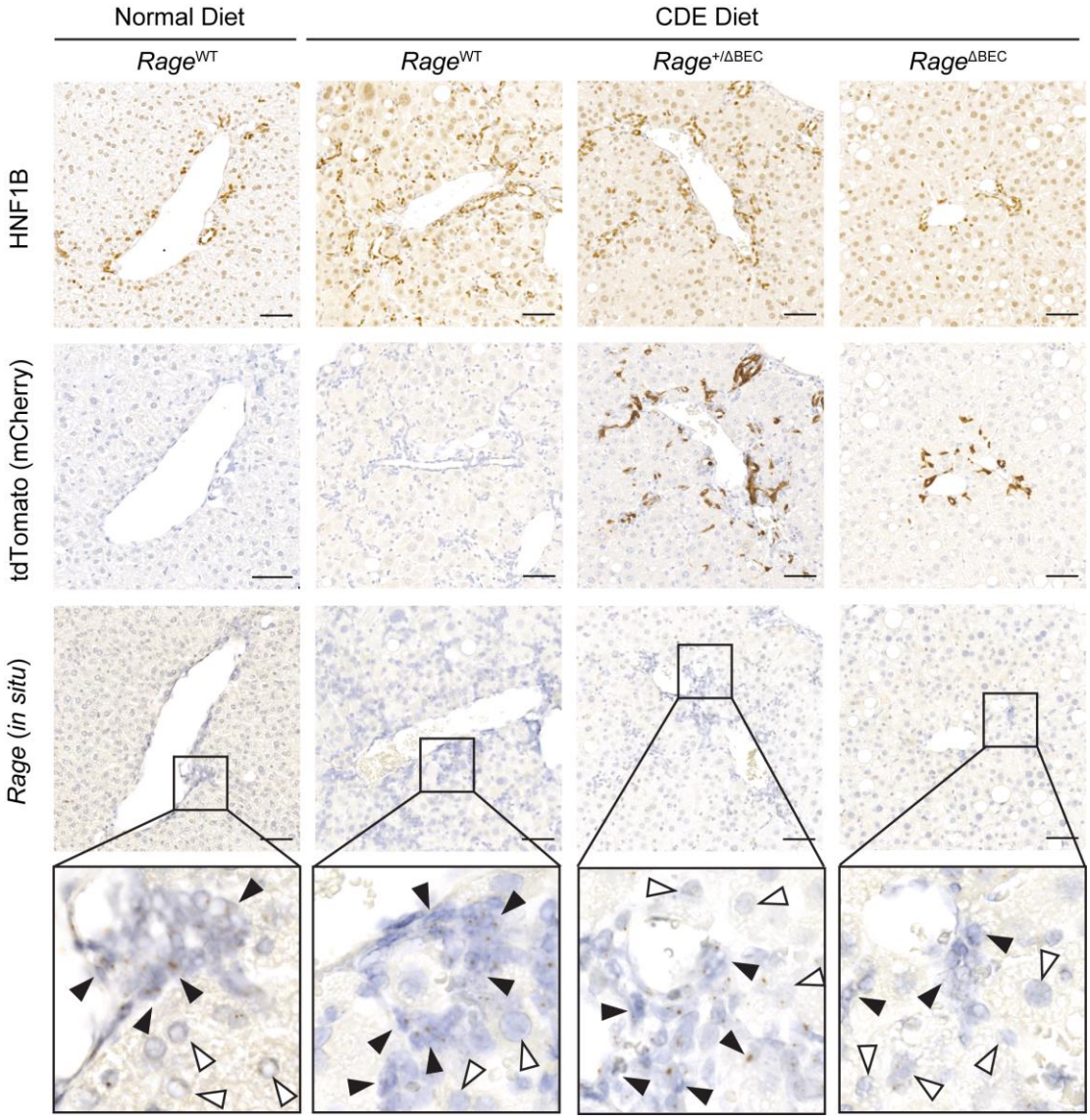


**Figure 3-4. Validation of *Rage* deletion in BECs in *R26TomHnf1b-CreER* reporter mice**.

Representative images of IHC staining of HNF1B, mCherry and *in situ* hybridization of *Rage* on consecutively sectioned liver tissues in normal diet-treated *Rage*$^{WT}$ mice or CDE diet-challenged *Rage*$^{WT}$, *Rage*$^{+/\Delta BEC}$ and *Rage*$^{\Delta BEC}$ mice. ▲ indicates BECs; Δ indicates hepatocytes. Scale bar, 50 µm.

### 3.1.3 RAGE on BEC is neither associated with CDE-induced inflammation nor steatosis

To investigate the role of RAGE in BECs in inflammation, steatosis and immune responses, H&E and histopathological analyses were employed to assess the histopathological features of diseased livers. The histological features of lobular inflammation were graded based on the number of inflammatory foci per 400X field while portal inflammation was graded based on severity as described previously [139, 141]. H&E staining and respective histological evaluation of

inflammation showed that *Rage*$^{WT}$, *Rage*$^{+/\Delta BEC}$ and *Rage*$^{\Delta BEC}$ mice fed with normal diet displayed normal hepatic architecture despite tamoxifen treatment. In contrast, CDE diet induced inflammation but at a rather comparable level in the host livers regardless of the expression of *Rage* in BECs (Figure 3-5A-C). For lobular inflammation, approximately 20-30% of the mice in each group displayed more than 1 inflammatory foci per 400X field; whereas 33.3% of *Rage*$^{WT}$ and *Rage*$^{\Delta BEC}$, and a majority of *Rage*$^{+/\Delta BEC}$ mice (70%) displayed 0.5-1 foci per 400X field (Figure 3-5B). Similarly, 22-25% of *Rage*$^{WT}$ mice displayed mild to moderate portal inflammation, and 50% of *Rage*$^{+/\Delta BEC}$ mice as well as 25% of *Rage*$^{\Delta BEC}$ displayed only mild portal inflammation (Figure 3-5C). As the degree of lobular and portal inflammation was not affected significantly despite the deletion of *Rage* in BEC, this suggests that RAGE in BEC does not contribute to CDE diet-induced inflammation.

Common diagnostic serum biochemical markers for liver functions including (1) hepatic injury markers: alanine aminotransferase (ALT), aspartate aminotransferase (AST), total bile acids, and (2) biliary tract function markers: alkaline phosphatase (ALP) and total bilirubin (TBIL) were analyzed (Figure 3-6). All CDE-challenged mice showed elevated AST, ALT and total bile acids levels when compared with the normal diet-treated mice; nevertheless, this is regardless of the activity of RAGE on BECs, indicating that hepatic injury caused by CDE treatment is independent of RAGE expression. Interestingly, the elevated ALP levels in CDE-challenged mice were significantly reduced upon the ablation of *Rage* on BECs. The elevated TBIL levels also showed a trend of reduction upon heterozygous or homozygous deletion of *Rage*. This indicates that RAGE activity on BEC might play a functional role in the biliary tract functions.

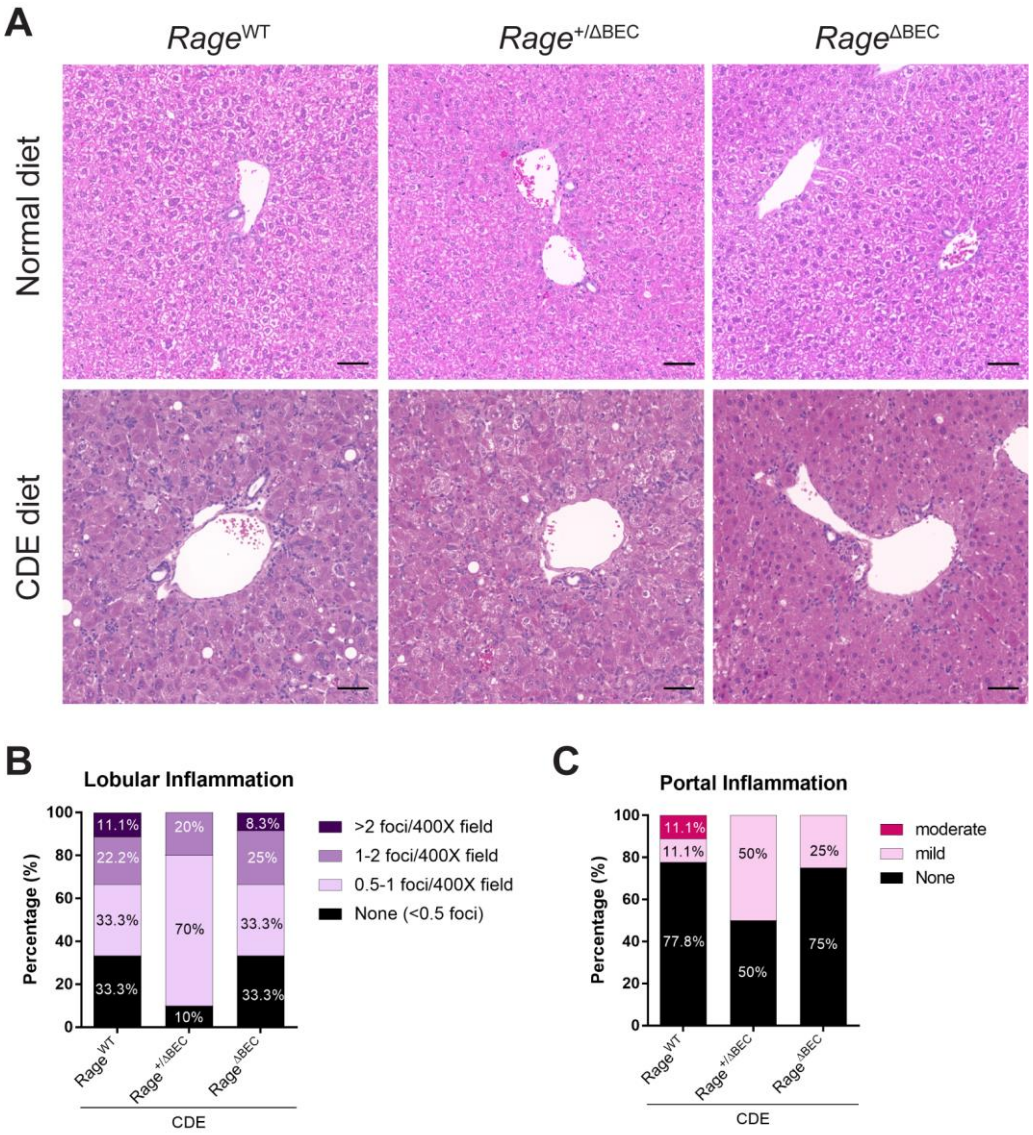


**Figure 3-5. RAGE on BECs is not involved in inflammation during cholestatic injury**.

(A) Hematoxylin & Eosin (H&E) staining of liver sections from *Rage*$^{WT}$, *Rage*$^{+/\Delta BEC}$ and *Rage*$^{\Delta BEC}$ mice fed with 3 weeks of normal or CDE diet. (B) Histopathological evaluation of lobular inflammation and portal inflammation based on H&E staining in CDE diet-challenged mice. ND-treated mice: *Rage*$^{WT}$ (*n*=12), *Rage*$^{+/\Delta BEC}$ (*n*=12), *Rage*$^{\Delta BEC}$ (*n*=11); CDE-treated mice: *Rage*$^{WT}$ (*n*=9), *Rage*$^{+/\Delta BEC}$ (*n*=10), *Rage*$^{\Delta BEC}$ (*n*=12). Scale bar, 50 μm.

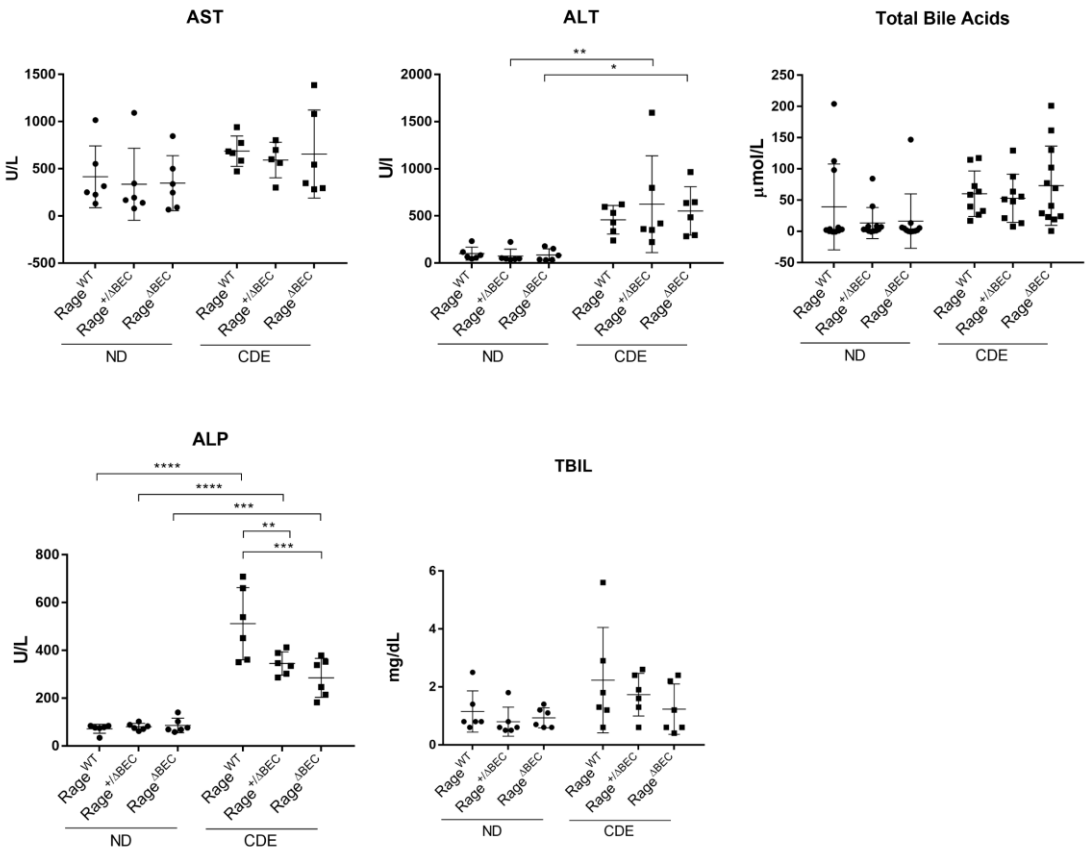


**Figure 3-6. RAGE on BECs may affect biliary tract functions**.

Biochemical serum analysis of hepatic function markers: aspartate aminotransferase (AST), alanine aminotransferase (ALT), total bile acids, and biliary tract function markers: alkaline phosphatase (ALP) and total bilirubin (TBIL) in *Rage*$^{WT}$, *Rage*$^{+/\Delta BEC}$ and *Rage*$^{\Delta BEC}$ mice fed for three weeks with normal or CDE diet (*n*=6 each group). Data are shown in mean± *s.d*. Two-way ANOVA Turkey's multiple comparisons test was used for statistical comparison. A *p*-value < 0.05 with 95% confidence interval was considered to be statistically significant (**p* < 0.05, ***p* < 0.01, ****p* < 0.001, *****p* < 0.0001).

Next, immune cell recruitments in this current model was also analyzed by IHC staining, including CD11b for neutrophils, F4/80 for macrophage, and CLEC4F for Kupffer cells (Figure 3-7). Interestingly, although different populations of immune cells were increased upon CDE-induced cholestasis, the degree of infiltration into the liver parenchyma was independent of the expression of RAGE in BECs. Collectively, these data suggested that RAGE on BECs is not associated with CDE diet-induced immune cell infiltration.

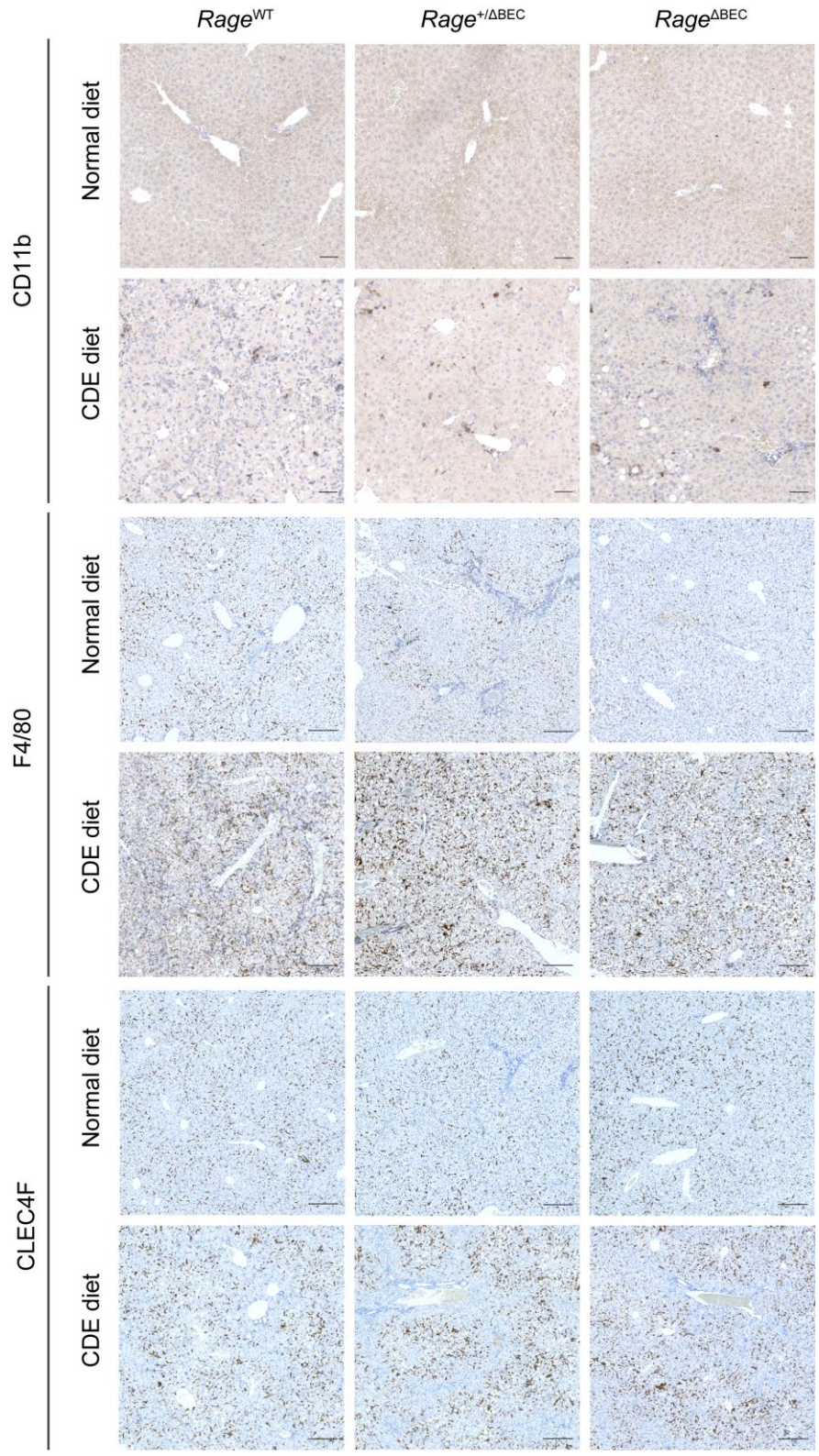


**Figure 3-7. Immune cell infiltrates into injured liver parenchyma regardless of RAGE activity during cholestatic injury**.

Representative images of IHC staining of immune cells, including CD11b for neutrophil, F4/80 for macrophages and CLEC4F for Kupffer cells in *Rage*$^{WT}$, *Rage*$^{+/\Delta BEC}$ and *Rage*$^{\Delta BEC}$ mice fed for 3 weeks with normal or CDE diet. IHC staining was repeated on liver tissues from at least 3 animals per group. Scale bar, 50 µm for CD11b; 200 µm for F4/80 and CLEC4F.

To investigate whether BECs influence CDE-induced lipid accumulation and steatosis, the abundance of neutral triglycerides and lipids was assessed by Oil Red O staining and quantified based on the percentage of the area of stained lipid droplets (Figure 3-8). In summary, CDE diet induced hepatocellular steatosis significantly but the amount of fat accumulation between *Rage*$^{WT}$, *Rage*$^{+/\Delta BEC}$ and *Rage*$^{\Delta BEC}$ mice upon CDE-induced chronic injury were not significantly different (Figure 3-8A & B). Moreover, hepatocellular steatosis were evaluated histopathologically based on H&E staining using a semi-quantitative scoring system [140]. Three features of steatosis, including macrovesicular steatosis (large lipid droplet present in hepatocytes), microvesicular steatosis (small lipid droplets present in hepatocytes) and hepatocellular hypertrophy, were graded based on the percentage of the total area affected: 0 (<5%), 1 (5-33%), 2 (34-66%) and 3 (>66%), which gives a sum of score (Figure 3-8C). In line with the Oil Red O staining, there was no significant difference of CDE-induced steatosis between *Rage*$^{WT}$, *Rage*$^{+/\Delta BEC}$ and *Rage*$^{\Delta BEC}$ mice, indicating the RAGE on BEC is not associated with steatosis.

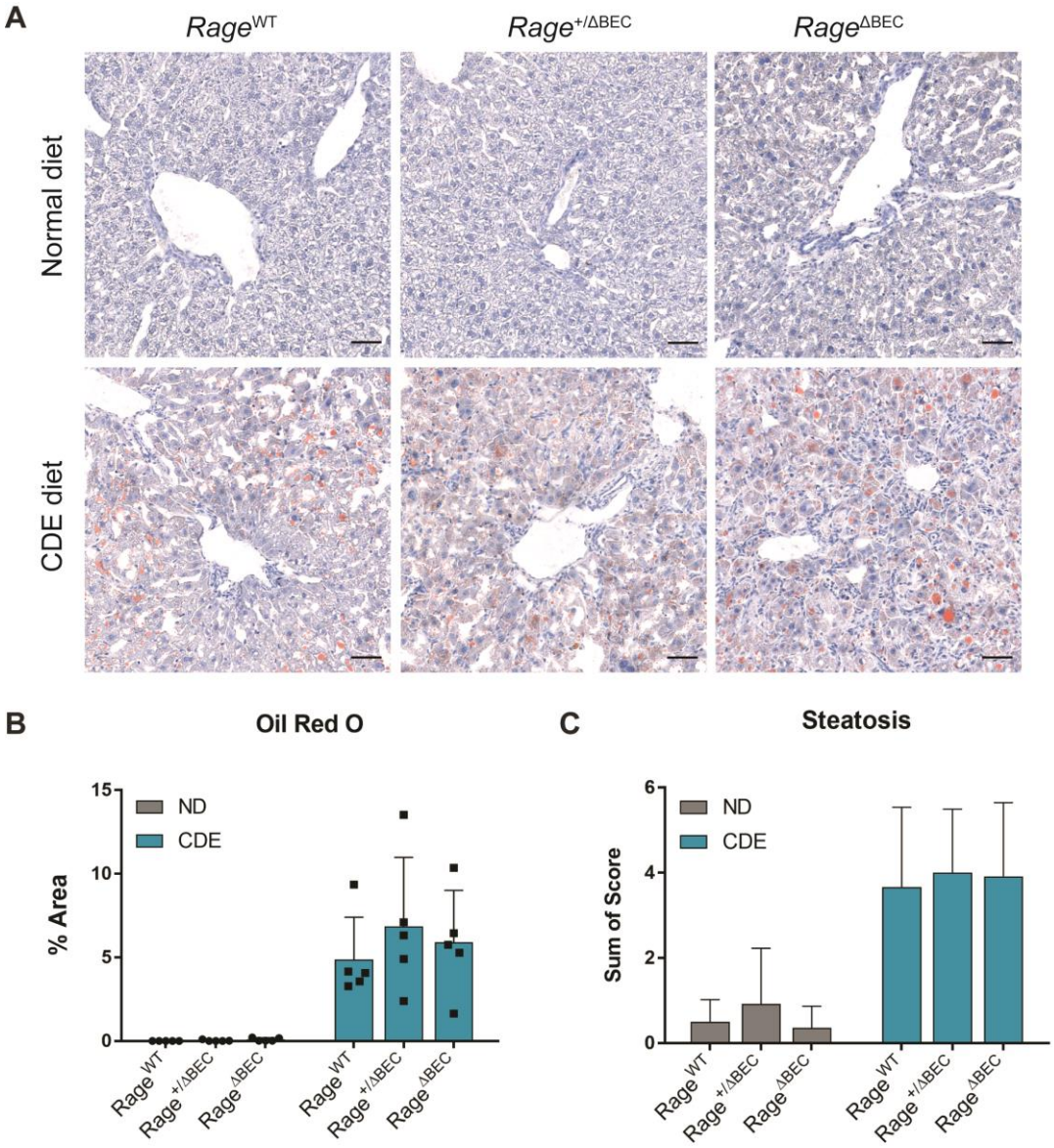


**Figure 3-8. RAGE on BECs is not associated with steatosis during cholestatic injury**.

(A) Representative images of Oil Red O staining, (B) Oil Red O quantification and (C) histopathological evaluation of steatosis (based on H&E staining in **Figure 3-5**) in *Rage*$^{WT}$, *Rage*$^{+/\Delta BEC}$ and *Rage*$^{\Delta BEC}$ mice fed with three weeks of normal or CDE diet. At least five animals were analyzed for each group. Data are shown in mean± *s.d*. Two-way ANOVA Turkey's multiple comparisons test was used for statistical comparison. The oil red O staining was performed by Heide Danijela (DKFZ, Division of chronic inflammation and cancer). Scale bar, 50 µm.

### 3.1.4 RAGE on BEC is indispensable for ductular reaction

To test with the hypothesis that RAGE is a critical mediator for DR in the context of cholestasis, the degree of DR and the abundance of proliferative bile ducts were analyzed histopathologically based on H&E staining on the liver tissues of CDE-challenged mice (Figure 3-9A & B). The abundance of BECs is accounted as the degree of DR. BECs appear as an oval-shaped nucleus and high nuclear-to-cytoplasmic ratio, whereas proliferative bile ducts are characterized by the formation of a bile duct lumen from the BECs. Both phenotypes can occur independently, but can be also associated with each other and develop cholangiofibrosis [151]. *Rage*$^{WT}$ mice exhibited an enhanced level of DR and bile duct proliferation upon CDE-induced cholestasis (around 80% with moderate to severe, 20% with mild DR; 45% with moderate and 55% with mild bile duct proliferation), whereas *Rage*$^{+/\Delta BEC}$ mice exhibited an intermediate level of DR and bile duct proliferation (40% with moderate to severe, 60% with mild DR; 60% with moderate to severe, 30% with mild bile duct proliferation). In the majority of *Rage*$^{\Delta BEC}$ mice, DR and bile duct proliferation are abrogated or attenuated, with a reduction to only 8.3% of mice exhibited a moderate phenotype, 58.3% with mild phenotype, and mice displaying no DR has increased to 33.3%. Similarly, around 17% of mice displayed no bile duct proliferation, whereas 75% showed mild condition and only 8% exhibited moderate level of bile duct proliferation.

Next, I performed co-IF analysis of BEC-specific markers (CK19 and A6) and tdTom on liver tissues from untreated and CDE-treated mice and the percentage of the area of the staining was determined (Figure 3-9C-F). IF analysis showed that CK19+ or A6+ BECs were restricted to the biliary compartments of the portal vein under normal condition. Upon three weeks of induction of chronic injury by CDE diet, both *Rage*$^{WT}$, and *Rage*$^{+/\Delta BEC}$ mice displayed massive expansion of BECs within the liver parenchyma as shown by total CK19 staining (6.1 ± 3.93% in *Rage*$^{WT}$ mice, $n$=9; 4.91 ± 3.68% in *Rage*$^{+/\Delta BEC}$ mice, $n$=10) and total A6 staining (9.15 ± 4.58% in *Rage*$^{WT}$ mice, $n$=9; 6.47 ± 4.88% in *Rage*$^{+/\Delta BEC}$ mice, $n$=10). Strikingly, loss of *Rage* in BECs resulted in a prominent reduction of total CK19 (1.64 ± 1.04%, $n$=12) and total A6 (2.95 ± 2.28%, $n$=12) staining. To assess whether the CK19 and A6 positive cells are the progeny of the HNF1B+ ductal compartment, co-IF analysis of both markers and tdTom was performed. Representative images showed that, on average, 70% of CK19+ and A6+ cells co-stained for tdTom, indicating that the vast majority of BECs arise from HNF1B+ ductal cells. Taken together, BECs are severely compromised in their capability to expand into the injured liver parenchyma upon deletion of *Rage* during CDE-induced cholestasis. This demonstrated that RAGE is required for efficient BEC activation.

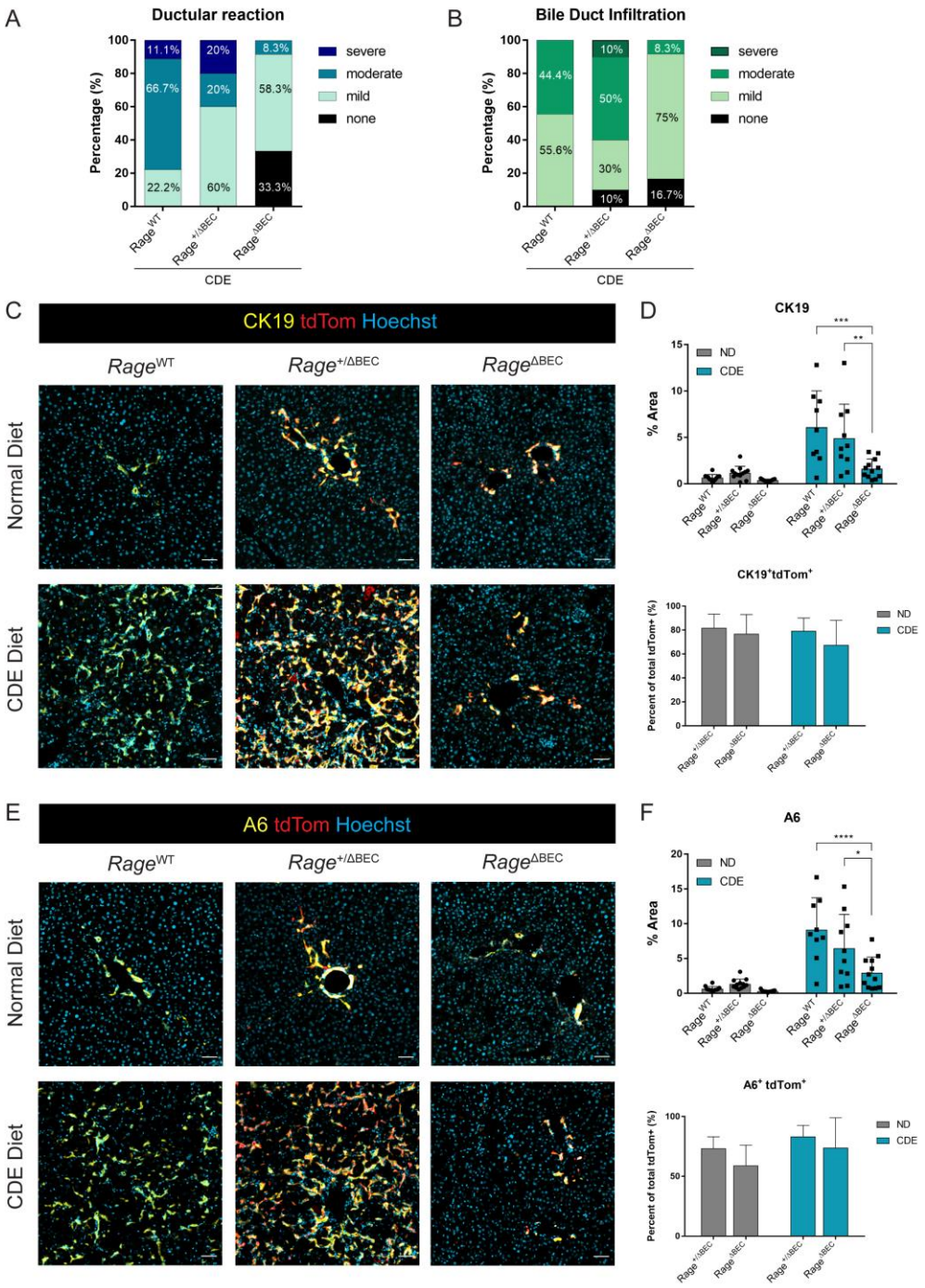


**Figure 3-9. RAGE on BECs is indispensable for ductular reaction during cholestasis**.

(A) Histopathological evaluation of ductular reaction and (B) bile duct infiltration in *Rage*$^{WT}$, *Rage*$^{+/\Delta BEC}$ and *Rage*$^{\Delta BEC}$ mice fed for three weeks with normal diet (ND) or CDE diet based on H&E staining. (C) Representative images of IF of tdTom and CK19 and (D) quantification of percent area of CK19 staining alone or CK19/tdTom double positive staining. (E) Representative images of IF of tdTom and A6 and (F) quantification of percent area of A6 staining alone or A6/tdTom double positive staining. ND-treated mice: *Rage*$^{WT}$ (*n*=12), *Rage*$^{+/\Delta BEC}$ (*n*=12), *Rage*$^{\Delta BEC}$ (*n*=11); CDE-treated mice: *Rage*$^{WT}$ (*n*=9), *Rage*$^{+/\Delta BEC}$ (*n*=10), *Rage*$^{\Delta BEC}$ (*n*=12). Data are shown in mean± *s.d*. Two-way ANOVA Turkey's multiple comparisons test was used for statistical comparison. A $p$-value < 0.05 with 95% confidence interval was considered to be statistically significant (*$p$ < 0.05, **$p$ < 0.01, ***$p$ < 0.001, ****$p$ < 0.0001). Scale bar, 50 µm.

## Section 3.2 Functional role of BEC-specific RAGE activity in fibrosis

### 3.2.1 Bulk RNA-sequencing reveals the functional role of RAGE on BECs in extracellular matrix organization[1]

To identify *Rage*-dependent genetic program in BECs in response to chronic injury, primary BECs were isolated from tamoxifen-treated, CDE-challenged mice by liver perfusion and density gradient separation, followed by FACS using a gating strategy based on high tdTom and GFP expression and subsequent bulk RNA sequencing (RNA-seq) to identify *Rage*-dependent signaling pathways in BECs (Figure 3-10A & B). Corresponding mice containing one intact *Rage* allele ($Rage^{+/\Delta BEC}$), which express high levels of tdTom and only marginal levels of GFP, was served as control (*Rage* control) for the RNA-seq analysis. Differential gene expression analysis demonstrated that loss of *Rage* in BECs resulted in a significant decrease in the expression of extracellular matrix (ECM)-associated genes such as *Col4a1*, *Col16a1*, *Ltbp2* (latent transforming growth factor beta-binding protein 2), *Timp1* (tissue inhibitor of matrix metalloproteinase 1), *Cdh17* (Cadherin 17); inflammation-associated mediators, such as *Ccl2* (C-C motif ligand 2), *Tnfaip2* (tumor necrosis factor alpha-induced protein 2), *Csf1* (colony stimulating factor 1), *Cd40* (cluster of differentiation 40); and stem cell markers, such as *Cd44* and *Nes* (nestin) (Figure 3-10C).

KEGG and REACTOME pathway analyses showed that a majority of the enriched pathways (*p.adj.* value <0.05) of the differentially expressed genes were associated with ECM modulation and cell-cell interactions as well as pro-inflammatory pathways, such as TNF- and IL-17-induced signaling (Figure 3-11A, Table 3-1, Table 3-2). Remarkably, Ingenuity pathway analysis (IPA) revealed that pathways, which are typically associated with hepatic fibrosis and hepatic stellate cell activation were dependent on *Rage* in BECs. Classical fibrotic mediators and markers (including *Tgfb1*, *Timp1* and *Vcam1*), collagen of the ECM (including *Col4a1*, *Col4a2*, *Col16A1* and *Col18a1*) and cell surface adhesion and signaling integrin (*Itga2*, *Itga5*) were found to be differentially expressed in the enriched hepatic fibrosis pathways (Figure 3-11B & C). The expression of the differentially expressed genes in the enriched hepatic fibrosis/ stellate cell activation and extracellular matrix organization pathways were visualized in heatmap (Figure 3-11D).

[1] The text of this section has been taken from a manuscript in preparation and was originally written by myself.

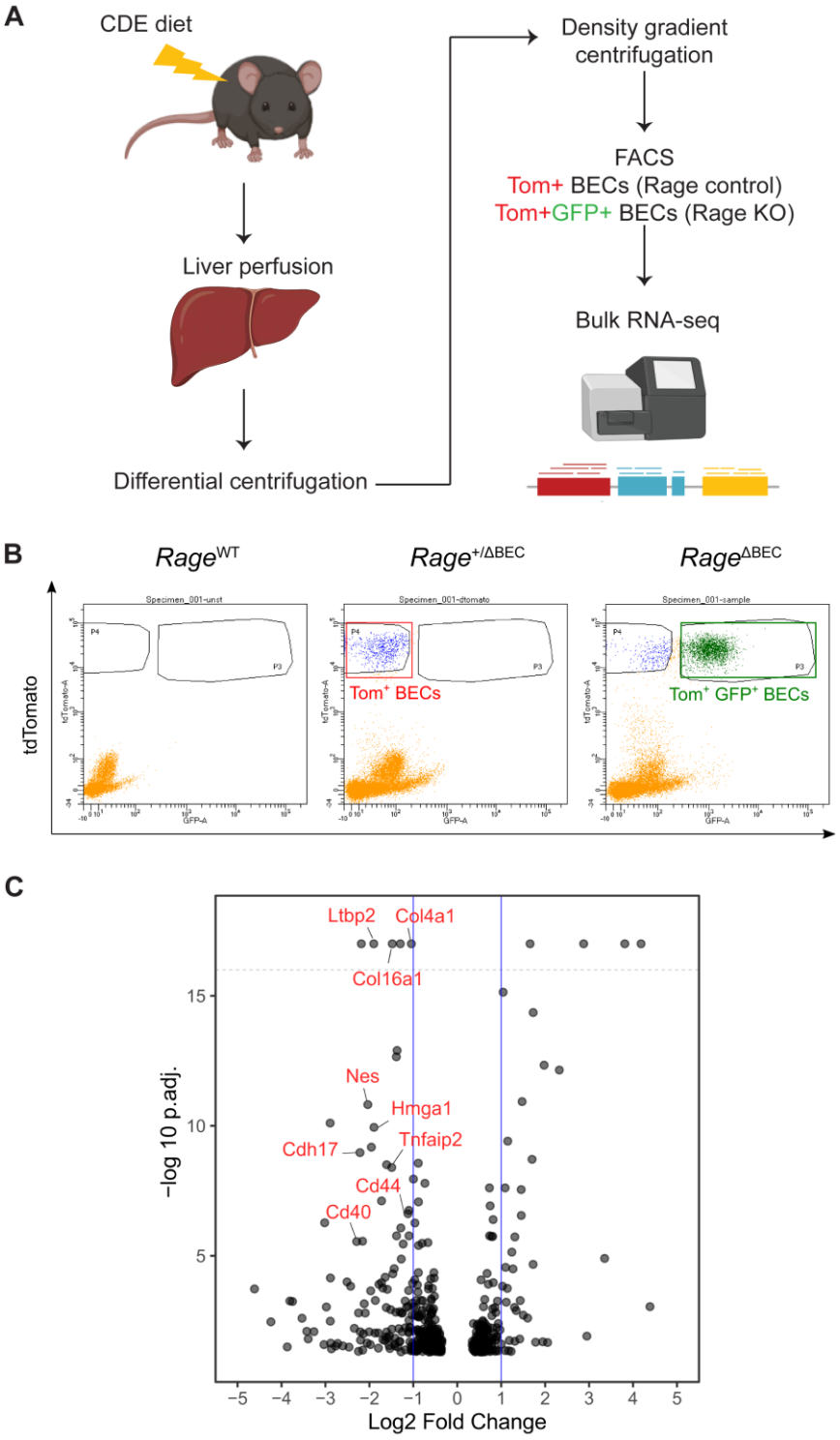


**Figure 3-10. Identification of differentially expressed genes between *Rage* control and knockout BECs from CDE-challenged mice**.

(A) Schematic diagram of the procedures to isolate primary BECs from CDE diet-challenged mice for bulk RNA-seq. (B) Representative FACS analysis of the primary BECs isolated from CDE diet-challenged *Rage*$^{WT}$, *Rage*$^{+/\Delta BEC}$ and *Rage*$^{\Delta BEC}$ mice. tdTom-positive BECs from *Rage*$^{+/\Delta BEC}$ mice ($n$=4) and tdTom and GFP-double positive BECs from *Rage*$^{\Delta BEC}$ ($n$=4) were sorted for direct RNA isolation followed by RNA-seq. tdTom+ BECs from *Rage*$^{+/\Delta BEC}$ mice were taken as *Rage* control group for analysis. (C) Volcano plot of differentially expressed (DE) genes (*p.adj.* value < 0.05) between *Rage* control and knockout BECs.

A

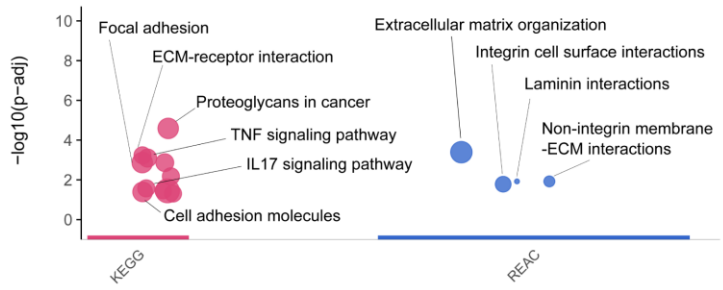


B

**Top Canonical Pathways**

| Name | p-value | Overlap | Molecules |
|---|---|---|---|
| Hepatic Fibrosis / Hepatic Stellate Cell Activation | 1.39E-07 | 9.1 % 17/186 | BAMBI,CD40,COL16A1,COL18A1,COL4A1,COL4A2,CSF1, CXCL3,FGFR1,FLT4,IGFBP3,MYH9,PDGFB,TGFB1,TIMP1, TNFRSF1B,VCAM1 |
| Caveolar-mediated Endocytosis Signaling | 1.14E-05 | 12.3 % 9/73 | ALB,FLNA,FLNB,FLNC,HLA-A,HLA-F,ITGA2,ITGA5,ITGAV |
| Leukocyte Extravasation Signaling | 3.20E-05 | 7.1 % 14/197 | BCAR1,CD44,CLDN2,CLDN8,ITGA2,ITGA5,MAPK11,MMP24, MSN,PLCG2,TIMP1,TIMP3,VAV2,VCAM1 |
| Hepatic Fibrosis Signaling Pathway | 3.71E-05 | 5.4 % 20/368 | BAMBI,CD40,CEBPB,COL18A1,FGFR1,FLT4,ITGA2,ITGA5, MAPK11,PDGFB,PLCG2,RND1,SIRT3,SUCNR1,Tcf7,TGFB1, TIMP1,TNFRSF1B,VCAM1,WNT7B |
| Granulocyte Adhesion and Diapedesis | 4.87E-05 | 7.3 % 13/179 | Ccl2,Ccl7,CLDN2,CLDN8,CXCL2,CXCL3,ITGA2,ITGA5,MMP24, MSN,SDC3,TNFRSF1B,VCAM1 |

C

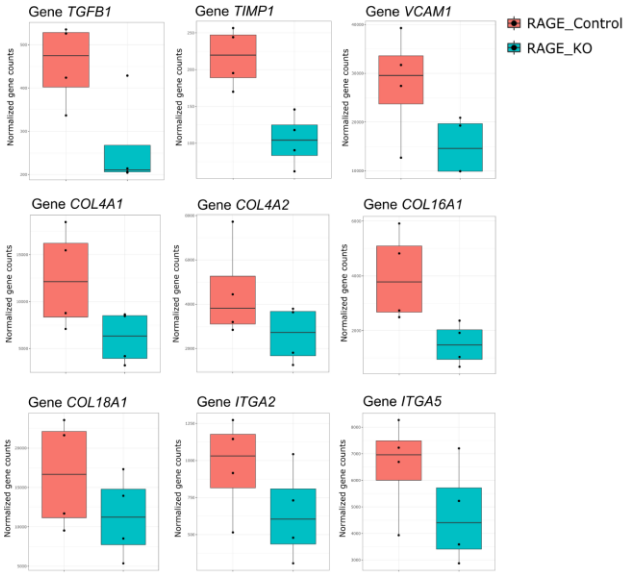


D

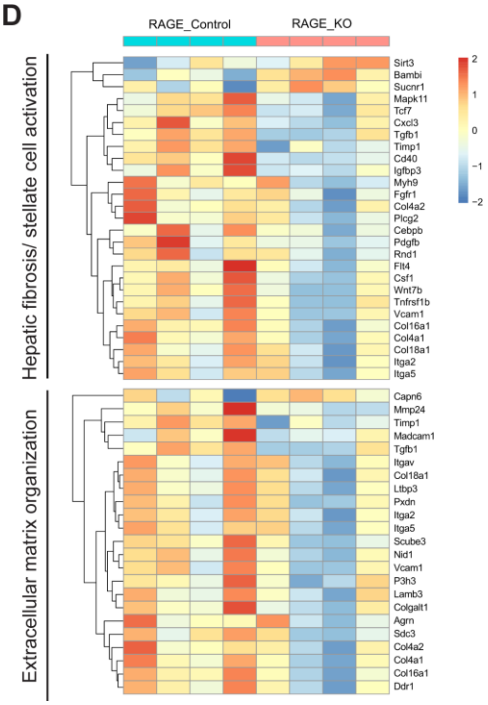


**Figure 3-11. RNA-seq data reveals the significant role of BEC-specific RAGE activity in extracellular matrix organization, hepatic stellate cell activation and fibrosis**.

(A) Enriched KEGG and REACTOME pathways (*p.adj.* value < 0.05) of DE genes. (B) Top five enriched canonical pathways of identified by Ingenuity Pathway Analysis and the respective DE gene list. (C) Box plots of DE fibrotic genes, ECM organizational genes and cell surface adhesion and signaling integrins. (D) Heatmaps of the DE genes between *Rage* control and knockout BECs in the corresponding enriched pathways, including hepatic fibrosis/ stellate cell activation and extracellular matrix organization. Color scale bar represents regularized log transformed reads. The RNA-seq data processing and analysis was performed by Dr. Giesela Gabernet (Quantitative Biology Center (QBiC); University of Tübingen).

**Table 3-1. KEGG enriched pathways between *Rage* control and *Rage* knockout BECs.**

| Pathway names | Pathway code | DE genes | Pathway size | Fraction (DE/pathway size) | *p.adj.* value |
|---|---|---|---|---|---|
| Proteoglycans in cancer | KEGG:05205 | 21 | 196 | 0.107143 | 2.57E-05 |
| ECM-receptor interaction | KEGG:04512 | 12 | 87 | 0.137931 | 0.000582 |
| TNF signaling pathway | KEGG:04668 | 13 | 109 | 0.119266 | 0.0008 |
| Focal adhesion | KEGG:04510 | 17 | 194 | 0.087629 | 0.001357 |
| Amoebiasis | KEGG:05146 | 12 | 103 | 0.116505 | 0.001357 |
| Small cell lung cancer | KEGG:05222 | 10 | 88 | 0.113636 | 0.006649 |
| IL-17 signaling pathway | KEGG:04657 | 9 | 88 | 0.102273 | 0.026794 |
| Salmonella infection | KEGG:05132 | 8 | 75 | 0.106667 | 0.035034 |
| Pathways in cancer | KEGG:05200 | 27 | 522 | 0.051724 | 0.035895 |
| Cell adhesion molecules (CAMs) | KEGG:04514 | 12 | 159 | 0.075472 | 0.040351 |
| Rheumatoid arthritis | KEGG:05323 | 8 | 83 | 0.096386 | 0.049291 |

**Table 3-2. REACTOME enriched pathways between *Rage* control and *Rage* knockout BECs.**

| Pathway names | Pathway code | DE genes | Pathway size | Fraction (DE/pathway size) | *p.adj.* value |
|---|---|---|---|---|---|
| Extracellular matrix organization | REAC:R-MMU-1474244 | 23 | 253 | 0.090909 | 0.000405 |
| Laminin interactions | REAC:R-MMU-3000157 | 6 | 25 | 0.24 | 0.011944 |
| Non-integrin membrane-ECM interactions | REAC:R-MMU-3000171 | 7 | 34 | 0.205882 | 0.011944 |
| Integrin cell surface interactions | REAC:R-MMU-216083 | 9 | 67 | 0.134328 | 0.016526 |

To validate the RNA-seq data, qPCR analysis was performed using total RNA from whole liver tissue from CDE-challenged *Rage*$^{+/\Delta BEC}$ and *Rage*$^{\Delta BEC}$ mice. Indeed, ECM and fibrotic markers, including *Col1a1*, *Col1a2*, *Col4a1*, *Col16a1*, *Col18a1*, *Tgfb1*, *Timp1* and *Ctgf* were markedly reduced in livers of *Rage*$^{\Delta BEC}$ mice when compared to *Rage* controls (Figure 3-12A). The RNA-seq result was also validated on protein level by IHC staining. For instance, Vcam-1 and Cd44 are two cell adhesion-associated genes found to be differentially expressed between the isolated *Rage* control and KO BECs. In line with the RNA-seq results, *Rage* control mice exhibited more prominent expression levels of VCAM-1 and CD44 than *Rage*$^{\Delta BEC}$ mice in liver tissues, and both proteins were most notably expressed in BECs (Figure 3-12B).

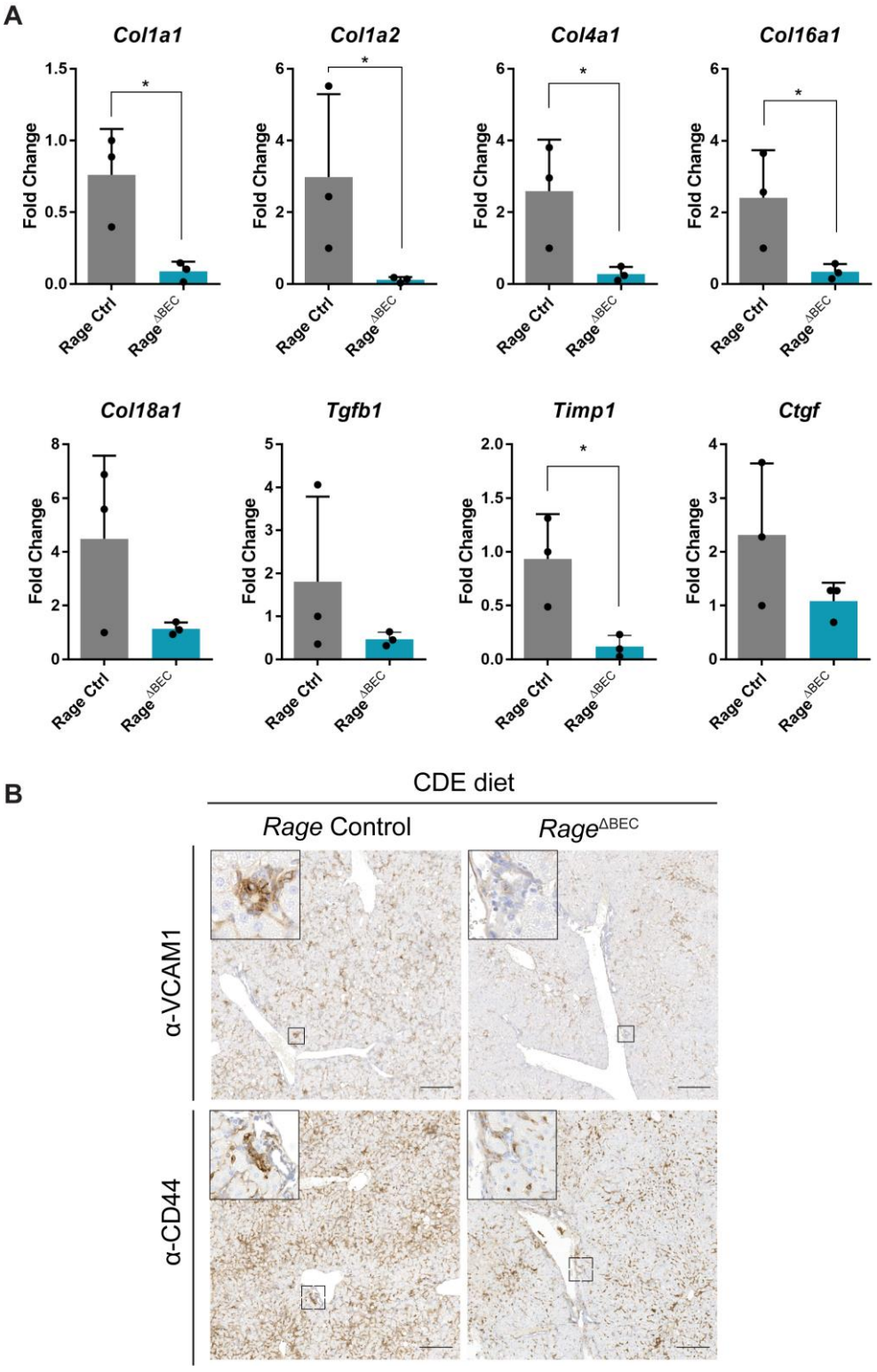


**Figure 3-12. Validation of RNA-seq data obtained from CDE-challenged *Rage* control and knockout mice**.

(A) qPCR analysis of mRNA expression of fibrotic markers, *Col1a1*, *Col1a2*, *Col4a1*, *Col16a1*, *Col18a1*, *Tgfb1*, *Timp1* and *Ctgf* in whole liver tissues of *Rage* control (*Rage*$^{+/\Delta BEC}$) and knockout mice (*Rage*$^{\Delta BEC}$). (B) Representative images of IHC staining of VCAM1 and CD44 on liver tissues of CDE-challenged BEC-specific *Rage* control and *Rage* knockout mice ($n$=3). Data are shown in mean± *s.d*. Two-tailed *t*-test was used for statistical comparison. A $p$-value < 0.05 with 95% confidence interval was considered to be statistically significant (*$p$ < 0.05). Scale bar, 200 μm.

### 3.2.2 BEC-specific RAGE activity is linked to stellate cell activation and fibrosis *in vivo*

Based on the RNA-seq result, the expression of RAGE on BECs is implicated in HSCs activation during cholestasis. To address the potential crosstalk between BECs and HSCs in the context of CDE-induced injury, the liver tissues were stained with markers of HSC activation, including Vimentin and Desmin. Co-IF analysis of tdTom-labelled BECs and markers of HSC activation was performed. In normal diet-treated mice, both HSC markers stained only the endothelial cells surrounding the portal veins and central veins. Upon CDE-induced chronic injury in the liver, the abundance of the Vimentin- and Desmin-positive HSCs expanded abundantly into the liver parenchyma in *Rage*$^{WT}$ and *Rage*$^{+/\Delta BEC}$ mice. Remarkably, ablation of *Rage* in BECs leads to a significant reduction of activated HSCs concomitant with the reduction of tdTom-positive BECs during cholestasis (Figure 3-13). For Vimentin, *Rage*$^{\Delta BEC}$ mice exhibited approximately 2-fold less Vimentin-positive HSC than *Rage*$^{WT}$ and *Rage*$^{+/\Delta BEC}$ mice (20.3 ± 7.31% of *Rage*$^{WT}$; 16.98 ± 5.69% of *Rage*$^{+/\Delta BEC}$; 8.84 ± 5.93% of *Rage*$^{\Delta BEC}$) (Figure 3-13A & B). For Desmin, *Rage*$^{\Delta BEC}$ mice exhibited approximately 4- to 5-fold less Desmin-positive HSC than *Rage*$^{WT}$ and *Rage*$^{+/\Delta BEC}$ mice (6.3 ± 3.99% of *Rage*$^{WT}$; 8.3 ± 3.79% of *Rage*$^{+/\Delta BEC}$; 1.64 ± 0.1% of *Rage*$^{\Delta BEC}$) (Figure 3-13C & D). Of note, tdTom expression and Vimentin or Desmin staining were mutually exclusive but adjacent to each other within the liver parenchyma under conditions of chronic injury.

During chronic injury, reduced turnover of extracellular matrix (ECM) molecules eventually leads to excessive accumulation of collagens, resulting in increased tissue stiffness and subsequent pathogenesis of fibrosis. In light of the RNA-seq data suggesting that fibrosis is dependent on RAGE activity in BECs, Picro-sirius Red staining for collagen fibers on liver tissues in normal diet and CDE diet-treated *Rage*$^{WT}$, *Rage*$^{+/\Delta BEC}$ and *Rage*$^{\Delta BEC}$ was performed, and the percent area of Sirius Red staining was quantified (Figure 3-14A & B). In normal diet-treated mice, Sirius Red stained only the pericytes of the blood vessels, whilst little to no collagen fibers were deposited in the liver parenchyma. CDE diet induced a striking increase of collagen fibers in the livers as shown from the Sirius Red staining. *Rage*$^{WT}$ and *Rage*$^{+/\Delta BEC}$ mice displayed 3.5- and 2.5-fold more collagen staining than *Rage*$^{\Delta BEC}$ respectively (7.43 ± 4.32% of *Rage*$^{WT}$; 5.38 ± 3.92% of *Rage*$^{+/\Delta BEC}$; 2.09 ± 1.54% of *Rage*$^{\Delta BEC}$). In line with the histology staining, histopathological evaluation on Sirius red staining demonstrated that *Rage*$^{WT}$ and *Rage*$^{+/\Delta BEC}$ mice displayed a higher grade of fibrosis, with around 44% and 20% of the mice exhibited bridging fibrosis, respectively. In contrast, ablation of *Rage* in BECs significantly reduced the number of mice (around 8%) which developed bridging fibrosis (Figure 3-14C). Taken together, the RNA-seq data concomitant with histological analyses

revealed that CDE diet-induced hepatic fibrosis is promoted by BECs via RAGE.

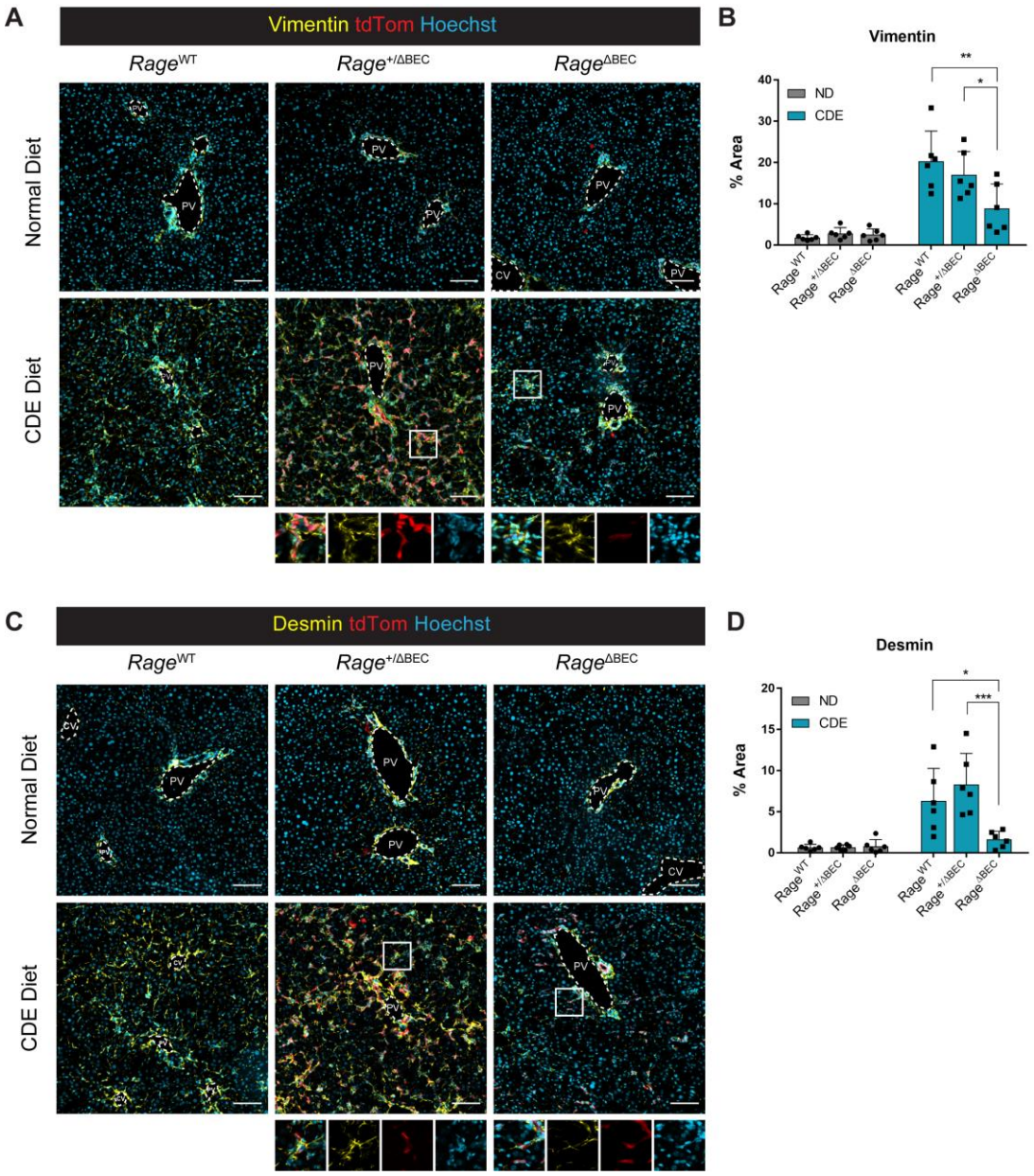


**Figure 3-13. RAGE in BECs contributes to stellate cell activation during cholestatic injury**.

(A) IF staining of stellate cell marker Vimentin and (B) quantification of the percent area of the Vimentin-positive cells. (C) IF staining of stellate cell marker Desmin and (B) quantification of the percent area of the Desmin-positive cells in *Rage*$^{WT}$, *Rage*$^{+/\Delta BEC}$ and *Rage*$^{\Delta BEC}$ mice fed with normal or CDE diet (*n*=6 each). Zoom in images of the cropped areas were shown in split channels. Data are shown in mean± *s.d*. Two-way ANOVA Turkey's multiple comparisons test was used for statistical comparison. A *p*-value < 0.05 with 95% confidence interval was considered to be statistically significant (**p* < 0.05, ***p* < 0.01, ****p* < 0.001). Scale bar, 100 µm. PV, portal vein. CV, central vein.

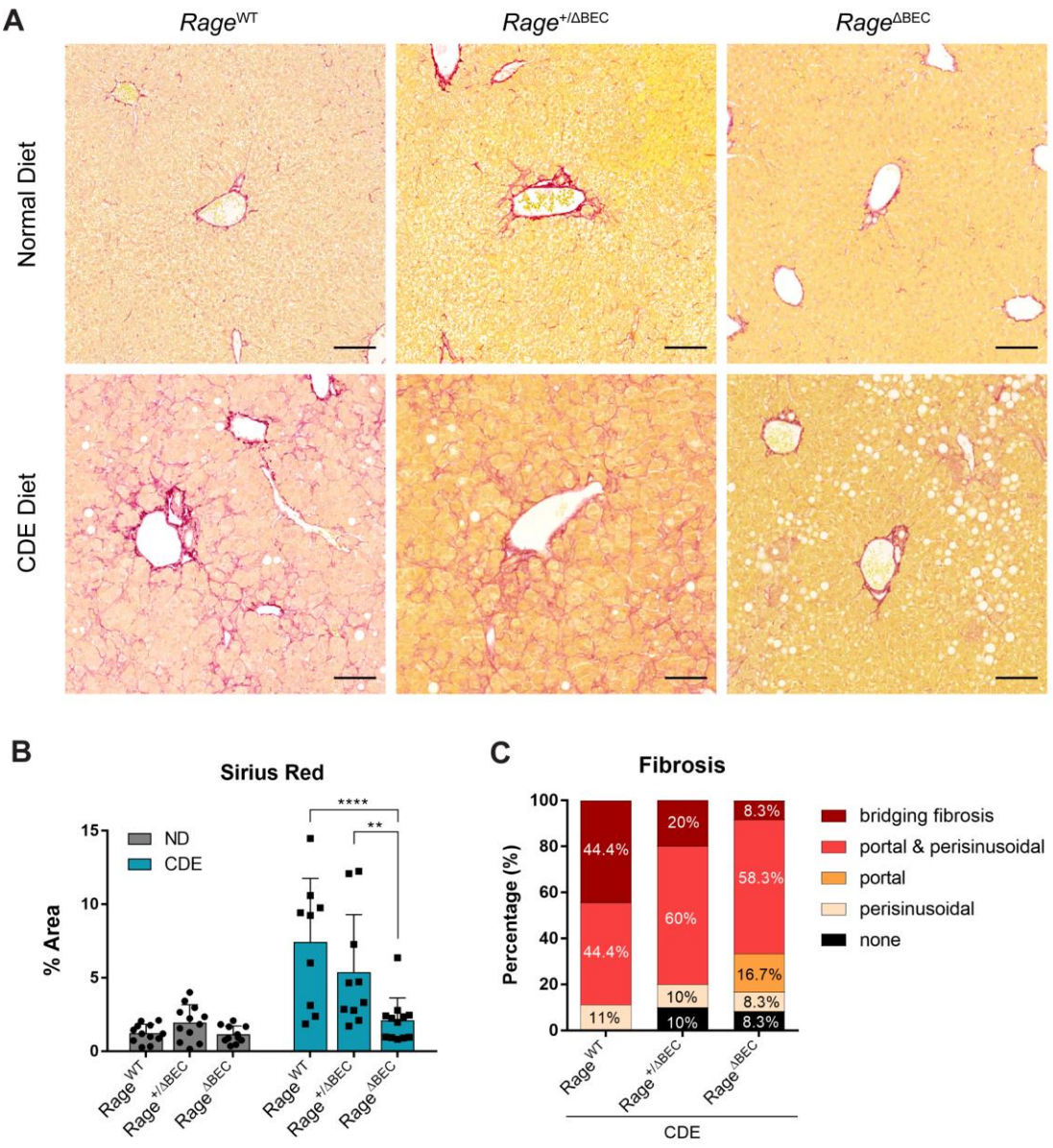


**Figure 3-14. BEC-specific RAGE activity is linked to cholestasis-associated fibrosis.**

(A) Picro Sirius Red staining, (B) Sirius Red staining quantification and (C) histopathological evaluation of fibrosis of *Rage*$^{WT}$, *Rage*$^{+/\Delta BEC}$ and *Rage*$^{\Delta BEC}$ mice fed with normal or CDE diet. ND-treated mice: *Rage*$^{WT}$ ($n$=12), *Rage*$^{+/\Delta BEC}$ ($n$=12), *Rage*$^{\Delta BEC}$ ($n$=11); CDE-treated mice: *Rage*$^{WT}$ ($n$=9), *Rage*$^{+/\Delta BEC}$ ($n$=10), *Rage*$^{\Delta BEC}$ ($n$=12). Data are shown in mean± *s.d.* Two-way ANOVA Turkey's multiple comparisons test was used for statistical comparison. A $p$-value < 0.05 with 95% confidence interval was considered to be statistically significant (**$p$ < 0.01, ****$p$ < 0.0001). Scale bar, 100 µm.

### 3.2.3 BECs activate HSCs in a RAGE-dependent manner via direct or indirect cell contact *in vitro*

Although HSCs were shown to be more activated in *Rage*$^{WT}$ mice when compared to *Rage*$^{\Delta BEC}$ under cholestatic conditions (Figure 3-13), it remains unclear whether BECs have a direct or indirect influence on stellate cells

activation. Therefore, I hypothesized that RAGE activity in BECs is essential for the intercellular communication between BECs and HSCs. To address this question, *Rage* WT or KO BECs were co-cultured directly with mCherry-labelled HSCs for four days to investigate the influence of RAGE on the direct interplay between these two cell types. The co-cultured cells were subjected to flow cytometry analysis to determine the activation status of the HSCs with the myofibroblast marker αSMA. The representative gating strategy showed that the cell debris was excluded based on forward scatter (FSC) and side scatter (SSC), followed by exclusion of cell doublets and dead cells (Figure 3-15A). The single live cells were gated for subsequent analysis based on GFP and mCherry to distinguish between *Rage* WT BEC, *Rage* KO BECs and HSCs (Figure 3-15B). Subsequently, HSCs were gated out for assessing αSMA expression in different conditions (Figure 3-15C & D). As the HSC cell line was generated from $p19^{ARF}$ null mice that underwent spontaneous activation through long-term passaging, this immortalized HSC cell line is considered to be in a pre-activated state. The HSC-alone control was used to determine the threshold of the percentage of αSMA-low or αSMA-high populations. Comparing to HSC-alone control, the proportion of αSMA-high HSCs increased by approximately 15% when the HSCs were co-cultured with *Rage* WT BECs, whereas those which were co-cultured with *Rage* KO BECs increased only by 7%. This suggested that BECs could activate HSCs under the influence of RAGE activity either via direct cell contact and/or soluble factor-mediated paracrine mechanisms.

Stellate cells are also known as fat-storing cell. It is the major cell type in the liver that stored vitamin A (retinol) in lipid droplets at quiescent state. However, these cells lose the retinol depots upon activation and transdifferentiate into fibrogenic myofibroblasts. To investigate whether HSCs can be activated by BECs via paracrine signaling, the conditioned medium produced by BECs was collected and cultured with HSCs. As TGFβ1 is known to be a potent molecule for HSC activation, the HSCs were also treated with recombinant TGFβ1 as a positive control. IF staining of αSMA for actin cytoskeleton were performed to assess the activation status of HSC. Additionally, BODPIY staining for lipid droplets was used as a second read-out for stellate cell activation, as it is more quantifiable to confirm that a given HSC is activated when it loses the vitamin A-containing lipid droplets (Figure 3-16A). The BODIPY lipid droplets were counted and quantified (Figure 3-16B). Furthermore, qPCR analysis was performed to examine mRNA levels of activated HSC markers, including *Acta2* and *Col1a1*, in HSC under the untreated and treated conditions (Figure 3-16C). In untreated control, HSCs expressed low level of αSMA and presented a significant number of BODIPY-positive lipid droplets, as well as relatively low *Acta2* and *Col1a1* mRNA expressions. When HSCs were treated with recombinant TGFB1 or BEC *Rage* WT conditioned medium (CM), the HSCs expressed higher αSMA level with increased abundance of visible actin

filaments. The number of BODIPY-positive lipid droplets were significantly reduced concomitantly with relatively higher *Acta2* and *Col1a1* mRNA expressions. In contrast, when HSCs were treated with CM collected from *Rage* KO BECs, the HSCs expressed comparable αSMA levels and more BODIPY-positive lipid droplets as in the untreated control, as well as relatively low *Acta2* and *Col1a1* mRNA expressions. Collectively, these data demonstrated that RAGE-dependent secretory factor(s) from BEC are present to induce HSC activate via paracrine mechanism.

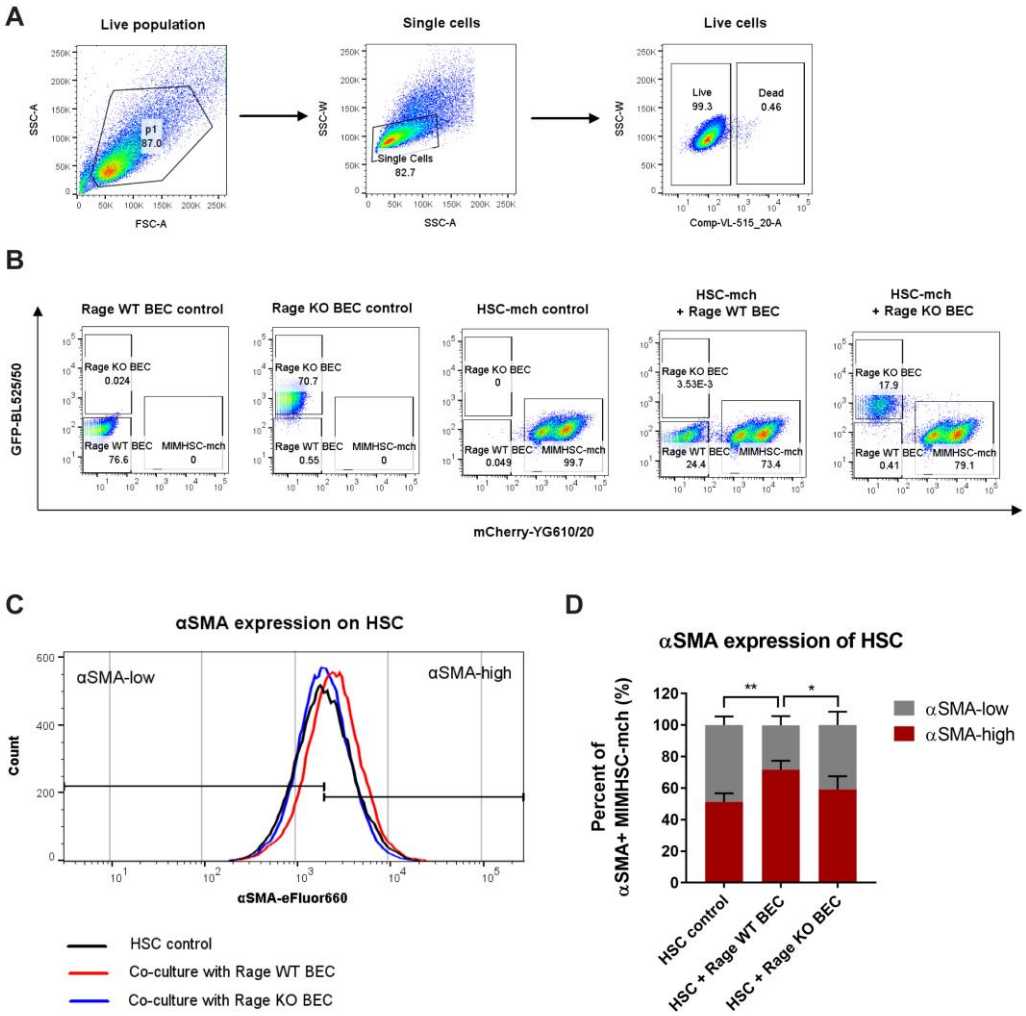


**Figure 3-15. BECs activate stellate cells in a RAGE-dependent manner**.

(A) Representative gating strategy for the live population, followed by single cell population and live cells that were negatively selective by LIVE/DEAD™ Fixable Aqua Dead Cell Stain. (B) Flow cytometry analysis of GFP and/or mCherry expressions in the abovementioned gated populations in conditions of single or co-cultured *Rage* wildtype BECs, *Rage* knockout BECs and mCherry-labelled HSCs. (C) Histogram plot of eFluor660-conjugated αSMA expression in HSC-mch and (D) quantification of the percent of αSMA-low and αSMA-high HSC-mch when cultured alone or co-culture with *Rage* WT or KO BECs. WT, wildtype; KO, knockout; HSC-mch, mCherry-labelled HSC. Two-way ANOVA Turkey's multiple comparisons test was used for statistical comparison. A *p*-value < 0.05 with 95% confidence interval was considered to be statistically significant (**p* < 0.05, ***p* < 0.01).

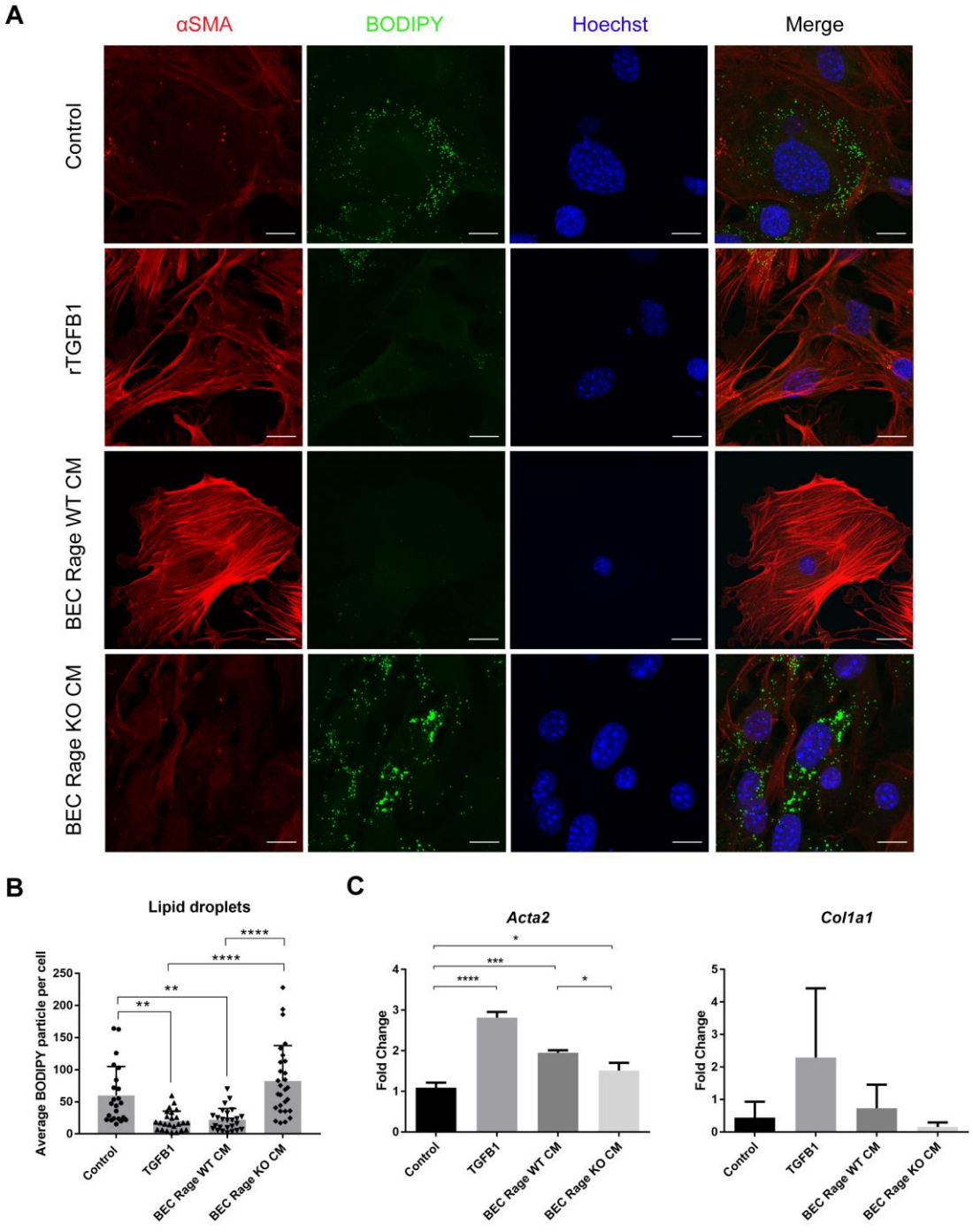


**Figure 3-16. BECs induce HSC activation in *trans* in RAGE-dependent manner**.

(A) IF staining of α-SMA for actin cytoskeleton and BODIPY for retinol-containing lipid droplets in HSCs treated with PBS control, 5 ng/ml rTGFB1, or conditioned medium (CM) collected from *Rage* WT or *Rage* KO BECs for 96 hours. (B) Quantification of the number of BODIPY-positive lipid droplet per cell in treated HSCs. (C) qPCR analysis of mRNA expression of *Acta2* or *Col1a1* in HSCs treated for 48 hours. Scale bar, 20 μm. Data are shown in mean± *s.d*. Two-way ANOVA Turkey's multiple comparisons test was used for statistical comparison. A *p*-value < 0.05 with 95% confidence interval was considered to be statistically significant (**p* < 0.05, ***p* < 0.01, ****p* < 0.001, *****p* < 0.0001).

### 3.2.4 BEC-derived JAG1 signals HSC activation in *trans*

Abovementioned results indicate that BECs secrete soluble factors in a RAGE-dependent manner, thus inducing HSC activation. To identify the paracrine signaling molecules from BECs that potentially activate HSCs, the conditioned medium was analyzed by mass spectrometry. A number of secretory factors that are differentially expressed between *Rage* WT and KO BEC CM were identified and were visualized in a volcano plot (Figure 3-17A). A p-adjusted value at 0.05 was used as a threshold cut-off to identify secretory factors that are significantly and differentially expressed. Out of 21 differentially expressed secretory factors, some were either unassociated with liver diseases or are listed as hypothetical proteins. Interestingly, NCAM1 and GOLM1, which were found to be mainly expressed in epithelial cells of bile duct in liver [152, 153], were downregulated in the BEC *Rage* KO CM. Of note, JAG1, an essential component in the evolutionarily conserved Notch signaling pathway for developmental and cellular processes, was also found to be downregulated in the secretome of BEC upon *Rage* deletion. JAG1 is known to be an essential niche factor for the development of biliary tree in fetal liver. In terms of pathological consequences, mutation in JAG1 causes Alagille syndrome characterized by intrahepatic bile duct paucity in infants and children. Aberrant Jag/Notch signaling is also implicated in fibrosis, HCC or ICC [154].

As JAG1 is directly linked to the pathogenesis of biliary diseases and fibrosis, it appeared to be an ideal candidate secretory protein in BECs in this current DR-associated fibrosis study. To validate the mass spectrometry analysis result, ELISA measurement of secretory JAG1 in the corresponding BEC conditioned medium, and qPCR analysis of mRNA expression of *Jag1* in BEC *Rage* WT and KO cells were performed. Indeed, the concentration of secretory JAG1 in BEC-derived conditioned medium (Figure 3-17B) and intrinsic mRNA expression of *Jag1* were significantly downregulated in BEC upon the deletion of *Rage* (Figure 3-17C). Furthermore, when HSCs were treated with recombinant JAG1 *in vitro*, as expected, JAG1 induces mRNA expressions of the Notch downstream target genes, including *Hes1*, *Hey1* and *Hey2*, concomitant with an induction of αSMA expression and loss of BODIPY-positive lipid droplets in HSCs (Figure 3-17D & E). This suggests that JAG1 is indeed a RAGE-dependent factor derived from BECs that induces Notch signaling and activates HSC myofibroblastic differentiation.

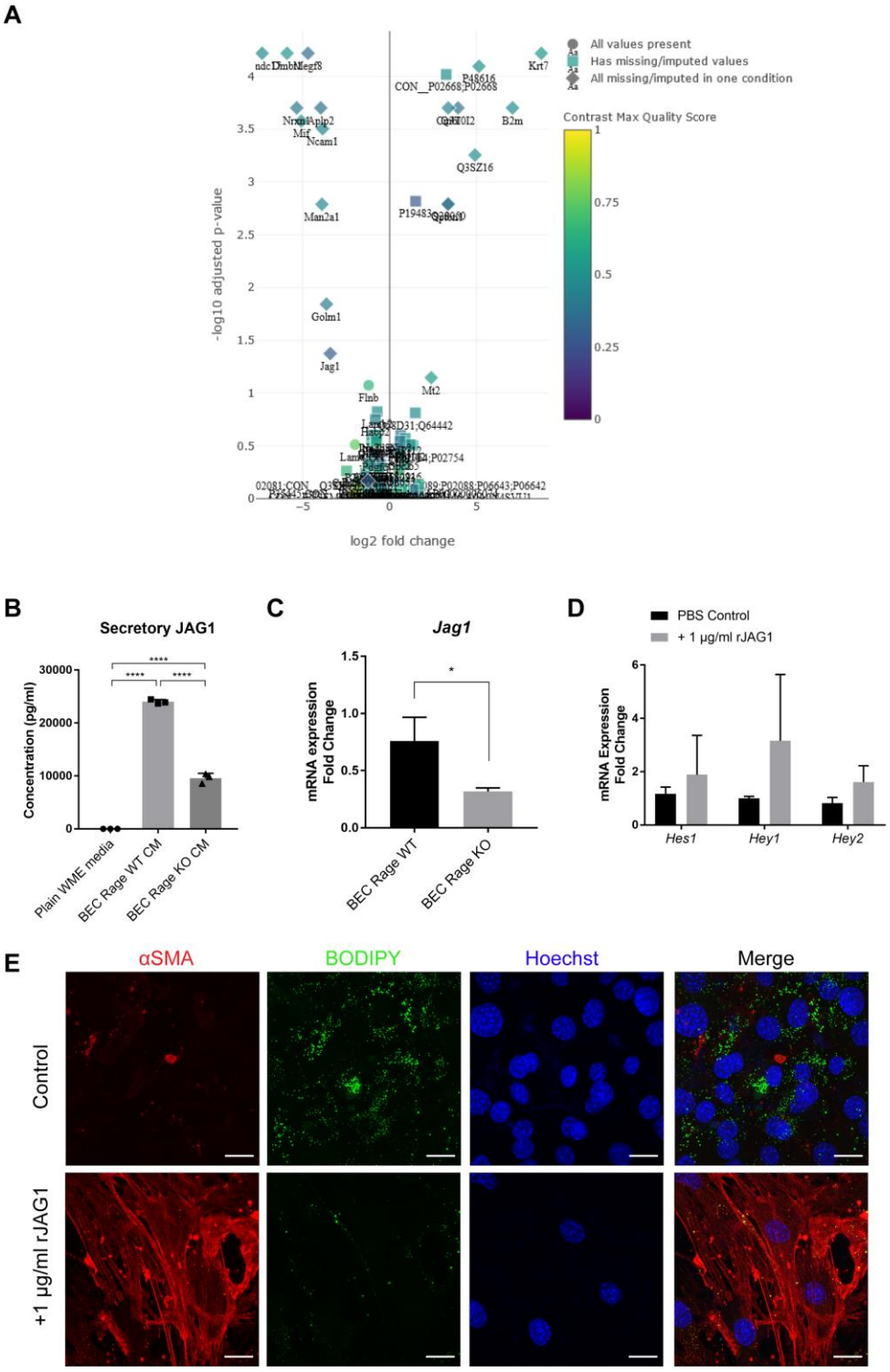


**Figure 3-17. BEC-derived secretory JAG ligands activate Notch signaling in HSCs**.

(A) Mass spectrometry analysis of the differential secretory proteomic profile between the conditioned medium of *Rage* WT and KO BECs. (B) ELISA measurement of the concentration of secretory JAG1 in plain William's E (WME) media, and BEC *Rage* WT and KO conditioned medium (CM). (C) qPCR analysis of endogenous mRNA expression of *Jag1* in *Rage* WT and KO BECs. (D) qPCR analysis of mRNA expressions of Notch genes, *Hes1*, *Hey1* and *Hey2* in HSCs treated with PBS control or 1 µg/ml of recombinant JAG1. (E) IF staining of αSMA and BODIPY in HSCs treated with PBS control or 1 µg/ml of recombinant JAG1. Scale bar, 20 µm. Data are shown in mean± *s.d*. Two-tailed *t*-test was used for statistical comparison.

Next, IHC staining of HES1 as a read-out for Notch activation was performed on liver tissues to determine whether Notch signaling is activated in the CDE diet injury model (Figure 3-18). As expected, HES1 was mainly expressed in BECs surrounding the portal vein in normal diet-treated mice since Notch signaling is crucial for the cellular process of the ductular cells. Under CDE diet regime, HES1 expression was substantially increased in CDE-diet induced cholestatic *Rage*$^{WT}$ and *Rage*$^{+/\Delta BEC}$ mice. In contrast, HES1 expression is significantly reduced in *Rage*$^{\Delta BEC}$ mice, suggesting Notch signaling is inhibited upon deletion of *Rage* in BEC. Of note, HES1 is not only expressed in the periportal BECs, but also in the stromal cells (potentially to be myofibroblasts and immune cells) in the disease state. Taken together, I propose that BEC-derived secretory Jag are released in a RAGE-dependent manner, and activates HSC via Notch signaling in *trans* upon chronic injury, thus promoting fibrosis during CDE-induced cholestasis.

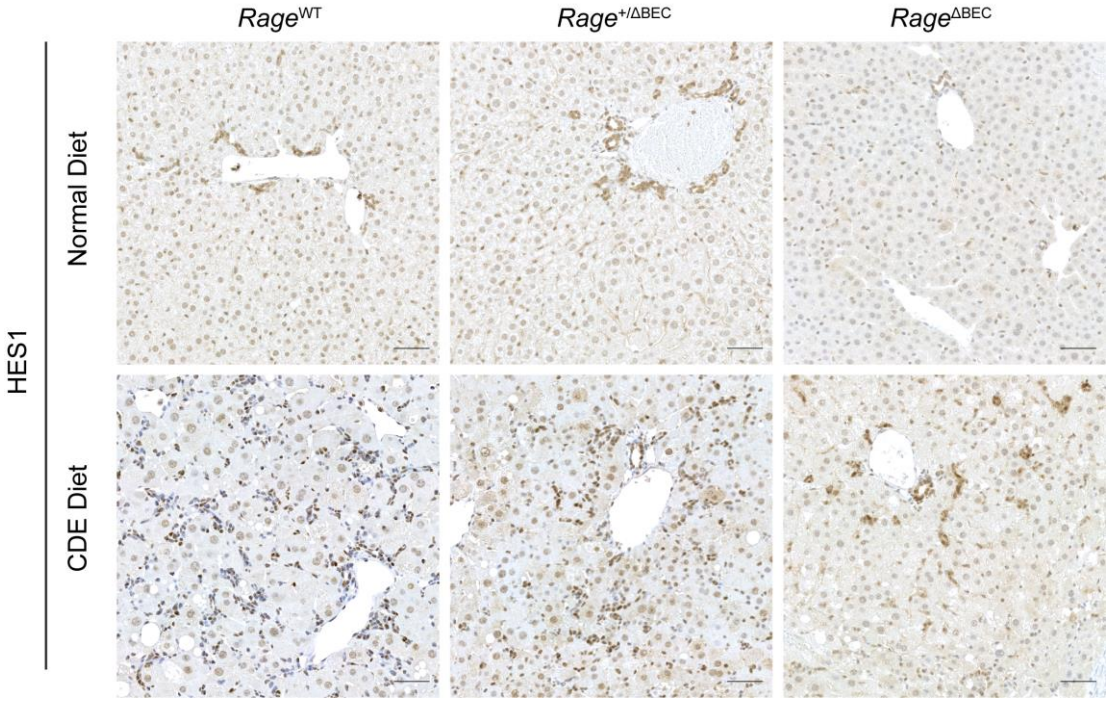


**Figure 3-18. BEC-specific RAGE activates Notch signaling in cholestatic mice**.

Representative images showing IHC staining of HES1 in *Rage*$^{WT}$, *Rage*$^{+/\Delta BEC}$ and *Rage*$^{\Delta BEC}$ mice fed with normal or CDE diet. The staining was repeated on liver tissues from three mice per group. Scale bar, 50 µm.

# Chapter 4
## Discussion

## Section 4.1 The functional role of RAGE in chronic liver injury and cholestasis

RAGE is a pattern recognition receptor commonly involved in inflammation-associated diseases, including atherosclerosis, neurodegenerative diseases, diabetes and cancer. Although it is merely expressed in liver cells and tissues under physiological conditions, multiple studies have suggested that RAGE is involved in inflammation-associated liver injuries and diseases [111, 155-157]. More specifically, it was proposed that RAGE is required to mediate HMGB1-induced DR and tumor progression in autophagy-deficient and MDR2-deficient tumor models [97, 111]. Furthermore, although Pusterla and colleagues showed that RAGE is not involved in immune cell recruitment in the biliary disease *Mdr2*-knockout model [111], on the contrary, it was suggested that RAGE is required for HMGB1-mediated neutrophil migration to necrotic tissues in acetaminophen model [156]. This suggested that RAGE may play a pivotal role in immunomodulation during liver injury, but it is rather context-dependent. The upstream stimuli and the underlying causes of the diseases may largely play a role in regulating the signal transduced via RAGE. Nevertheless, none of these studies conclusively clarify the identity of the cell type mediating RAGE-dependent DR, nor the molecular mechanisms of RAGE-mediated fibrosis.

In this dissertation, I have employed a well-established diet-induced cholestatic injury mouse model that mirrors cholangiopathies-associated DR and fibrosis. Combining the animal approach, whole transcriptomic analysis and *in vitro* studies, I have uncovered the specific pathophysiological role of RAGE on BEC during cholestatic injury from two perspectives: (1) the presence and expression of RAGE on BECs is required for DR but not necessary for the inflammatory response, and (2) BEC-specific RAGE activity fosters a pro-fibrotic milieu, and contributes to stellate cell activation and fibrosis in a paracrine manner.

### 4.1.1 RAGE is predominantly expressed in activated BECs and influences BECs expanding capacity *in vitro*

Previous studies have proposed that RAGE is expressed on hepatocytes and stellate cells in the liver [83, 158], suggesting the role of RAGE in the malignant transformation in these cell types during liver injury. However, in this dissertation, by comparing the mRNA expression of primary hepatocytes, BECs and stellate cells using qPCR and *in situ* hybridization, I have shown for the first time that RAGE is merely expressed in hepatocytes and other cell types, but is predominantly expressed in BECs during CDE-diet induced cholestatic injury. This suggests that RAGE may have a specific regulatory role on BECs but not in other cell types during chronic liver injury.

RAGE signaling axis has been demonstrated to regulate cell proliferation in various cell types, including HCC cells [159], pancreatic cancer cells [160], prostate cancer cell [161] and others. Although it was proposed that RAGE is a key regulator of DR, it remains unclear whether it intrinsically regulates the proliferation and expansion capacity of BECs. Due to the limitation of monolayer 2D culture conditions, I have employed the organoid culture to model and investigate the influence of RAGE in BEC proliferation in a 3D culture environment. The organoid culture is a system either originating from pluripotent stem cells or adult progenitor cells, with the capacity to self-organize into a complex that recapitulate the physiology and pathogenesis of the respective cell types or organs [162, 163]. It is a powerful tool to overcome the limitations of many *in vitro* 2D cell culture systems, including preserving the cell heterogeneity, tissue structure and gene expression of the organoid culture, thus it is often utilized to model organogenesis, as well as cellular and mechanical communications [163]. In conventional 2D culture, I did not observe a significant difference in the proliferation rate between *Rage* WT and KO BECs (data not shown). However, by utilizing the 3D organoid culture with matrigel matrix that mimics an *in vivo* tissue microenvironment, I found that the ablation of *Rage* in BECs attenuates the formation and proliferation of the bile duct organoids. In particular, *Rage* WT BECs were able to form larger organoids with bigger lumens when compared to *Rage* KO BECs after eight days of initiating the organoid culture, suggesting that RAGE regulates the expansion capacity of BECs, and potentially their ability to maintain their architectures. This implies that RAGE may support BEC expansion and tubular structure formation of ductular response that was observed during chronic injury *in vivo*.

The Hippo pathway is an important regulator of cell fate, organ size and homeostasis. Emerging studies have shown the profound significance of this pathway also in liver regeneration [31, 164, 165] and diseases [30, 166, 167]. Previous studies reported that Yes-associated protein (YAP), the downstream effector of the Hippo pathway, is enriched in the biliary compartment and favors DR upon liver injury [30, 31], whereas activation of YAP in mature hepatocytes would lead to their de-differentiation into ductal- or progenitor-like cells [31]. Interestingly, in this current CDE diet-induced cholestasis model, a robust YAP expression and activity in both hepatocytes and BECs in CDE-challenged wild type mice was observed (data not shown). Deletion of RAGE in BECs completely abolished YAP expression in hepatocytes despite the challenge of the mice by CDE diet. Furthermore, RNA-seq analysis using the *in vitro* established BEC *Rage* WT and KO cell lines was also performed, with Hippo pathway identified as one the most significantly enriched pathway in the whole transcriptomic analysis (data not shown). This preliminary result suggests that RAGE might be a mediator for YAP activation in both BECs and hepatocytes during cholestasis. BEC-specific RAGE might mediate YAP inducers through paracrine signaling within the local microenvironment and facilitates

dedifferentiation of hepatocytes into BECs. At the same time, RAGE-mediated YAP activation in BECs might also confer the increased proliferative capacity of the BEC pool, such that a more robust DR phenotype in the RAGE wildtype mice was observed upon liver injury. However, how RAGE modulate YAP signaling in BEC remains elusive. The homolog of Drosophila Salvador WW45, is an adaptor for the Hippo kinase and plays a crucial role in Hippo-dependent cell proliferation and differentiation. Two studies have demonstrated that ablation of WW45 leads to hyper-proliferation and immature differentiation of the epithelial cells [32, 168]. More specifically in DDC-induced liver injury, ablation of WW45 increased the abundance of YAP and induced its activation in BECs, thereby results in increase BEC proliferation and liver overgrowth [32]. Furthermore, the loss of the serine/threonine protein kinases MST1 and MST2, two key upstream regulators of YAP, promotes BEC proliferation [169]. This suggests that the Hippo-Salvador signaling axis is crucial in regulating the activation of YAP, thus controlling BEC proliferation and liver growth. Nevertheless, it is well-known that YAP is a downstream effector of the G-protein-coupled receptors (GPCRs) [170]. Herein, I propose that RAGE might regulate BEC proliferation via crosstalk with GPCR signaling and modulates YAP activation, but this would require further investigation.

### 4.1.2 BEC-specific RAGE activity is not involved in immune cell recruitment during cholestasis

RAGE binds to a diverse range of endogenous and exogenous inflammation-associated ligands including AGEs, HMGB1, S100 proteins and others, and mediate a broad range of cellular effects that sustains inflammation. For instance, HMGB1 is a prevalent pro-inflammatory cytokine that is passively released by dying cells and functions as ‘danger signals’ that recruits immune cells and stimulates pro-inflammatory cascades. It was suggested that HMGB1 activates the pro-inflammatory features of various cell type including monocytes, neutrophils, endothelial cells and cancer cells via binding to RAGE [171, 172]. RAGE promotes immune cell recruitment upon binding with the heterodimeric ligand S100A8/A9 in various cancer-associated models, such as TPA-induced skin carcinogenesis and colitis-associated colorectal cancer [102, 173]. In the perspective of liver injury, it is evident that RAGE is the receptor for HMGB1 and promotes neutrophil infiltration to necrotic tissues in acetaminophen-induced injury mouse model [156]. However, ablation of *Rage* in the classical *Mdr2*-knockout cholestasis-associated and inflammation-driven HCC model [111], or deletion of RAGE ligand S100A9 in DEN-induced HCC model has no major impact on immune cell recruitment during pre-malignant and malignant stage [104].

In this dissertation, the aspect of immune cell recruitment has been investigated in the context of cholestasis-induced injury and inflammation. All in all, the mice

administrated with three weeks CDE diet displayed induced lobular and portal inflammation as shown by the H&E staining and histopathological evaluation, as well as an elevated hepatic injury serum markers including AST and ALT; however, ablation of RAGE on BEC in the CDE-treated mice does not affect the degree of inflammation. Immune cell infiltrations were evaluated by IHC staining of CD11b for neutrophils, F4/80 for macrophage and CLEC4F for Kupffer cells. Although inflammation caused by CDE diet induced abundant infiltration of these immune cells, there was no significant difference between *Rage*$^{WT}$, *Rage*$^{+/\Delta BEC}$ and *Rage*$^{\Delta BEC}$ mice during CDE-induced injury. In line with the previous results in the *Mdr2*-knockout model, which is also a cholestasis-associated mouse model, I hereby further confirmed and demonstrated that RAGE, despite its predominant expression on BEC, is not involved in inflammation and immune cell recruitment under cholestasis condition as shown from the CDE diet mouse model.

### 4.1.3 BEC-specific RAGE activity does not contribute to CDE-induced steatosis

RAGE may be involved in obesity [89, 174] as well as aging-associated hepatic steatosis [157], which are the major clinical feature of NAFLD. NAFLD is a global health burden and has become one of the most common cause of chronic liver disease nowadays. It is a liver disease referred to the presence of hepatic steatosis, but not associated with heavy alcohol consumption or other underlying cause of liver disease. Apart from obesity and insulin resistance, dietary intake with high sugar, fructose, saturated fat and cholesterol contents are the major risk factors of NAFLD. Of note, saturated fatty acids from these diets are the major sources of the RAGE ligand, AGEs. In a study of aging-associated NAFLD, AGEs and RAGE were found to be upregulated in the aged mice (20-month-old) when compared to the young mice (3-month-old). The upregulated AGE/RAGE axis suppressed hepatic PPARα activity for mitochondrial free fatty acid *β*-oxidation, thus resulting in hepatic triglyceride accumulation, accompanied with hyperglycemia and insulin resistance in aged mice [157]. Likewise, other reports also showed that RAGE plays a regulatory role in metabolic responses in high fat diet-induced obesity and insulin resistance [88, 89].

In this dissertation, I have employed the CDE dietary model involving the deficiency of choline in the food intake for the mice. Under physiological conditions, choline is obtained via food intake and functions as the major source for metabolism and the component of phospholipids of the cell membranes. Deficiency in choline thereby results in the decrease of phosphatidylcholine, which is crucial for the structure of cell membrane and the formation of the very low-density lipoprotein (VLDL) produced by hepatocytes to export triglycerides. Consequently, this results in fat accumulation and damage in the hepatocytes

[175, 176]. Therefore, CDE diet is a relevant model for the investigation on steatosis in NAFLD. Predominantly, CDE diet is utilized as a model for cholestasis and DR. Interestingly, ductular reaction is positively correlated with the disease stage of NAFLD [9]. As RAGE is playing a regulatory role in steatosis and BEC remodeling in DR, it is interesting to elucidate whether BEC-specific RAGE activity is the cause of fat accumulation in the CDE model. Indeed, steatosis is induced in the hepatic parenchyma of the mice treated with CDE as shown by the Oil Red O staining for neutral triglycerides and histopathological evaluation. However, there is no significant difference in the degree of steatosis between the *Rage*$^{WT}$, *Rage*$^{+/\Delta BEC}$ and *Rage*$^{\Delta BEC}$ mice, suggesting that CDE diet-induced triglyceride accumulation occurs independent of RAGE activity in BEC. In line with the results of the CDE diet model, my preliminary data from a western diet model study, which is a classical NASH model, also revealed that lipid accumulation is not associated with BEC-specific RAGE activity (data not shown).

### 4.1.4 BEC-specific RAGE activity is indispensable for DR *in vivo*

RAGE is a master regulator that mediates DR in a chronic inflammation-associated HCC model either in a cell-autonomous, or via a more indirect manner [111]. DR is observed among a broad etiologies of liver diseases. It is served as an escape mechanism to compensate for the function loss of the bile ducts upon chronic injuries, especially in the occasions of cholestasis. In a study using DDC diet-induced liver injury mouse model with *Rage* deletion, in combination with *in vitro* model using RAGE-specific blocking antibodies, the HMGB1/RAGE axis was found to be the main driver of DAMP-induced DR [96]. Other studies also reported that HMGB1/RAGE signaling modulates DR that may contribute to the tumor microenvironment in enhancing tumorigenesis in autophagy-deficient livers [97, 177]. Nevertheless, none of these studies have conclusive results to show which specific cell type is predominantly regulated by RAGE in ductular responses during the liver pathogenesis. As BECs represent the epithelial cell type that lined the bile duct, and in this current study, *Rage* was found to be predominantly expressed in BECs but not in other hepatic cell types, I hypothesized that RAGE is a key regulator for BEC expansion and contributes to the DR phenotype in liver diseases. Here, I have utilized a lineage tracing approach and delete *Rage* in BEC specifically to investigate whether its growth is under the regulation of RAGE. Indeed, CDE diet induced substantial DR as shown by BEC markers CK19 and A6; in contrast, DR was completely abrogated upon deletion of *Rage* in BECs. In line with the above-mentioned results in the *in vitro* organoid model study, I have demonstrated the novel and unique role of RAGE on BEC expansions also in an animal model. BECs are severely compromised in their capability to expand into the liver parenchyma upon deletion of *Rage* under the condition of CDE-

induced injury, demonstrating that BEC-specific RAGE activity is indispensable for DR.

The functional role and impact of DR in liver diseases have not been clearly defined. Although it was postulated that DR occurs to compensate for the functional loss of biliary ducts and to regenerate liver during injury, many other studies have also reported their adverse impact on liver diseases progression. Apparently, DR mediates liver regeneration only when hepatocyte replication is severely impaired or undergoing senescence [26]; otherwise, it is evident that DR has a detrimental impact on the pathogenesis of liver diseases [60, 62]. Hepatocytes are known the be the primary source for liver regeneration in various mouse models; however, as the CDE diet model does neither provoke hepatocyte senescence nor impair hepatocyte replication efficiently, thus it is not an ideal model to investigate the functional role of DR relevant to the condition of hepatocellular senescence. Indeed, in line with previous study utilizing also the Hnf1b-Cre lineage tracing mouse line [27], the Hnf1b-positive BECs in our current study merely give rise to new hepatocytes upon CDE-induced cholestasis, suggesting that BEC-mediated DR does not contribute to liver regeneration, irrespective of the presence of RAGE on BECs. Without appropriate tools and techniques, it remained obscure speculating about the specific function of the increased branching of DR during chronic injury.

Until recent years, the advancement in multidimensional intravital imaging technologies have provided a new platform and approach to study the structural and functional dynamics in the liver of mouse models. As DR suggested to function as a compensatory mechanism of the ducts, it was proposed that the increased number of BECs relates to the bile excretion during injury conditions. Bile is synthesized in the hepatocytes and secreted into the bile canaliculi that is directly connected with the bile duct. To examine the bile flow and transport kinetics, the synthetic fluorescent-labeled bile analog, cholyl-lysyl-fluorescein (CLF), can be injected into the mice intravenously and imaged with fluorescence microscopy simultaneously (Figure 4-1) [178]. When the CLF reaches the liver, it is first rapidly taken up by the sinusoidal blood, followed by influx into the hepatocytes, then into the bile canaliculi, and eventually into the bile ducts. In a study utilizing DDC diet-induced cholestasis or TAA-induced non-cholestasis associated fibrosis, Kamimoto and colleagues have utilized this state-of-the-art intravital imaging method to examine the functional and structural change in the biliary network [135]. The authors revealed that hepatocellular injury caused by DDC diet or TTA administration leads to the collapse of bile canaliculi irrespective of the cholestatic conditions, followed by induction of DR. Though hepatocytes were detached from the bile canaliculi networks due to parenchymal injury, they re-established connection with the newly formed bile ducts, [135]. The authors suggested that DR occurs to restore the loss of functional bile excretion channels; nevertheless, the CLF uptake

kinetics was not quantified and compared between the physiological and cholestatic condition, therefore it cannot be fully stated that the bile excretion was rescued by the neogenesis of the ductular network. It remains elusive how the constructions of these biliary structures were regulated under injury conditions.

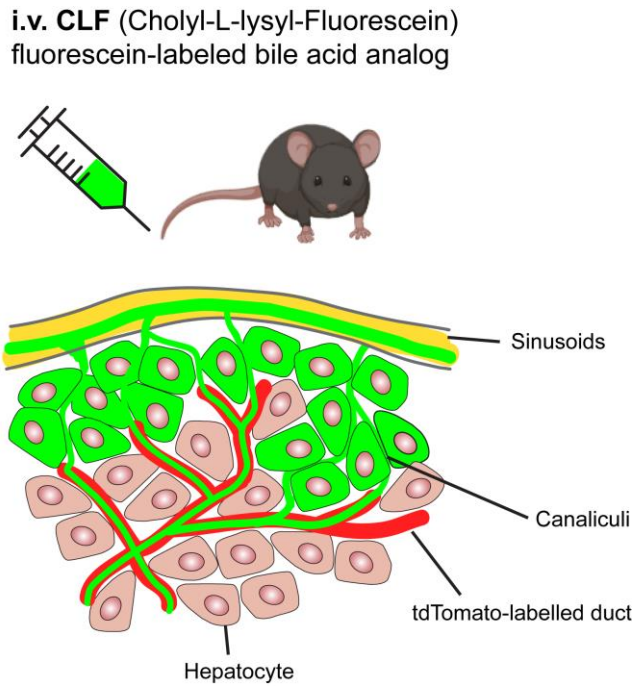


**Figure 4-1. Schematic diagram of the cholyl-lysyl-fluorescein uptake kinetics to trace bile acid transport via intravital imaging**.

The synthetic fluorescent-labeled bile analog, cholyl-lysyl-fluorescein (CLF), is injected into the mice via tail vein injection. The CLF is first taken up by the sinusoidal blood, followed by the hepatocytes, bile canaliculi, and then eventually transported out of the live via the bile duct. i.v., intravenous.

In this dissertation, I have already demonstrated that the ductular network was blunted upon the deletion of *Rage* in BECs, signifying a regulatory role of RAGE in the functional and structural dynamics of the ducts under CDE diet-induced cholestatic condition. To investigate further into the functional impact of RAGE in bile excretion based on Kamimoto's experimental study, our group has established collaboration with Dr. Fabian Geisler (Klinik und Poliklinik für Innere Medizin II, TUM), Dr. Jan Hengtsler (Systems toxicology, IfADo) and Dr. Nachiket Vartak (Systems toxicology, IfADo). In this on-going investigation, my results as well as additional data from this group has shed light on the regulatory mechanism of RAGE on DR in bile flow [179]. We utilized similar intravital imaging method to examine the bile flow. CDE diet was used as our cholestatic injury model and the *Hnf1b*-Cre mice was used for lineage tracing of the ducts. Similarly, *Rage* was deleted in the HNF1B-positive BECs as described in this dissertation. As expected, upon CDE diet treatment, the bile canaliculi were drastically destroyed and fragmented regardless of the presence or absence of

RAGE in BECs, even though DR was blunted in *Rage*$^{\Delta BEC}$ mice. The uptake kinetics of CLF was severely disrupted and these bile acid analogues tended to retain in the hepatocytes in these mice in the CDE-challenged wildtype mice. Surprisingly, although the loss of RAGE on BEC blunted DR, it completely reversed the severely compromised CLF uptake kinetics in cholestatic condition and displayed comparable normal kinetics as shown in normal untreated mice. Our results fully illustrated the dynamic changes of bile transport kinetics in the mice under both physiological and cholestatic conditions. Most importantly, it was evident that RAGE-dependent DR is required to sustain cholestasis, thus it is detrimental to the health status of the mice during injury. In contrast, mice lacking RAGE on BECs showed less DR, but surprisingly more efficient bile transport, thus less accumulation of bile in the liver, implying that deletion of RAGE rescues the mice from cholestatic injury. Previous studies have proposed that the newly formed ducts from DR function as an escape route of the accumulated bile in the liver. However, our latest results have provided a counter-argument to this hypothesis. Although DR can function as an excretion channel for the bile, one cannot eliminate the possibility that bile excreting into these channels might in turn facilitate the crosstalk between BECs with other cell types in the damaged tissue microenvironment in a RAGE-dependent manner, such that the injury is amplified.

## Section 4.2 The functional role of RAGE in cholestasis-associated fibrosis

Cholestasis is a chronic liver disease characterized by obstruction of bile flow and bile acid accumulation. In cholangiopathies, the increased number of proliferating small bile duct referred to as DR, is positively correlated with diseases stage and the degree of fibrosis. Liver fibrosis is characterized by HSC activation and extracellular matrix deposition upon persistent injury and inflammation. The importance of HSC activation for the progression of liver diseases is well recognized [43]. Multiple reports suggested that the paracrine crosstalk between BECs and HSC or portal fibroblasts contributes to fibrosis under cholestatic conditions. Therefore, the link between DR and fibrosis has been investigated by both *in vitro* and *in vivo* approaches in this dissertation. A better understanding of the underlying mechanisms controlling the interaction between BECs and HSCs would open a door in the development of novel therapies to treat fibrosis. In this section, the potential role of RAGE on BEC in cholestasis-associated fibrosis, and the interplay between BECs and HSCs will be discussed.

### 4.2.1 Ablation of RAGE ameliorated fibrosis in cholestasis-associated injury by modulating ECM organization

In light of the strong association between DRs and stages of fibrosis in various etiologies of human liver diseases [122, 131, 180, 181], and my findings of the functional role of RAGE in BEC expansion, I hypothesized that BECs might contribute to fibrosis in a RAGE-dependent manner, and in particular via RAGE activity on BECs. Indeed, in this current study, I have observed a more robust DR concomitantly with a more aggressive fibrotic phenotype in the CDE diet-challenged mice. Most importantly, I have shown that deletion of *Rage* in BEC solely diminish the severity of fibrosis. By bulk RNA-seq analysis of the isolated BECs from the CDE-challenged *Rage* control (*Rage*$^{+/\Delta BEC}$) and *Rage* knockout (*Rage*$^{\Delta BEC}$) mice, I have uncovered unprecedented RAGE-regulated gene expression patterns and pathways specifically in BECs. Of note, BEC-specific RAGE expression is closely associated with HSC activation, hepatic fibrosis, extracellular matrix (ECM) organization and ECM-receptor interaction pathways, accompanied with differential gene expressions in classical fibrotic markers and ECM-associated genes. These results signified the role of BEC-specific RAGE expression in mediating fibrosis in the context of CDE diet-induced cholestasis. Several pathways might be involved RAGE-mediated fibrotic responses, which would be discussed as follows.

### 4.2.2 RAGE on BECs does not contribute to TGFβ1-associated fibrosis

Transforming growth factor beta (TGFβ) family members play a pivotal role in fibrosis. They mediate epithelial-mesenchymal transition and foster the activation of HSCs directly or indirectly, resulting in enhanced synthesis of matrix proteins as well as the upregulation of the inhibitors for matrix degradation, thus favoring a pro-fibrotic milieu [182]. It was suggested that BECs are the source of transforming growth factor beta (TGFβ) in the 2-acetylaminofluorene (AAF)/carbon tetrachloride ($CCl_4$) chronic injury models, and triggered the fibroblasts to get transformed into myofibroblastic HSCs in injured liver [183]. In line with this earlier report, RNA-seq results described in this dissertation demonstrated that the gene expression of *Tgfb1*, accompanied by its key mediators, *Ltbp1* and *Timp1*, were downregulated in the isolated *Rage*-knockout BECs when compared to *Rage* control. To be more specific, LTBP1 is essential for TGFβ1 proper protein folding, secretion and association with the ECM [184], whereas TGFβ1-derived TIMP-1 was shown to mediate crosstalk between HSCs and HCC cells [185]. To investigate whether TGFβ1 is secreted by the BECs in RAGE-dependent manner, I have further analyzed the conditioned medium from the *Rage* wildtype (WT) and knockout (KO) BEC cells lines by mass spectrometry. However, the secretory protein level of TGFβ1 between the *Rage* WT and KO BECS were not differentially expressed. The differential expression results between the mRNA and protein expressions

of TGFβ1 indicates that there might be post-translational modifications, resulting in somewhat contradictory results. Moreover, western blot analysis of a TGFβ1 intracellular mediator, phosphorylated SMAD, in whole cell lysates from the normal diet- and CDE diet-treated mice showed that TGFβ1 signaling is activated upon CDE-induced chronic injury irrespective of RAGE expression in BECs (data not shown). These results suggested that BEC-specific RAGE activity may be involved in TGFβ1-associated signaling and genetic programs, but not necessary in producing TGFβ1 ligands. Therefore, I speculated that BEC-specific RAGE activity does not drive HSC activation and fibrosis via the TGFβ1 pathway, but is plausibly via other signaling programs.

### 4.2.3 Integrins may be regulated in BECs in a RAGE-dependent manner and are associated with fibrosis

Integrins constitute a family of transmembrane receptors that mediate cell-cell and cell-ECM interactions. They play a significant role in physiological processes, such as embryonic development, organogenesis, and normal tissue development, as well as pathological role in chronic inflammation and fibrosis. A universal feature of fibrosis is the complex interplay between the epithelial and inflammatory cells with myofibroblast and the ECM in the tissue microenvironment of various disease states. The integrin family of cell adhesion molecules is the key mediator in the cellular communications that govern the initiation, maintenance and the resolution of fibrosis [186]. Moreover, integrins are also found be associated with the classical pro-fibrotic TGFβ1 pathways. To be more specific, the αv integrins family plays a key role in the activation of latent TGFβ1 [186]. In liver fibrosis, integrin αvβ6 expression is upregulated in patients with fibrosis associated with various liver diseases and is exclusively present in epithelial cells [187, 188]. Pharmacological inhibition of αvβ6 in *Mdr2*-knockout mice or in BECs *in vitro*, or genetic ablation of *Itgb6* in *Mdr2*-knockout and DDC diet-induced cholestasis models, effectively suppressed DR and diminished biliary fibrosis, suggesting a prominent role of integrin αvβ6 in DR-mediated fibrosis [188, 189]. Interestingly, CCN1, a secreted ECM-associated signaling protein, promotes DR via integrin αvβ5/αvβ3, and activates Jag/Notch signaling via NF-κB to sustain BEC proliferation [190]. Here in the present study, the RNA-seq data also showed downregulation of *Itgav*, *Itga2* and *Itga5* (encoded for integrin subunit alpha V, subunit alpha 2 and subunit alpha 5 respectively) gene expressions in freshly isolated primary BECs from *Rage*$^{\Delta BEC}$ when compared to those from *Rage*$^{WT}$ mice, suggesting that RAGE directly regulate expressions of these distinct integrin genes and mediates integrin-dependent pathways. However, answering the question whether the altered RAGE-mediated integrin-dependent pathways are associated with fibrosis would require further investigation. In view of the promising results from earlier studies, I hereby speculated that RAGE may regulate BEC proliferation via integrin pathways and promote fibrosis.

### 4.2.4 BEC secretes soluble JAG1 in RAGE-dependent manner and confers HSC activation *in vitro*[2]

A HSC-specific fate tracing study indicated that activated HSCs are the dominant contributor of ECM production in mouse models of toxic-induced, biliary and fatty liver-associated fibrosis [37]. The interplay between activated HSCs and BECs has frequently been reported. For instance, it was proposed that activated HSC-derived paracrine factors eventually evoke a protective response by inducing BEC-mediated liver regeneration [191-193]. In a classical 2-acetylaminofluorene/partial hepatectomy (2AAF/PH)-induced BEC response model, it was shown that inhibition of HSC activation by administration of a L-cysteine diet suppresses DR during the process of liver regeneration, suggesting that HSCs are required for BEC expansion [192]. More recently, a study also showed that HSC-derived growth factor triggers BEC regenerative response and ameliorates liver fibrosis [194]. On the contrary, some studies also proposed that BEC proliferation exacerbates fibrosis [130, 183].

In this dissertation, I have demonstrated that DR and fibrosis are indeed closely linked and positively correlated with each other *in vivo*. Most important, since it was demonstrated that RAGE in BEC has a direct impact on DR, I speculated that DR is an event that preceded fibrosis during cholestatic liver, and these sequential responses occur in a BEC-specific RAGE-dependent manner.

In line with previous reports [192, 195, 196], BECs and HSCs localized in close proximity with each other upon CDE-induced injury as shown from the co-IF analysis of the tdTomato-labelled BECs and HSC-specific markers, Desmin and Vimentin, respectively. Moreover, the abundance of HSCs reduced significantly and this is accompanied by the reduction of RAGE-mediated DR. In light of the remarkable correlation between DR, HSCs activation and severity of fibrosis, and combining the whole transcriptomic data from the primary BECs from *Rage* control ($Rage^{+/\Delta BEC}$) and *Rage* knockout ($Rage^{\Delta BEC}$) mice, I hypothesized that RAGE-driven DR facilitates the cellular and molecular role of HSCs in promoting fibrosis during cholestatic injury.

Although the interplay between BECs and HSCs has been extensively studied, to date, the direct influence of BECs on HSCs has not been reported. Herein, I have utilized both direct and indirect co-culture of BECs with HSCs to investigate the specific role of RAGE on BEC in HSC activation *in vitro*. By direct co-culture and flow cytometry analysis, or indirect co-culture utilizing conditioned medium from BECs on HSCs, I have demonstrated that HSCs are more activated by BECs in the presence of RAGE, providing evidence for RAGE-mediated HSC activation by BECs either via direct contact or paracrine

[2] The discussion content in this sub-section is adapted from a manuscript in preparation.

signaling. To investigate how HSCs are activated by BEC in a RAGE-dependent manner in *trans*, mass spectrometry was utilized to identify the secretory factors that are release by BECs dependent on the presence of RAGE. Among 14 differentially expressed secretory proteins between the conditioned medium from *Rage* WT and *Rage* KO BECs, JAG1 is the most interesting candidate in relation to the context of BEC-mediated HSC activation, as it is an essential component of the Notch signaling that is crucial for biliary lineage cell fate and is commonly dysregulated in liver diseases.

Notch signaling is an evolutionarily conserved pathway that is essential for cell fate decision, differentiation and homeostasis. During liver development, Notch signaling is particularly crucial for the biliary lineage specification and biliary tree development. In mammals, there are five known Notch ligands: JAG1, JAG2, and Delta-like ligands (DLL) 1, 3 and 4, and four Notch receptors: Notch 1-4. [154]. Notch signaling is activated and the signals are transduced upon the engagement of the integral membrane protein JAG1 with membrane receptor Notch. Upon the binding of JAG/NOTCH, it leads subsequent processing and cleavage of Notch intracellular domain (NICD) by γ-secretase. The cleaved NICD then translocates to the nucleus, where it interacts with (RBP)-Jκ to regulate gene transcription of NOTCH downstream target genes [197]. The classical NOTCH genes belongs to the *HES* and *HEY* families, which play a pivotal role in most of the biological processes and cell fate decision. In pathogenesis of liver diseases, aberrant activation of Notch signaling is frequently implicated in hepatocellular carcinoma (HCC) [198, 199] and intrahepatic cholangiocarcinoma (ICC) [200]. Moreover, the Notch gene *Hes1* plays a critical role in induction of BEC proliferation and ICC initiation [201]. In terms of DR and fibrosis, the significant role of Notch signaling in hepatocytes, biliary cells and non-parenchymal cells have been extensively described in mouse injury models. For instance, Notch signal is important for determining the biliary lineage cell fate and expansion in an acute hepatocyte senescence *Mdm2* deletion model [202], as well as in CDE and DDC-induced cholestatic models [22]. Aberrant JAG1 activity from hepatocyte is likely to be mediated by TLR4-NFκB signaling and is necessary for Notch activation in NASH-induced liver fibrosis [203]. To resolve Notch-induced hepatic injury, inhibition of Notch components seemingly has a protective effect on hepatocytes and ameliorates HSCs activation and fibrosis as described in two experimental models of $CCl_4$ hepatotoxin-induced liver injury [204, 205]. Previous work has generated opposing results about the source of JAG1 in injury models, with one study suggested that JAG1 is produced by BEC-associated myofibroblast [22], while another study proposed that it is produced by BECs themselves [202]. Furthermore, the upstream regulator contributing to JAG/NOTCH signaling is currently unknown. Moreover, whether or not the expansion of BECs is required for supporting HSCs differentiation have not been investigated.

In this present study, I demonstrated that RAGE on BECs controls JAG1 expression in enhancing a more pro-fibrotic milieu by activating Notch signaling in HSCs both *in vitro* and *in vivo*. In the *in vitro* experimental studies, it was demonstrated that BEC-derived secretory JAG1 is indeed controlled by RAGE activity, and it is sufficient to induce the transformation of HSCs into a more myofibroblastic-like status. Likewise, the *in vivo* analysis also demonstrated that RAGE-deficiency in BECs ameliorated CDE diet-induced fibrosis, alongside with reduced NOTCH activity as demonstrated by HES1 staining. In line with previous studies, Notch signaling was upregulated in activated HSCs and *Hes1* is transcriptionally active during fibrosis progression [204, 206]. Nonetheless, whether the induced HES1 expression is present exclusively in HSCs in this current CDE diet model would require further IHC staining analyses. Additionally, as proposed by earlier studies, it would also be plausible that the activated HSCs can further activate BECs, such that it forms a positive feedback loop and sustain Notch activation within the entire tissue environment in promoting DR and fibrosis simultaneously, but this would require more sophisticated lineage tracing models for further confirmation. Taken together, the results in this current study indicate that the increased DR results in more secretory JAG1 from BECs under cholestatic conditions, thereby inducing prominently Notch activation in HSCs, and enhancing transformation of HSCs into myofibroblast yielding accelerated fibrosis.

## Section 4.3 Limitations of the current study

### 4.3.1 The *Hnf1b*-Cre mouse line might not fully represent the BEC population

BEC is a rather heterogeneous cell population. Recent single-cell RNA-seq studies revealed the plasticity and heterogeneity of BECs, and suggested that the BEC population comprises a dynamic gene expression profile [15, 16]. However, in this dissertation, I have only utilized the *Hnf1b-Cre* mouse model, which might indeed underrepresent the BEC pool and neglect other BECs or liver epithelial progenitors which might also contribute to DR or fibrosis. To date, there are multiple Cre mouse lines, including *Ck19-CreER*, *Lgr5-CreER*, *Opn-CreER*, *Sox9-CreER* and *Foxl1-CreER*, shown to be capable of specifically targeting either the naïve or activated form of BECs [207]. Indeed, as indicated by the co-IF analysis of CK19 or A6 and tdTom in the CDE-challenged mice, around 45% of CK19+ or A6+ BECs were not targeted by *Hnf1b-Cre* (data not shown). These cells may either represent the BECs that are regulated by other promoters or the dedifferentiated hepatocytes. As a matter of fact, the use of a multiple Cre lines rather than a single one will be needed to overcome the challenges of cellular heterogeneity in BECs.

### 4.3.2 CDE dietary mouse model does not represent all forms of liver injury

The underlying mechanisms of different types of liver injuries are rather context-dependent. In this dissertation, I have focused on the use of the CDE diet-induced cholestasis mouse model to investigated the role of BEC-specific RAGE activity. This injury model is exclusively used to examine cholestasis-induced DR and fibrosis. Although I have clearly shown that DR and fibrosis are mediated via RAGE on BEC in this model, it is not clear whether the results would be consistent in other types of injury mouse models due to different underlying causes (described in Table 4-1), thus the subsequent mechanisms to cope with the corresponding injuries. In the perspective of cholestasis, several classical cholestasis mouse models have been extensively used to investigate biliary-associated disease. Although these models all consistently lead to DR, chronic inflammation, bridging fibrosis and tumor formation, the malignant transformation and oncogenic events can arise from various underlying causes. For instance, systemic thioacetamide (TAA) administration is known to induce cell death of hepatocytes located around the central vein [208], whereas CDE or DDC diet models mainly damage hepatocytes around the portal vein [209]. Additionally, bile duct ligation (BDL) is a surgical mouse model that causes acute obstruction of bile flow, resulting in rapid cholestatic damage particularly in the biliary tree [210]. To fully address the of cholestasis-induced liver fibrosis, multiple mouse models would have to be used to interrogated whether different forms of cholestatic injuries leads to fibrosis via the same mechanisms. Moreover, to elucidate how other types of liver injuries associated with fibrosis, appropriate mouse models would have to be carefully chosen.

**Table 4-1. Underlying causes of liver disease mouse models.**

| Mouse models | Major type of liver diseases | Underlying causes | References |
|---|---|---|---|
| Choline-deficient ethionine-supplemented (CDE) diet | Cholestasis | Damage hepatocytes around portal vein, inhibit phosphatidylcholine synthesis that is required for very low-density lipoprotein (VLDL) production | [111, 179, 209, 211] |
| 3,5-diethoxycarbonyl 1,4-dihydrocollidinen (DDC) diet | Cholestasis | Damage hepatocytes around portal vein, steatosis | [209] |
| Thioacetamide (TAA) | Cholestasis, Fibrosis | Cell death of hepatocytes around central vein | [208] |
| Bile duct ligation (BDL) | Cholestasis, biliary fibrosis | Acute bile duct obstruction | [212] |

| Mouse models | Major type of liver diseases | Underlying causes | References |
|---|---|---|---|
| Carbon tetrachloride ($CCl_4$) | Fibrosis | Hepatotoxicity due to DNA adduct formation | [213] |
| Multidrug-resistant protein 2 knockout / Abcb4 -/- | Cholestasis, HCC | Defect in phospholipid and cholesterol secretion due to the deletion of the phosphatidylcholine translocation | [111, 214, 215] |
| Diethylnitrosamine (DEN)/ dimethylnitrosamine (DMN) | HCC | Hepatic damage necrosis due to DNA adducts formation | [216] |
| Western diet | NASH | Obesity and insulin resistance induced by high-fat, high-cholesterol and high-fructose content diet | [217, 218] |
| Choline-deficient high-fat diet (CD-HFD) | NASH | Inhibit phosphatidylcholine synthesis that is required for very low-density lipoprotein (VLDL) production, accumulation of triglycerides | [219] |
| Methionine and choline-deficient (MCD) diet | NASH | Impairs synthesis of phosphatidylcholine, accumulation of triglycerides | [220] [221] |

## Section 4.4 Conclusion and future perspectives

### 4.4.1 Conclusion of present study

RAGE is an immunoglobulin and pattern recognition receptor that engages a variety of damage-associated ligands. In the context of inflammation-associated hepatic injury, RAGE is known to play a pivotal role in sustaining inflammation, DR, onset of liver fibrosis and carcinogenesis. In this dissertation, I have clarified the RAGE-dependent mechanistic linkage between DR and fibrosis during cholestatic injury, and have provided further insights on the functional role of RAGE in BECs specifically. Here, I have addressed the following topics:

(1) RAGE is predominantly expressed on BECs, which counter-argued previous claims about the expression of RAGE on other hepatic resident cells such as hepatocytes or stellate cells.
(2) BEC-specific RAGE activity is not directly involved in immune cells recruitment or linked with the degree of steatosis.
(3) The presence and expression of RAGE on BECs is indispensable for DR in a cell-intrinsic manner during cholestatic injury.

(4) BEC-specific RAGE-mediated DR is positively correlated with the severity of fibrosis, signifying that BEC is modulating fibrotic events either directly or indirectly in RAGE-dependent manner.
(5) BECs secrete JAG1 in a RAGE-dependent manner and activate Notch signaling in HSCs in *trans*, thereby triggering the HSCs to transform into a more myofibroblastic-like status.

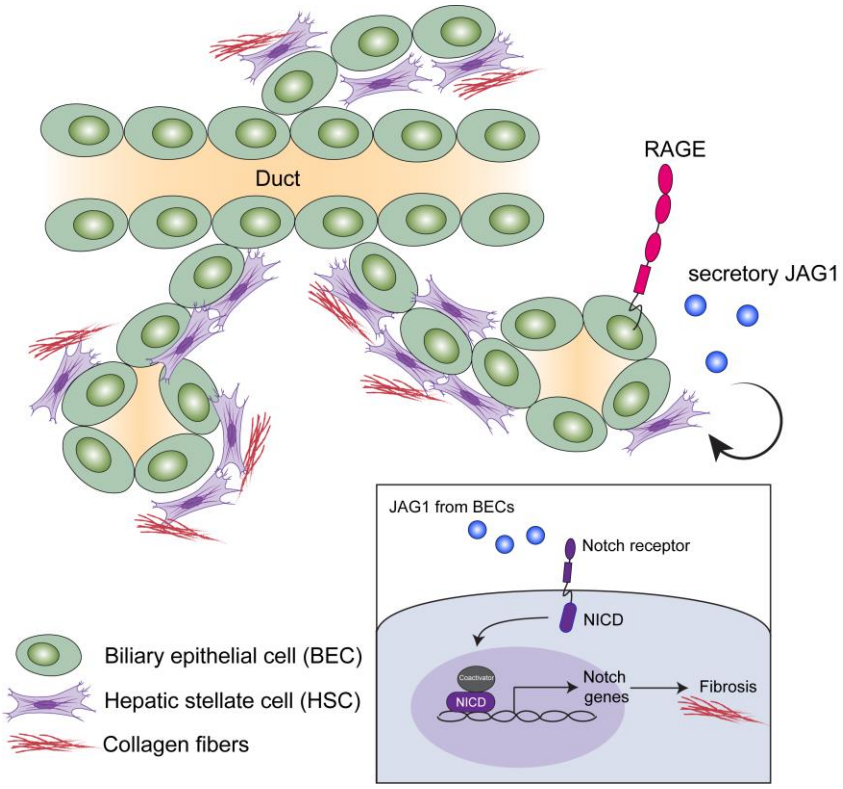


**Figure 4-2. Graphical summary of BEC-mediated DR and fibrosis in a RAGE-dependent manner**.

Predominant expression of RAGE in BECs drive BEC proliferation, thus ductular reaction during cholestasis. Furthermore, RAGE controls secretory JAG1 released by BECs, which triggers Notch activation in HSCs in a paracrine manner. Notch genes including *Hes1*, *Hey1* and *Hey2* are transcribed in HSCs in support of HSC transformation into a more myofibroblastic-like state, thus promoting fibrosis.

In conclusion, this current study demonstrated that RAGE is a master regulator of DR and fibrosis in cholestasis-associated liver diseases (Figure 4-2). Instead of resolving inflammation and promoting liver regeneration, DR was found to be detrimental to the progression of cholestasis and fibrosis. This study suggests a novel model of a RAGE-dependent interplay between BECs and HSCs. Under cholestatic condition, RAGE plays a crucial role in modulating JAG1-induced HSCs activation in promoting fibrosis.

In light of the specific expression of RAGE in BECs and its significant role in DR-mediated fibrosis, targeting RAGE may represent a novel vulnerability in

DR- or fibrosis-associated liver diseases. As *Rage*-knockout mice are viable and appear physiologically normal, it might be a feasible approach to therapeutically target RAGE in clinical settings.

### 4.4.2 Future perspectives in treating cholestasis and cholestasis-associated fibrosis

To date, there are only a few known RAGE small molecular inhibitors available for pre-clinical and early clinical trials in various inflammatory diseases. For instance, Azeliragon, the orally bioavailable small molecule inhibitor of RAGE, has been used as an agent in preclinical studies focused on diabetic complications, cardiovascular disease or Alzheimer's disease. Another RAGE inhibitor, FPS-ZM1, is a small molecule that is able to inhibit the interaction between RAGE and its ligands. It was shown that FPS-ZM1 is able to block inflammatory signaling in mouse brain or reduced inflammation in cardiac tissues during cardiac hypertrophy [172]. In view of its efficacy in preclinical studies of other inflammatory diseases, the RAGE inhibitors Azeliragon or FPS-ZM1 might have the potential to be the pharmacological tools in treating cholestasis or cholestasis-associated fibrosis.

#### 4.4.2.1 RAGE is a potential therapeutic target for cholestasis

Common chronic primary cholestatic diseases includes primary biliary cholangitis (PBC) and primary sclerosing cholangitis (PSC), are caused by the scarring of the bile ducts due to inflammation, leading to subsequent blockade of the bile flow. Other common primary cholestatic diseases include progressive familial intrahepatic cholestasis (PFIC) and Alagille syndrome (ALGS), which are rare hereditary diseases in children and infants. Chronic intrahepatic cholestatic diseases commonly results from impaired bile secretion or biliary phospholipid secretion [59]. Patients exhibiting this phenotype are at high risk of developing periportal fibrosis. Progression to biliary cirrhosis with prominent proliferating bile ducts and liver failure are commonly observed at advanced stage of the disease, which ultimately leads to hepatocellular carcinoma or cholangiocarcinoma [59, 222]. Recently, two ileal bile acid transporter (IBAT) inhibitors, maralixibat and odevixibat, have been approved for treatment of pruritus in patients with Alagille Syndrome or Progressive Familial Intrahepatic Cholestasis (PFIC), respectively. It was proven that these inhibitors are effective in reducing the intrahepatic retention of bile acids. However, these drugs do not target the root cause of cholestasis. Latest studies on the usage of FXR agonists and FGF19 analogues to reduce bile acid synthesis have also shed light on anti-cholestatic management. Nevertheless, the additional benefits of these potential agents on complications arising from cholestasis would require further investigations and monitoring. To date, there are still a limited FDA-approved therapeutic options to cure cholestatic diseases, by so

far only liver transplantation is served as a complete resolution to abrogate the risk of liver failure and tumorigenic progression [222]. In this present study, RAGE is demonstrated to express mainly on BECs in the liver, and functions as a master regulator of DR, which is a prevalent feature of cholestatic diseases. Moreover, it was also discovered that RAGE might be involved in attenuating bile transport, making the liver to be more cholestatic due to the accumulation of bile. Therefore, targeting RAGE might be a plausible approach to inhibit DR and reverse the attenuated bile transport during cholestasis. In view of the cell type-specific function of RAGE in the context of cholestasis, I hereby propose that RAGE may serve as an attractive target for anti-cholestatic therapy.

#### 4.4.2.2 RAGE may represent a novel preventive treatment for cholestasis-associated fibrosis

Progressive fibrosis typically follows chronic liver damage due to hepatitis viral infection, metabolic diseases, cholestatic insult, and heavy alcohol consumptions. Eventually, fibrosis leads to hepatic failure and end-stage liver diseases such as HCC and ICC. Research progresses in liver diseases over the past decades has enable us to further understand the pathogenesis of fibrosis and its clinical consequences. To date, numerous anti-fibrotic therapeutic strategies have been proposed in various experimental models and are being investigated in clinical trials (Table 4-2). These strategies include: (1) targeting liver lipid metabolism and oxidative stress, (2) targeting liver inflammation and cell death, and (3) targeting fibrosis. Yet, none of the investigative pharmacological agents have been approved by the FDA or EMA so far, as they neither show clear efficacies in fibrosis reduction, nor have progressed to larger scale clinical trials.

**Table 4-2. Anti-fibrotic pharmacological agents in clinical trials.**

| | Compounds | Target effects | Clinical trials; Phase | Anti-fibrotic effects | Ref. |
|---|---|---|---|---|---|
| Targeting lipid metabolism and oxidative stress | Firsocostat (GS-0976) | Acetyl coA carboxylase (ACC) inhibition | NCT04971785 (Recruiting); Phase II | Reduced liver stiffness | [223] |
| | Aramchol | Stearoyl-CoA desaturase 1 (SCD1) inhibition | NCT04104321; Phase III | Improvement in fibrosis by at least one stage but not statistically significant | [224] |
| | Aldafermin (NGM282) | FGF19 analog, serve as FGF agonist | NCT04210245; Phase IIb | Improved fibrosis by at least one stage but not statistically significant | [225] |

| | Compounds | Target effects | Clinical trials; Phase | Anti-fibrotic effects | Ref. |
|---|---|---|---|---|---|
| Targeting lipid metabolism and oxidative stress | Pegbelfermin (BMS-986036) | Pegylated FGF21 analog, serve as FGF agonist | NCT03486899, NCT03486912; Phase IIb | Improvement in fibrosis by at least one stage | [226] |
| | Resmetirom (MGL-3196) | Thyroid hormone receptor agonist | NCT03900429; Phase III | Reduced fibrosis markers and liver stiffness | [227] |
| | Obeticholic acid | Farnesoid X receptor (FXR) agonist | NCT02548351; Phase III | Improvement in fibrosis | [228, 229] |
| | Cilofexor (GS-9674) | Farnesoid X receptor (FXR) agonist | NCT03890120; Phase III | No significant improvement in fibrosis | [230] |
| | Elafibranor | Peroxisomal proliferator-activated receptors (PPARs) agonist | NCT02704403; Phase III | Resolved NASH without fibrosis worsening | [231] |
| | Liraglutide | Glucagon-like peptide-1 (GLP-1) receptor agonist | NCT01237119; Phase II | Reduced fibrosis progression | [232] |
| | Semaglutide | GLP-1 receptor agonist | NCT02970942; Phase II | No significant improvement in fibrosis | [233] |
| | Anti-FGFR1c/KLB agonist antibody (BFKB8488A) | Activates FGFR1 in KLB-dependent manner | NCT04171765; Phase IIb | Reduced fibrosis | [234, 235] |
| Targeting inflammation and apoptosis | Selonsertib | Apoptosis signal-regulating kinase 1 (ASK1) inhibition in hepatocytes | NCT03053063; Phase III | No reduction in fibrosis | [236] |
| | CM-101 | CCL24 blocking antibody | NCT04595825 (Recruiting); Phase II | N/A | [237] |
| | Silymarin | Anti-oxidant, anti-inflammatory and anti-fibrotic effects | NCT02006498; Phase II | Reduced fibrosis | [238] |
| Targeting fibrosis | Pioglitazone | PPARγ agonist, blocks activation of HSCs | NCT00063622; Phase III | No improvement in fibrosis | [239] |
| | Simtuzumab (SIM, GS-6624) | Monoclonal antibody against lysyl oxidase homologue 2 (LOXL2); blocks collagen cross-linking | NCT01672866; Phase II | No improvement in fibrosis | [240] |

| | Compounds | Target effects | Clinical trials; Phase | Anti-fibrotic effects | Ref. |
|---|---|---|---|---|---|
| Targeting fibrosis | Losartan | Angiotensin II Type 1 receptor antagonist, blocks HSC activation | NCT01051219; Phase III (enrollment suspended) | N/A | [241] |
| | BMS-986263 | A siRNA-delivering lipid nanoparticle that degrade HSP47 mRNA | NCT03420768; Phase II | Improvement in fibrosis | [242] |

Activated HSCs are well recognized as key effectors of fibrosis as they are the major cell types that contribute to fibrosis. Currently, several other agents targeting HSC activation have been investigated in experimental models and showed promising results in suppressing fibrosis progression. TGFβ is one of the most potent stimuli to induce myofibroblast activities, thus it serves as an attractive target to inhibit HSC activation. Targeting TGFβ signaling using neutralizing anti-TGFβ antibodies 1 [243] or TGFβ-activated ALK5 signaling [244] diminished fibrosis in experimental TAA-administered or dimethylnitrosamine (DMN)-administered mouse respectively. Additionally, selective inhibition of integrin αvβ6 (a binding partner of the latent TGFβ binding protein which activates latent TGFβ [245] ) by monoclonal antibody 3G9 [188] or small molecule CWHM12 [246] effectively attenuated liver fibrosis. Other classes of molecules, such as NADPH oxidase (NOX) inhibitor GKT137831 [247, 248], Hedgehog inhibitor cyclopamine [249], YAP inhibitor verteporfin [249], anti-vascular adhesion protein-1 (VAP-1) monoclonal antibody [250] were shown to be able to inhibit HSC activation or migration, thereby attenuating fibrosis.

In this dissertation, I have uncovered and redefined the cell-cell interactions between BECs and HSCs in cholestasis-associated fibrosis, providing new evidence for a critical interplay between these two cell types in RAGE-dependent manner. Moreover, I have demonstrated that DR is directly linked to fibrosis under the regulation of BEC-specific RAGE activity via secretory JAG1. Abolishing RAGE activity on BECs may seem to be indirect yet promising approaches to limit DR-mediated HSC activation. However, whether RAGE inhibition can be used for preventive care or therapeutic treatment has to be strategically defined and investigated. In my on-going study utilizing the *Mdr2*-knockout mouse model when biliary fibrosis spontaneously develops starting at week 2 of age, I have investigated whether the deletion of *Rage* in BEC could reverse or diminish fibrosis. *Rage* was deleted in BEC specifically at the age of week 4, and was sacrificed at the age of 3-month, 6-month and 9-month. Importantly, the deletion of *Rage* could not effectively reverse or attenuate

biliary fibrosis progression, however, the average size of the HCC tumor nodules, which were developed at the age of 9-month old were smaller in the mice with BEC-specific *Rage* deletion. In contrast, as demonstrated in the CDE diet model in this dissertation, the deletion of *Rage* in BECs prior to the initiation and perpetuation of fibrosis effectively diminished HSC activation and attenuated fibrosis progression, suggesting that fibrosis can be prevented by limiting RAGE activity at an early stage. Collectively, this suggests that RAGE might serve as an attractive diagnostic target for the prevention of cholestasis-associated fibrosis, or a therapeutic target of HCC development, but not as a therapeutic target for anti-fibrotic therapy.

# Chapter 5
## References

1. Manco, R. and S. Itzkovitz, *Liver zonation.* Journal of Hepatology, 2021. **74**(2): p. 466-468.
2. Ma, R., et al., *Metabolic and non-metabolic liver zonation is established non-synchronously and requires sinusoidal Wnts.* eLife, 2020. **9**: p. e46206.
3. Birchmeier, W., *Orchestrating Wnt signalling for metabolic liver zonation.* Nature Cell Biology, 2016. **18**(5): p. 463-465.
4. Wang, B., et al., *Self-renewing diploid Axin2+ cells fuel homeostatic renewal of the liver.* Nature, 2015. **524**(7564): p. 180-185.
5. Planas-Paz, L., et al., *The RSPO–LGR4/5–ZNRF3/RNF43 module controls liver zonation and size.* Nature Cell Biology, 2016. **18**(5): p. 467-479.
6. Lin, S., et al., *Distributed hepatocytes expressing telomerase repopulate the liver in homeostasis and injury.* Nature, 2018. **556**(7700): p. 244-248.
7. Chen, F., et al., *Broad Distribution of Hepatocyte Proliferation in Liver Homeostasis and Regeneration.* Cell Stem Cell, 2020. **26**(1): p. 27-33.e4.
8. He, L., et al., *Proliferation tracing reveals regional hepatocyte generation in liver homeostasis and repair.* Science, 2021. **371**(6532): p. eabc4346.
9. Gadd, V.L., N. Aleksieva, and S.J. Forbes, *Epithelial Plasticity during Liver Injury and Regeneration.* Cell Stem Cell, 2020. **27**(4): p. 557-573.
10. Mullany, L.K., et al., *Distinct proliferative and transcriptional effects of the D-type cyclins in vivo.* Cell Cycle, 2008. **7**(14): p. 2215-24.
11. Higgins, G.M., *Experimental pathology of the liver.* Arch pathol, 1931. **12**: p. 186-202.
12. Michalopoulos, G.K. and B. Bhushan, *Liver regeneration: biological and pathological mechanisms and implications.* Nature Reviews Gastroenterology & Hepatology, 2021. **18**(1): p. 40-55.
13. Font-Burgada, J., et al., *Hybrid Periportal Hepatocytes Regenerate the Injured Liver without Giving Rise to Cancer.* Cell, 2015. **162**(4): p. 766-779.
14. Miyajima, A., M. Tanaka, and T. Itoh, *Stem/Progenitor Cells in Liver Development, Homeostasis, Regeneration, and Reprogramming.* Cell Stem Cell, 2014. **14**(5): p. 561-574.
15. Aizarani, N., et al., *A human liver cell atlas reveals heterogeneity and epithelial progenitors.* Nature, 2019. **572**(7768): p. 199-204.
16. Segal, J.M., et al., *Single cell analysis of human foetal liver captures the transcriptional profile of hepatobiliary hybrid progenitors.* Nature Communications, 2019. **10**(1): p. 3350.
17. Takase, H.M., et al., *FGF7 is a functional niche signal required for stimulation of adult liver progenitor cells that support liver regeneration.* Genes Dev, 2013. **27**(2): p. 169-81.
18. Hu, M., et al., *Wnt/beta-catenin signaling in murine hepatic transit amplifying progenitor cells.* Gastroenterology, 2007. **133**(5): p. 1579-91.
19. Kitade, M., et al., *Specific fate decisions in adult hepatic progenitor cells driven by MET and EGFR signaling.* Genes Dev, 2013. **27**(15): p. 1706-17.
20. Fiorotto, R., et al., *Notch signaling regulates tubular morphogenesis during repair from biliary damage in mice.* Journal of Hepatology, 2013. **59**(1): p. 124-130.
21. Lu, J., et al., *Notch Signaling Coordinates Progenitor Cell-Mediated Biliary Regeneration Following Partial Hepatectomy.* Scientific Reports, 2016. **6**(1): p. 22754.
22. Boulter, L., et al., *Macrophage-derived Wnt opposes Notch signaling to specify hepatic progenitor cell fate in chronic liver disease.* Nature Medicine, 2012. **18**(4): p. 572-579.
23. Fukano, S., et al., *Bile acid metabolism in partially hepatectomized rats.* Steroids, 1985. **45**(3-4): p. 209-227.
24. Sato, K., et al., *Ductular Reaction in Liver Diseases: Pathological Mechanisms and Translational Significances.* Hepatology, 2019. **69**(1): p. 420-430.
25. Yanger, K., et al., *Adult hepatocytes are generated by self-duplication rather than stem cell differentiation.* Cell Stem Cell, 2014. **15**(3): p. 340-349.
26. Lu, W.-Y., et al., *Hepatic progenitor cells of biliary origin with liver repopulation capacity.* Nature Cell Biology, 2015. **17**(8): p. 971-983.
27. Jörs, S., et al., *Lineage fate of ductular reactions in liver injury and carcinogenesis.* The Journal of Clinical Investigation, 2015. **125**(6): p. 2445-2457.
28. Bird, T.G., et al., *Bone marrow injection stimulates hepatic ductular reactions in the absence of injury via macrophage-mediated TWEAK signaling.* Proceedings of the National Academy of Sciences, 2013. **110**(16): p. 6542-6547.

29. Tirnitz-Parker, J.E., et al., *Tumor necrosis factor-like weak inducer of apoptosis is a mitogen for liver progenitor cells.* Hepatology, 2010. **52**(1): p. 291-302.
30. Planas-Paz, L., et al., *YAP, but Not RSPO-LGR4/5, Signaling in Biliary Epithelial Cells Promotes a Ductular Reaction in Response to Liver Injury.* Cell Stem Cell, 2019. **25**(1): p. 39-53.e10.
31. Yimlamai, D., et al., *Hippo pathway activity influences liver cell fate.* Cell, 2014. **157**(6): p. 1324-38.
32. Lee, K.-P., et al., *The Hippo-Salvador pathway restrains hepatic oval cell proliferation, liver size, and liver tumorigenesis.* Proceedings of the National Academy of Sciences of the United States of America, 2010. **107**(18): p. 8248-53.
33. Kisseleva, T. and D. Brenner, *Molecular and cellular mechanisms of liver fibrosis and its regression.* Nature Reviews Gastroenterology & Hepatology, 2021. **18**(3): p. 151-166.
34. Turnpenny, P.D. and S. Ellard, *Alagille syndrome: pathogenesis, diagnosis and management.* European Journal of Human Genetics, 2012. **20**(3): p. 251-257.
35. Iwaisako, K., et al., *Origin of myofibroblasts in the fibrotic liver in mice.* Proc Natl Acad Sci U S A, 2014. **111**(32): p. E3297-305.
36. Kisseleva, T., et al., *Bone marrow-derived fibrocytes participate in pathogenesis of liver fibrosis.* Journal of Hepatology, 2006. **45**(3): p. 429-438.
37. Mederacke, I., et al., *Fate tracing reveals hepatic stellate cells as dominant contributors to liver fibrosis independent of its aetiology.* Nature Communications, 2013. **4**(1): p. 2823.
38. Trivedi, P., S. Wang, and S.L. Friedman, *The Power of Plasticity—Metabolic Regulation of Hepatic Stellate Cells.* Cell Metabolism, 2021. **33**(2): p. 242-257.
39. De Smet, V., et al., *Initiation of hepatic stellate cell activation extends into chronic liver disease.* Cell Death & Disease, 2021. **12**(12): p. 1110.
40. Mannaerts, I., et al., *The Hippo pathway effector YAP controls mouse hepatic stellate cell activation.* J Hepatol, 2015. **63**(3): p. 679-88.
41. Mannaerts, I., et al., *Unfolded protein response is an early, non-critical event during hepatic stellate cell activation.* Cell Death & Disease, 2019. **10**(2): p. 98.
42. Puche, J.E., Y. Saiman, and S.L. Friedman, *Hepatic stellate cells and liver fibrosis.* Compr Physiol, 2013. **3**(4): p. 1473-92.
43. Tsuchida, T. and S.L. Friedman, *Mechanisms of hepatic stellate cell activation.* Nature Reviews Gastroenterology & Hepatology, 2017. **14**(7): p. 397-411.
44. Getachew, A., et al., *SAA1/TLR2 axis directs chemotactic migration of hepatic stellate cells responding to injury.* iScience, 2021. **24**(5): p. 102483.
45. Olsen, A.L., et al., *Fibronectin extra domain-A promotes hepatic stellate cell motility but not differentiation into myofibroblasts.* Gastroenterology, 2012. **142**(4): p. 928-937.e3.
46. Bachem, M.G., R. Melchior, and A.M. Gressner, *The role of thrombocytes in liver fibrogenesis: effects of platelet lysate and thrombocyte-derived growth factors on the mitogenic activity and glycosaminoglycan synthesis of cultured rat liver fat storing cells.* J Clin Chem Clin Biochem, 1989. **27**(9): p. 555-65.
47. Borkham-Kamphorst, E., et al., *Pro-fibrogenic potential of PDGF-D in liver fibrosis.* J Hepatol, 2007. **46**(6): p. 1064-74.
48. Cai, B., et al., *Macrophage MerTK Promotes Liver Fibrosis in Nonalcoholic Steatohepatitis.* Cell Metab, 2020. **31**(2): p. 406-421.e7.
49. Friedman, S.L. and M.J. Arthur, *Activation of cultured rat hepatic lipocytes by Kupffer cell conditioned medium. Direct enhancement of matrix synthesis and stimulation of cell proliferation via induction of platelet-derived growth factor receptors.* J Clin Invest, 1989. **84**(6): p. 1780-5.
50. Wang, J., et al., *Kupffer cells mediate leptin-induced liver fibrosis.* Gastroenterology, 2009. **137**(2): p. 713-23.
51. Karlmark, K.R., et al., *Hepatic recruitment of the inflammatory Gr1+ monocyte subset upon liver injury promotes hepatic fibrosis.* Hepatology, 2009. **50**(1): p. 261-274.
52. Liaskou, E., et al., *Monocyte subsets in human liver disease show distinct phenotypic and functional characteristics.* Hepatology, 2013. **57**(1): p. 385-398.
53. Pradere, J.P., et al., *Hepatic macrophages but not dendritic cells contribute to liver fibrosis by promoting the survival of activated hepatic stellate cells in mice.* Hepatology, 2013. **58**(4): p. 1461-73.

54. Nishio, T., et al., *Activated hepatic stellate cells and portal fibroblasts contribute to cholestatic liver fibrosis in MDR2 knockout mice.* J Hepatol, 2019. **71**(3): p. 573-585.
55. Duarte, S., et al., *Matrix metalloproteinases in liver injury, repair and fibrosis.* Matrix Biol, 2015. **44-46**: p. 147-56.
56. Lachowski, D., et al., *Matrix stiffness modulates the activity of MMP-9 and TIMP-1 in hepatic stellate cells to perpetuate fibrosis.* Scientific Reports, 2019. **9**(1): p. 7299.
57. Tam, P.K.H., et al., *Cholangiopathies – Towards a molecular understanding.* EBioMedicine, 2018. **35**: p. 381-393.
58. Jacquemin, E., *Progressive familial intrahepatic cholestasis.* Clin Res Hepatol Gastroenterol, 2012. **36 Suppl 1**: p. S26-35.
59. Srivastava, A., *Progressive Familial Intrahepatic Cholestasis.* Journal of Clinical and Experimental Hepatology, 2014. **4**(1): p. 25-36.
60. Friedman, S.L. and M. Pinzani, *Hepatic fibrosis 2022: Unmet needs and a blueprint for the future.* Hepatology, 2022. **75**(2): p. 473-488.
61. Pinzani, M. and K. Rombouts, *Liver fibrosis: from the bench to clinical targets.* Digestive and Liver Disease, 2004. **36**(4): p. 231-242.
62. Penz-Österreicher, M., C.H. Österreicher, and M. Trauner, *Fibrosis in autoimmune and cholestatic liver disease.* Best Pract Res Clin Gastroenterol, 2011. **25**(2): p. 245-58.
63. Svegliati-Baroni, G., et al., *Bile acids induce hepatic stellate cell proliferation via activation of the epidermal growth factor receptor.* Gastroenterology, 2005. **128**(4): p. 1042-1055.
64. Fickert, P., et al., *Farnesoid X Receptor Critically Determines the Fibrotic Response in Mice but Is Expressed to a Low Extent in Human Hepatic Stellate Cells and Periductal Myofibroblasts.* The American Journal of Pathology, 2009. **175**(6): p. 2392-2405.
65. Stedman, C., et al., *Benefit of farnesoid X receptor inhibition in obstructive cholestasis.* Proceedings of the National Academy of Sciences, 2006. **103**(30): p. 11323-11328.
66. Tarocchi, M., et al., *Molecular mechanism of hepatitis B virus-induced hepatocarcinogenesis.* World J Gastroenterol, 2014. **20**(33): p. 11630-40.
67. Farazi, P.A. and R.A. DePinho, *Hepatocellular carcinoma pathogenesis: from genes to environment.* Nat Rev Cancer, 2006. **6**(9): p. 674-87.
68. Hoshida, Y., et al., *Pathogenesis and prevention of hepatitis C virus-induced hepatocellular carcinoma.* J Hepatol, 2014. **61**(1 Suppl): p. S79-90.
69. Schulze-Krebs, A., et al., *Hepatitis C virus-replicating hepatocytes induce fibrogenic activation of hepatic stellate cells.* Gastroenterology, 2005. **129**(1): p. 246-58.
70. Llovet, J.M., et al., *Hepatocellular carcinoma.* Nature Reviews Disease Primers, 2021. **7**(1): p. 6.
71. Seitz, H.K., et al., *Alcoholic liver disease.* Nature Reviews Disease Primers, 2018. **4**(1): p. 16-16.
72. Kwon, H.J., et al., *Aldehyde dehydrogenase 2 deficiency ameliorates alcoholic fatty liver but worsens liver inflammation and fibrosis in mice.* Hepatology, 2014. **60**(1): p. 146-57.
73. Jeong, W.I., O. Park, and B. Gao, *Abrogation of the antifibrotic effects of natural killer cells/interferon-gamma contributes to alcohol acceleration of liver fibrosis.* Gastroenterology, 2008. **134**(1): p. 248-58.
74. Heyens, L.J.M., et al., *Liver Fibrosis in Non-alcoholic Fatty Liver Disease: From Liver Biopsy to Non-invasive Biomarkers in Diagnosis and Treatment.* Frontiers in Medicine, 2021. **8**.
75. Brunt, E.M., et al., *Nonalcoholic fatty liver disease.* Nature Reviews Disease Primers, 2015. **1**(1): p. 15080.
76. Tomita, K., et al., *Free cholesterol accumulation in hepatic stellate cells: mechanism of liver fibrosis aggravation in nonalcoholic steatohepatitis in mice.* Hepatology, 2014. **59**(1): p. 154-69.
77. Neeper, M., et al., *Cloning and expression of a cell surface receptor for advanced glycosylation end products of proteins.* Journal of Biological Chemistry, 1992. **267**(21): p. 14998-15004.
78. Sessa, L., et al., *The Receptor for Advanced Glycation End-Products (RAGE) Is Only Present in Mammals, and Belongs to a Family of Cell Adhesion Molecules (CAMs).* PLOS ONE, 2014. **9**(1): p. e86903.
79. Bierhaus, A., et al., *Understanding RAGE, the receptor for advanced glycation end products.* Journal of Molecular Medicine, 2005. **83**(11): p. 876-886.

80. Sparvero, L.J., et al., *RAGE (Receptor for Advanced Glycation Endproducts), RAGE Ligands, and their role in Cancer and Inflammation.* Journal of Translational Medicine, 2009. **7**(1): p. 17.
81. Ding, Q. and J.N. Keller, *Evaluation of rage isoforms, ligands, and signaling in the brain.* Biochimica et Biophysica Acta (BBA) - Molecular Cell Research, 2005. **1746**(1): p. 18-27.
82. Yamagishi, S. and T. Matsui, *Role of receptor for advanced glycation end products (RAGE) in liver disease.* Eur J Med Res, 2015. **20**(1): p. 15.
83. Hyogo, H. and S. Yamagishi, *Advanced glycation end products (AGEs) and their involvement in liver disease.* Curr Pharm Des, 2008. **14**(10): p. 969-72.
84. Asadipooya, K., et al., *RAGE is a Potential Cause of Onset and Progression of Nonalcoholic Fatty Liver Disease.* Int J Endocrinol, 2019. **2019**: p. 2151302.
85. Hiwatashi, K., et al., *A novel function of the receptor for advanced glycation end-products (RAGE) in association with tumorigenesis and tumor differentiation of HCC.* Ann Surg Oncol, 2008. **15**(3): p. 923-33.
86. Sebeková, K., et al., *Markedly elevated levels of plasma advanced glycation end products in patients with liver cirrhosis - amelioration by liver transplantation.* J Hepatol, 2002. **36**(1): p. 66-71.
87. Hyogo, H., et al., *Elevated levels of serum advanced glycation end products in patients with non-alcoholic steatohepatitis.* J Gastroenterol Hepatol, 2007. **22**(7): p. 1112-9.
88. Song, F., et al., *RAGE Regulates the Metabolic and Inflammatory Response to High-Fat Feeding in Mice.* Diabetes, 2014. **63**(6): p. 1948-1965.
89. Gaens, K.H., et al., *Nε-(carboxymethyl)lysine-receptor for advanced glycation end product axis is a key modulator of obesity-induced dysregulation of adipokine expression and insulin resistance.* Arterioscler Thromb Vasc Biol, 2014. **34**(6): p. 1199-208.
90. Goodwin, M., et al., *Advanced glycation end products augment experimental hepatic fibrosis.* 2013. **28**(2): p. 369-376.
91. Basta, G., et al., *Advanced Glycation End Products Activate Endothelium Through Signal-Transduction Receptor RAGE.* 2002. **105**(7): p. 816-822.
92. Chen, R., et al., *Emerging Role of High-Mobility Group Box 1 (HMGB1) in Liver Diseases.* Molecular Medicine, 2013. **19**(1): p. 357-366.
93. Zhou, R.R., et al., *HMGB1 cytoplasmic translocation in patients with acute liver failure.* BMC Gastroenterol, 2011. **11**: p. 21.
94. Jung, J.H., et al., *Hepatitis C virus infection is blocked by HMGB1 released from virus-infected cells.* J Virol, 2011. **85**(18): p. 9359-68.
95. Wang, L.W., H. Chen, and Z.J. Gong, *High mobility group box-1 protein inhibits regulatory T cell immune activity in liver failure in patients with chronic hepatitis B.* Hepatobiliary Pancreat Dis Int, 2010. **9**(5): p. 499-507.
96. Hernandez, C., et al., *HMGB1 links chronic liver injury to progenitor responses and hepatocarcinogenesis.* The Journal of Clinical Investigation, 2019. **128**(6): p. 2436-2450.
97. Khambu, B., et al., *HMGB1 promotes ductular reaction and tumorigenesis in autophagy-deficient livers.* Journal of Clinical Investigation, 2018.
98. Ge, X., et al., *High Mobility Group Box-1 Drives Fibrosis Progression Signaling via the Receptor for Advanced Glycation End Products in Mice.* Hepatology, 2018. **68**(6): p. 2380-2404.
99. Arriazu, E., et al., *Signalling via the osteopontin and high mobility group box-1 axis drives the fibrogenic response to liver injury.* Gut, 2017. **66**(6): p. 1123-1137.
100. Yao, S., et al., *Role of the S100 protein family in liver disease (Review).* Int J Mol Med, 2021. **48**(3): p. 166.
101. Xia, C., et al., *S100 Proteins As an Important Regulator of Macrophage Inflammation.* Front Immunol, 2017. **8**: p. 1908.
102. Gebhardt, C., et al., *RAGE signaling sustains inflammation and promotes tumor development.* J Exp Med, 2008. **205**(2): p. 275-85.
103. Wiechert, L., et al., *Hepatocyte-specific S100a8 and S100a9 transgene expression in mice causes Cxcl1 induction and systemic neutrophil enrichment.* Cell Communication and Signaling, 2012. **10**(1): p. 40.
104. De Ponti, A., et al., *A pro-tumorigenic function of S100A8/A9 in carcinogen-induced hepatocellular carcinoma.* Cancer Letters, 2015. **369**(2): p. 396-404.

105. Németh, J., et al., *S100A8 and S100A9 are novel nuclear factor kappa B target genes during malignant progression of murine and human liver carcinogenesis.* Hepatology, 2009. **50**(4): p. 1251-1262.
106. Park, J.W., et al., *Increased Expression of S100B and RAGE in a Mouse Model of Bile Duct Ligation-induced Liver Fibrosis.* J Korean Med Sci, 2021. **36**(14): p. e90.
107. Weinhage, T., et al., *The Receptor for Advanced Glycation Endproducts (RAGE) Contributes to Severe Inflammatory Liver Injury in Mice.* Front Immunol, 2020. **11**: p. 1157.
108. Kierdorf, K. and G. Fritz, *RAGE regulation and signaling in inflammation and beyond.* Journal of Leukocyte Biology, 2013. **94**(1): p. 55-68.
109. Riehl, A., et al., *The receptor RAGE: Bridging inflammation and cancer.* Cell Communication and Signaling, 2009. **7**(1): p. 12-12.
110. Teissier, T. and É. Boulanger, *The receptor for advanced glycation end-products (RAGE) is an important pattern recognition receptor (PRR) for inflammaging.* Biogerontology, 2019. **20**(3): p. 279-301.
111. Pusterla, T., et al., *Receptor for advanced glycation endproducts (RAGE) is a key regulator of oval cell activation and inflammation-associated liver carcinogenesis in mice.* Hepatology (Baltimore, Md.), 2013. **58**(1): p. 363-73.
112. Burstein, A.H., et al., *Development of Azeliragon, an Oral Small Molecule Antagonist of the Receptor for Advanced Glycation Endproducts, for the Potential Slowing of Loss of Cognition in Mild Alzheimer's Disease.* J Prev Alzheimers Dis, 2018. **5**(2): p. 149-154.
113. Le Bagge, S., et al., *Targeting the receptor for advanced glycation end products (RAGE) in type 1 diabetes.* Medicinal Research Reviews, 2020. **40**(4): p. 1200-1219.
114. Singh, H. and D.K. Agrawal, *Therapeutic potential of targeting the receptor for advanced glycation end products (RAGE) by small molecule inhibitors.* Drug Development Research, 2022. **83**(6): p. 1257-1269.
115. Deane, R., et al., *A multimodal RAGE-specific inhibitor reduces amyloid β–mediated brain disorder in a mouse model of Alzheimer disease.* The Journal of Clinical Investigation, 2012. **122**(4): p. 1377-1392.
116. Abe, R., et al., *Regulation of human melanoma growth and metastasis by AGE-AGE receptor interactions.* J Invest Dermatol, 2004. **122**(2): p. 461-7.
117. Bro, S., et al., *A neutralizing antibody against receptor for advanced glycation end products (RAGE) reduces atherosclerosis in uremic mice.* Atherosclerosis, 2008. **201**(2): p. 274-80.
118. Lutterloh, E.C., et al., *Inhibition of the RAGE products increases survival in experimental models of severe sepsis and systemic infection.* Crit Care, 2007. **11**(6): p. R122.
119. Palma-Duran, S.A., et al., *Serum levels of advanced glycation end-products (AGEs) and the decoy soluble receptor for AGEs (sRAGE) can identify non-alcoholic fatty liver disease in age-, sex- and BMI-matched normo-glycemic adults.* Metabolism, 2018. **83**: p. 120-127.
120. Zhang, X., et al., *Reduced Circulating Soluble Receptor for Advanced Glycation End-products in Chronic Hepatitis B Are Associated with Hepatic Necroinflammation.* Inflammation, 2022. **45**(6): p. 2559-2569.
121. Ekong, U., et al., *Blockade of the receptor for advanced glycation end products attenuates acetaminophen-induced hepatotoxicity in mice.* J Gastroenterol Hepatol, 2006. **21**(4): p. 682-8.
122. Lowes, K.N., et al., *Oval cell numbers in human chronic liver diseases are directly related to disease severity.* Am J Pathol, 1999. **154**(2): p. 537-41.
123. Sancho-Bru, P., et al., *Liver progenitor cell markers correlate with liver damage and predict short-term mortality in patients with alcoholic hepatitis.* Hepatology, 2012. **55**(6): p. 1931-1941.
124. Jung, Y., et al., *Accumulation of hedgehog-responsive progenitors parallels alcoholic liver disease severity in mice and humans.* Gastroenterology, 2008. **134**(5): p. 1532-43.
125. Nobili, V., et al., *Hepatic progenitor cells activation, fibrosis, and adipokines production in pediatric nonalcoholic fatty liver disease.* 2012. **56**(6): p. 2142-2153.
126. Furuyama, K., et al., *Continuous cell supply from a Sox9-expressing progenitor zone in adult liver, exocrine pancreas and intestine.* Nature Genetics, 2011. **43**(1): p. 34-41.

127. Shin, S., et al., *Ablation of Foxl1-Cre–Labeled Hepatic Progenitor Cells and Their Descendants Impairs Recovery of Mice From Liver Injury.* Gastroenterology, 2015. **148**(1): p. 192-202.e3.
128. Huch, M., et al., *In vitro expansion of single Lgr5+ liver stem cells induced by Wnt-driven regeneration.* Nature, 2013. **494**(7436): p. 247-250.
129. Español–Suñer, R., et al., *Liver Progenitor Cells Yield Functional Hepatocytes in Response to Chronic Liver Injury in Mice.* Gastroenterology, 2012. **143**(6): p. 1564-1575.e7.
130. Kuramitsu, K., et al., *Failure of fibrotic liver regeneration in mice is linked to a severe fibrogenic response driven by hepatic progenitor cell activation.* Am J Pathol, 2013. **183**(1): p. 182-94.
131. Clouston, A.D., et al., *Fibrosis correlates with a ductular reaction in hepatitis C: roles of impaired replication, progenitor cells and steatosis.* Hepatology, 2005. **41**(4): p. 809-18.
132. Lee, J.-S., et al., *A novel prognostic subtype of human hepatocellular carcinoma derived from hepatic progenitor cells.* Nature Medicine, 2006. **12**(4): p. 410-416.
133. Tummala, K.S., et al., *Hepatocellular Carcinomas Originate Predominantly from Hepatocytes and Benign Lesions from Hepatic Progenitor Cells.* Cell Reports, 2017. **19**(3): p. 584-600.
134. Holczbauer, Á., et al., *Modeling Pathogenesis of Primary Liver Cancer in Lineage-Specific Mouse Cell Types.* Gastroenterology, 2013. **145**(1): p. 221-231.
135. Kamimoto, K., et al., *Multidimensional imaging of liver injury repair in mice reveals fundamental role of the ductular reaction.* Communications Biology, 2020. **3**(1): p. 289.
136. Proell, V., et al., *The plasticity of p19 ARF null hepatic stellate cells and the dynamics of activation.* Biochim Biophys Acta, 2005. **1744**(1): p. 76-87.
137. Madisen, L., et al., *A robust and high-throughput Cre reporting and characterization system for the whole mouse brain.* Nature Neuroscience, 2009. **13**: p. 133-133.
138. Constien, R., et al., *Characterization of a novel EGFP reporter mouse to monitor Cre recombination as demonstrated by a Tie2 Cre mouse line.* genesis, 2001. **30**(1): p. 36-44.
139. Kleiner, D.E., et al., *Design and validation of a histological scoring system for nonalcoholic fatty liver disease.* Hepatology, 2005. **41**(6): p. 1313-1321.
140. Liang, W., et al., *Establishment of a General NAFLD Scoring System for Rodent Models and Comparison to Human Liver Pathology.* PLoS ONE, 2014. **9**(12): p. e115922-e115922.
141. Brunt, E.M., et al., *Nonalcoholic steatohepatitis: a proposal for grading and staging the histological lesions.* Am J Gastroenterol, 1999. **94**(9): p. 2467-74.
142. Klingmüller, U., et al., *Primary mouse hepatocytes for systems biology approaches: a standardized in vitro system for modelling of signal transduction pathways.* Syst Biol (Stevenage), 2006. **153**(6): p. 433-47.
143. Ewels, P., et al., *MultiQC: summarize analysis results for multiple tools and samples in a single report.* Bioinformatics (Oxford, England), 2016. **32**(19): p. 3047-3048.
144. Dobin, A., et al., *STAR: ultrafast universal RNA-seq aligner.* Bioinformatics, 2013. **29**(1): p. 15-21.
145. Wang, L., S. Wang, and W. Li, *RSeQC: quality control of RNA-seq experiments.* Bioinformatics, 2012. **28**(16): p. 2184-5.
146. Liao, Y., G.K. Smyth, and W. Shi, *featureCounts: an efficient general purpose program for assigning sequence reads to genomic features.* Bioinformatics, 2014. **30**(7): p. 923-30.
147. Love, M.I., W. Huber, and S. Anders, *Moderated estimation of fold change and dispersion for RNA-seq data with DESeq2.* bioRxiv, 2014: p. 002832.
148. Strick-Marchand, H. and M.C. Weiss, *Inducible differentiation and morphogenesis of bipotential liver cell lines from wild-type mouse embryos.* Hepatology, 2002. **36**(4 Pt 1): p. 794-804.
149. Lee, H., et al., *R-spondins are BMP receptor antagonists in Xenopus early embryonic development.* Nature Communications, 2020. **11**(1): p. 5570.
150. Cox, J., et al., *Accurate proteome-wide label-free quantification by delayed normalization and maximal peptide ratio extraction, termed MaxLFQ.* Mol Cell Proteomics, 2014. **13**(9): p. 2513-26.

151. Haschek, W.M., C.G. Rousseaux, and M.A. Wallig, *Chapter 9 - The Liver*, in *Fundamentals of Toxicologic Pathology (Second Edition)*, W.M. Haschek, C.G. Rousseaux, and M.A. Wallig, Editors. 2010, Academic Press: San Diego. p. 197-235.
152. Libbrecht, L., et al., *Expression of neural cell adhesion molecule in human liver development and in congenital and acquired liver diseases.* Histochem Cell Biol, 2001. **116**(3): p. 233-9.
153. Yan, J., et al., *Recent advances of GOLM1 in hepatocellular carcinoma.* Hepat Oncol, 2020. **7**(2): p. Hep22.
154. Geisler, F. and M. Strazzabosco, *Emerging roles of Notch signaling in liver disease.* Hepatology, 2015. **61**(1): p. 382-392.
155. Zeng, S., et al., *Blockade of receptor for advanced glycation end product (RAGE) attenuates ischemia and reperfusion injury to the liver in mice.* Hepatology, 2004. **39**(2): p. 422-432.
156. Huebener, P., et al., *The HMGB1/RAGE axis triggers neutrophil-mediated injury amplification following necrosis.* The Journal of Clinical Investigation, 2015. **125**(2): p. 539-550.
157. Wan, J., et al., *Aging-induced aberrant RAGE/PPARα axis promotes hepatic steatosis via dysfunctional mitochondrial β oxidation.* Aging Cell, 2020. **19**(10): p. e13238.
158. Fehrenbach, H., et al., *Up-regulated expression of the receptor for advanced glycation end products in cultured rat hepatic stellate cells during transdifferentiation to myofibroblasts.* Hepatology, 2001. **34**(5): p. 943-52.
159. Li, J., et al., *Rage induces hepatocellular carcinoma proliferation and sorafenib resistance by modulating autophagy.* Cell Death & Disease, 2018. **9**(2): p. 225-225.
160. Swami, P., et al., *RAGE Up-Regulation Differently Affects Cell Proliferation and Migration in Pancreatic Cancer Cells.* Int J Mol Sci, 2020. **21**(20).
161. Bao, J.-M., et al. *AGE/RAGE/Akt pathway contributes to prostate cancer cell proliferation by promoting Rb phosphorylation and degradation*. American journal of cancer research, 2015. **5**, 1741-1750.
162. Huch, M., et al., *The hope and the hype of organoid research.* Development, 2017. **144**(6): p. 938-941.
163. Heydari, Z., et al., *Organoids: a novel modality in disease modeling.* Bio-Design and Manufacturing, 2021. **4**(4): p. 689-716.
164. Lu, L., M.J. Finegold, and R.L. Johnson, *Hippo pathway coactivators Yap and Taz are required to coordinate mammalian liver regeneration.* Experimental & Molecular Medicine, 2018. **50**(1): p. e423-e423.
165. Pepe-Mooney, B.J., et al., *Single-Cell Analysis of the Liver Epithelium Reveals Dynamic Heterogeneity and an Essential Role for YAP in Homeostasis and Regeneration.* Cell Stem Cell, 2019. **25**(1): p. 23-38.e8.
166. Hagenbeek, T.J., et al., *The Hippo pathway effector TAZ induces TEAD-dependent liver inflammation and tumors.* Sci Signal, 2018. **11**(547).
167. Aylon, Y., et al., *The LATS2 tumor suppressor inhibits SREBP and suppresses hepatic cholesterol accumulation.* Genes Dev, 2016. **30**(7): p. 786-97.
168. Lee, J.H., et al., *A crucial role of WW45 in developing epithelial tissues in the mouse.* Embo j, 2008. **27**(8): p. 1231-42.
169. Song, H., et al., *Mammalian Mst1 and Mst2 kinases play essential roles in organ size control and tumor suppression.* Proceedings of the National Academy of Sciences, 2010. **107**(4): p. 1431-1436.
170. Yu, F.-X., et al., *Regulation of the Hippo-YAP Pathway by G-Protein-Coupled Receptor Signaling.* Cell, 2012. **150**(4): p. 780-791.
171. Scaffidi, P., T. Misteli, and M.E. Bianchi, *Release of chromatin protein HMGB1 by necrotic cells triggers inflammation.* Nature, 2002. **418**: p. 191-191.
172. Hudson, B.I. and M.E. Lippman, *Targeting RAGE Signaling in Inflammatory Disease.* Annual Review of Medicine, 2018. **69**(1): p. 349-364.
173. Turovskaya, O., et al., *RAGE, carboxylated glycans and S100A8/A9 play essential roles in colitis-associated carcinogenesis.* Carcinogenesis, 2008. **29**(10): p. 2035-43.
174. Feng, Z., et al., *Role of RAGE in obesity-induced adipose tissue inflammation and insulin resistance.* Cell Death Discovery, 2021. **7**(1): p. 305.
175. Lombardi, B., P. Pani, and F.F. Schlunk, *Choline-deficiency fatty liver: impaired release of hepatic triglycerides.* J Lipid Res, 1968. **9**(4): p. 437-46.

176. Zeisel, S.H., et al., *Choline, an essential nutrient for humans.* Faseb j, 1991. **5**(7): p. 2093-8.
177. Khambu, B., et al., *The HMGB1-RAGE axis modulates the growth of autophagy-deficient hepatic tumors.* Cell Death & Disease, 2020. **11**(5): p. 333.
178. Milkiewicz, P., et al., *Visualization of the transport of primary and secondary bile acids across liver tissue in rats: in vivo study with fluorescent bile acids.* J Hepatol, 2001. **34**(1): p. 4-10.
179. Lam, W.L.M., et al., *OS042 - Biliary epithelial cell-specific RAGE controls ductular reaction-mediated fibrosis during cholestasis.* Journal of Hepatology, 2022. **77**: p. S38.
180. Richardson, M.M., et al., *Progressive Fibrosis in Nonalcoholic Steatohepatitis: Association With Altered Regeneration and a Ductular Reaction.* Gastroenterology, 2007. **133**(1): p. 80-90.
181. Roskams, T., et al., *Oxidative stress and oval cell accumulation in mice and humans with alcoholic and nonalcoholic fatty liver disease.* Am J Pathol, 2003. **163**(4): p. 1301-11.
182. Fabregat, I. and D. Caballero-Díaz, *Transforming Growth Factor-β-Induced Cell Plasticity in Liver Fibrosis and Hepatocarcinogenesis.* 2018. **8**(357).
183. Chobert, M.N., et al., *Liver precursor cells increase hepatic fibrosis induced by chronic carbon tetrachloride intoxication in rats.* Lab Invest, 2012. **92**(1): p. 135-50.
184. Troilo, H., et al., *Independent multimerization of Latent TGFβ Binding Protein-1 stabilized by cross-linking and enhanced by heparan sulfate.* Scientific Reports, 2016. **6**(1): p. 34347.
185. Park, S.-A., et al., *TIMP-1 mediates TGF-β-dependent crosstalk between hepatic stellate and cancer cells via FAK signaling.* Scientific Reports, 2015. **5**(1): p. 16492.
186. Henderson, N.C. and D. Sheppard, *Integrin-mediated regulation of TGFβ in fibrosis.* Biochim Biophys Acta, 2013. **1832**(7): p. 891-6.
187. Popov, Y., et al., *Integrin alphavbeta6 is a marker of the progression of biliary and portal liver fibrosis and a novel target for antifibrotic therapies.* J Hepatol, 2008. **48**(3): p. 453-64.
188. Peng, Z.-W., et al., *Integrin αvβ6 critically regulates hepatic progenitor cell function and promotes ductular reaction, fibrosis, and tumorigenesis.* Hepatology, 2016. **63**(1): p. 217-232.
189. Patsenker, E., et al., *Inhibition of integrin alphavbeta6 on cholangiocytes blocks transforming growth factor-beta activation and retards biliary fibrosis progression.* Gastroenterology, 2008. **135**(2): p. 660-70.
190. Kim, K.-H., et al., *CCN1 induces hepatic ductular reaction through integrin αvβ5–mediated activation of NF-κB.* The Journal of Clinical Investigation, 2015. **125**(5): p. 1886-1900.
191. Chang, W., et al., *Early activated hepatic stellate cell-derived paracrine molecules modulate acute liver injury and regeneration.* Laboratory Investigation, 2017. **97**(3): p. 318-328.
192. Pintilie, D.G., et al., *Hepatic stellate cells' involvement in progenitor-mediated liver regeneration.* 2010. **90**(8): p. 1199-1208.
193. Kordes, C., et al., *Hepatic stellate cells contribute to progenitor cells and liver regeneration.* J Clin Invest, 2014. **124**(12): p. 5503-15.
194. Dai, Z., et al., *Growth differentiation factor 11 attenuates liver fibrosis via expansion of liver progenitor cells.* Gut, 2019: p. gutjnl-2019-318812.
195. Paku, S., et al., *Origin and Structural Evolution of the Early Proliferating Oval Cells in Rat Liver.* The American Journal of Pathology, 2001. **158**(4): p. 1313-1323.
196. Van Hul, N.K., et al., *Relation between liver progenitor cell expansion and extracellular matrix deposition in a CDE-induced murine model of chronic liver injury.* Hepatology, 2009. **49**(5): p. 1625-35.
197. Bray, S.J., *Notch signalling: a simple pathway becomes complex.* Nat Rev Mol Cell Biol, 2006. **7**(9): p. 678-89.
198. Villanueva, A., et al., *Notch signaling is activated in human hepatocellular carcinoma and induces tumor formation in mice.* Gastroenterology, 2012. **143**(6): p. 1660-1669.e7.
199. Zhu, C., et al., *Notch activity characterizes a common hepatocellular carcinoma subtype with unique molecular and clinicopathologic features.* Journal of Hepatology, 2021. **74**(3): p. 613-626.

200. Zender, S., et al., *A Critical Role for Notch Signaling in the Formation of Cholangiocellular Carcinomas.* Cancer Cell, 2013. **23**(6): p. 784-795.
201. Matsumori, T., et al., *Hes1 Is Essential in Proliferating Ductal Cell–Mediated Development of Intrahepatic Cholangiocarcinoma.* Cancer Research, 2020. **80**(23): p. 5305-5316.
202. Minnis-Lyons, S.E., et al., *Notch-IGF1 signaling during liver regeneration drives biliary epithelial cell expansion and inhibits hepatocyte differentiation.* Sci Signal, 2021. **14**(688).
203. Yu, J., et al., *Hepatocyte TLR4 triggers inter-hepatocyte Jagged1/Notch signaling to determine NASH-induced fibrosis.* Science Translational Medicine, 2021. **13**(599): p. eabe1692.
204. Bansal, R., et al., *The interplay of the Notch signaling in hepatic stellate cells and macrophages determines the fate of liver fibrogenesis.* Scientific Reports, 2015. **5**(1): p. 18272.
205. Chen, Y., et al., *Inhibition of Notch Signaling by a γ-Secretase Inhibitor Attenuates Hepatic Fibrosis in Rats.* PLOS ONE, 2012. **7**(10): p. e46512.
206. Yang, T., et al., *NPAS2 Contributes to Liver Fibrosis by Direct Transcriptional Activation of Hes1 in Hepatic Stellate Cells.* Molecular Therapy - Nucleic Acids, 2019. **18**: p. 1009-1022.
207. Lemaigre, F.P., *Determining the fate of hepatic cells by lineage tracing: Facts and pitfalls.* Hepatology, 2015. **61**(6): p. 2100-2103.
208. Kamimoto, K., et al., *Heterogeneity and stochastic growth regulation of biliary epithelial cells dictate dynamic epithelial tissue remodeling.* eLife, 2016. **5**: p. e15034.
209. Wang, J., et al., *Dissecting the single-cell transcriptomeunderlying chronic liver injury.* Mol Ther Nucleic Acids, 2021. **26**: p. 1364-1373.
210. Mariotti, V., et al., *Animal models of cholestasis: An update on inflammatory cholangiopathies.* Biochimica et Biophysica Acta (BBA) - Molecular Basis of Disease, 2019. **1865**(5): p. 954-964.
211. Lee, S., et al., *Comparative study of liver injury induced by high-fat methionine- and choline-deficient diet in ICR mice originating from three different sources.* Laboratory Animal Research, 2019. **35**(1): p. 15.
212. Cameron, G.R. and C.L. Oakley, *Ligation of the common bile duct.* The Journal of Pathology and Bacteriology, 1932. **35**(5): p. 769-798.
213. Scholten, D., et al., *The carbon tetrachloride model in mice.* Lab Anim, 2015. **49**(1 Suppl): p. 4-11.
214. Takahashi, Y. and T. Fukusato, *Chapter 13 - Animal Models of Liver Diseases*, in *Animal Models for the Study of Human Disease (Second Edition)*, P.M. Conn, Editor. 2017, Academic Press. p. 313-339.
215. Smit, J.J., et al., *Homozygous disruption of the murine mdr2 P-glycoprotein gene leads to a complete absence of phospholipid from bile and to liver disease.* Cell, 1993. **75**(3): p. 451-62.
216. Tolba, R., et al., *Diethylnitrosamine (DEN)-induced carcinogenic liver injury in mice.* Lab Anim, 2015. **49**(1 Suppl): p. 59-69.
217. Charlton, M., et al., *Fast food diet mouse: novel small animal model of NASH with ballooning, progressive fibrosis, and high physiological fidelity to the human condition.* American Journal of Physiology-Gastrointestinal and Liver Physiology, 2011. **301**(5): p. G825-G834.
218. Tsuchida, T., et al., *A simple diet- and chemical-induced murine NASH model with rapid progression of steatohepatitis, fibrosis and liver cancer.* J Hepatol, 2018. **69**(2): p. 385-395.
219. Pfister, D., et al., *NASH limits anti-tumour surveillance in immunotherapy-treated HCC.* Nature, 2021. **592**(7854): p. 450-456.
220. Yao, Z.M. and D.E. Vance, *The active synthesis of phosphatidylcholine is required for very low density lipoprotein secretion from rat hepatocytes.* Journal of Biological Chemistry, 1988. **263**(6): p. 2998-3004.
221. Raubenheimer, P.J., M.J. Nyirenda, and B.R. Walker, *A Choline-Deficient Diet Exacerbates Fatty Liver but Attenuates Insulin Resistance and Glucose Intolerance in Mice Fed a High-Fat Diet.* Diabetes, 2006. **55**(7): p. 2015-2020.
222. Ibrahim, S.H., et al., *Cholestatic Liver Diseases of Genetic Etiology: Advances and Controversies.* Hepatology, 2022. **n/a**(n/a).

223. Lawitz, E.J., et al., *Acetyl-CoA Carboxylase Inhibitor GS-0976 for 12 Weeks Reduces Hepatic De Novo Lipogenesis and Steatosis in Patients With Nonalcoholic Steatohepatitis.* Clin Gastroenterol Hepatol, 2018. **16**(12): p. 1983-1991.e3.
224. Ratziu, V., et al., *Aramchol in patients with nonalcoholic steatohepatitis: a randomized, double-blind, placebo-controlled phase 2b trial.* Nature Medicine, 2021. **27**(10): p. 1825-1835.
225. Harrison, S.A., et al., *Aldafermin in patients with non-alcoholic steatohepatitis (ALPINE 2/3): a randomised, double-blind, placebo-controlled, phase 2b trial.* The Lancet Gastroenterology & Hepatology, 2022. **7**(7): p. 603-616.
226. Abdelmalek, M.F., et al., *The FALCON program: Two phase 2b randomized, double-blind, placebo-controlled studies to assess the efficacy and safety of pegbelfermin in the treatment of patients with nonalcoholic steatohepatitis and bridging fibrosis or compensated cirrhosis.* Contemp Clin Trials, 2021. **104**: p. 106335.
227. Harrison, S.A., et al., *Effects of Resmetirom on Noninvasive Endpoints in a 36-Week Phase 2 Active Treatment Extension Study in Patients With NASH.* Hepatol Commun, 2021. **5**(4): p. 573-588.
228. Rinella, M.E., et al., *Non-invasive evaluation of response to obeticholic acid in patients with NASH: Results from the REGENERATE study.* J Hepatol, 2022. **76**(3): p. 536-548.
229. Younossi, Z.M., et al., *Obeticholic Acid Impact on Quality of Life in Patients With Nonalcoholic Steatohepatitis: REGENERATE 18-Month Interim Analysis.* Clin Gastroenterol Hepatol, 2022. **20**(9): p. 2050-2058.e12.
230. Patel, K., et al., *Cilofexor, a Nonsteroidal FXR Agonist, in Patients With Noncirrhotic NASH: A Phase 2 Randomized Controlled Trial.* Hepatology, 2020. **72**(1): p. 58-71.
231. Ratziu, V., et al., *Elafibranor, an Agonist of the Peroxisome Proliferator−Activated Receptor−α and −δ, Induces Resolution of Nonalcoholic Steatohepatitis Without Fibrosis Worsening.* Gastroenterology, 2016. **150**(5): p. 1147-1159.e5.
232. Armstrong, M.J., et al., *Liraglutide safety and efficacy in patients with non-alcoholic steatohepatitis (LEAN): a multicentre, double-blind, randomised, placebo-controlled phase 2 study.* Lancet, 2016. **387**(10019): p. 679-690.
233. Newsome, P.N., et al., *A Placebo-Controlled Trial of Subcutaneous Semaglutide in Nonalcoholic Steatohepatitis.* N Engl J Med, 2021. **384**(12): p. 1113-1124.
234. Wong, C., et al., *Fibroblast growth factor receptor 1/Klothoβ agonist BFKB8488A improves lipids and liver health markers in patients with diabetes or NAFLD: A phase 1b randomized trial.* Hepatology, 2022.
235. Baruch, A., et al., *Antibody-mediated activation of the FGFR1/Klothoβ complex corrects metabolic dysfunction and alters food preference in obese humans.* Proceedings of the National Academy of Sciences, 2020. **117**(46): p. 28992-29000.
236. Harrison, S.A., et al., *Selonsertib for patients with bridging fibrosis or compensated cirrhosis due to NASH: Results from randomized phase III STELLAR trials.* J Hepatol, 2020. **73**(1): p. 26-39.
237. Segal-Salto, M., et al., *A blocking monoclonal antibody to CCL24 alleviates liver fibrosis and inflammation in experimental models of liver damage.* JHEP Reports, 2020. **2**(1): p. 100064.
238. Wah Kheong, C., N.R. Nik Mustapha, and S. Mahadeva, *A Randomized Trial of Silymarin for the Treatment of Nonalcoholic Steatohepatitis.* Clin Gastroenterol Hepatol, 2017. **15**(12): p. 1940-1949.e8.
239. Sanyal, A.J., et al., *Pioglitazone, Vitamin E, or Placebo for Nonalcoholic Steatohepatitis.* New England Journal of Medicine, 2010. **362**(18): p. 1675-1685.
240. Harrison, S.A., et al., *Simtuzumab Is Ineffective for Patients With Bridging Fibrosis or Compensated Cirrhosis Caused by Nonalcoholic Steatohepatitis.* Gastroenterology, 2018. **155**(4): p. 1140-1153.
241. McPherson, S., et al., *A randomised controlled trial of losartan as an anti-fibrotic agent in non-alcoholic steatohepatitis.* PLoS One, 2017. **12**(4): p. e0175717.
242. Lawitz, E.J., et al., *BMS-986263 in patients with advanced hepatic fibrosis: 36-week results from a randomized, placebo-controlled phase 2 trial.* Hepatology, 2022. **75**(4): p. 912-923.
243. Ling, H., et al., *Transforming growth factor β neutralization ameliorates pre-existing hepatic fibrosis and reduces cholangiocarcinoma in thioacetamide-treated rats.* PLoS One, 2013. **8**(1): p. e54499.

244. de Gouville, A.C., et al., *Inhibition of TGF-beta signaling by an ALK5 inhibitor protects rats from dimethylnitrosamine-induced liver fibrosis.* Br J Pharmacol, 2005. **145**(2): p. 166-77.
245. Munger, J.S., et al., *A Mechanism for Regulating Pulmonary Inflammation and Fibrosis: The Integrin αvβ6 Binds and Activates Latent TGF β1.* Cell, 1999. **96**(3): p. 319-328.
246. Henderson, N.C., et al., *Targeting of αv integrin identifies a core molecular pathway that regulates fibrosis in several organs.* Nat Med, 2013. **19**(12): p. 1617-24.
247. Lan, T., T. Kisseleva, and D.A. Brenner, *Deficiency of NOX1 or NOX4 Prevents Liver Inflammation and Fibrosis in Mice through Inhibition of Hepatic Stellate Cell Activation.* PLoS One, 2015. **10**(7): p. e0129743.
248. Aoyama, T., et al., *Nicotinamide adenine dinucleotide phosphate oxidase in experimental liver fibrosis: GKT137831 as a novel potential therapeutic agent.* Hepatology, 2012. **56**(6): p. 2316-27.
249. Du, K., et al., *Hedgehog-YAP Signaling Pathway Regulates Glutaminolysis to Control Activation of Hepatic Stellate Cells.* Gastroenterology, 2018. **154**(5): p. 1465-1479.e13.
250. Weston, C.J., et al., *Vascular adhesion protein-1 promotes liver inflammation and drives hepatic fibrosis.* J Clin Invest, 2015. **125**(2): p. 501-20.

# Chapter 6
## Supplements

## Section 6.1 Declaration

I hereby declare that except where specific reference is made to the work of others, the contents of this dissertation are original and based on results of my own investigations. This dissertation has not been submitted for consideration for any other degree or qualification.

Heidelberg, _____

Wai Ling Macrina Lam

## Section 6.2 Acknowledgements

It feels unrealistic – I cannot believe it has finally come to an end of my PhD despite lots of ups and downs and frustrations in the past five years. Never have I thought of doing a PhD during my Bachelor study, yet after being inspired by few mentors along the way, and here I am, achieving my personal goal in my academic career. I am thankful to many people, who have accompanied me along this journey.

First of all, I would like to express my deepest gratitude to my supervisor, **Prof. Peter Angel**, for offering me an opportunity to receive my PhD training in his lab. I would like to thank you for your patience and guidance, for giving me the freedom and support to develop my skills and ideas, and especially for putting your trust on me throughout my PhD. Thank you for also giving me lots of chances to attend international conferences and summer school each year, which has given me opportunities to learn from other scientists in the hepatology field.

I would also like to thank **Prof. Mathias Heikenwälder** and **Prof. Kai Breuhahn** for being my TAC committee and provided lots of stimulating scientific discussions during the TAC meetings. I would also like to thank Mathias and the support from his lab technician **Danijela Heide** on part of the IHC staining.

My heartfelt gratitude to my mentor, **Dr. Doris Schneller**, for writing the SFB proposal and animal licenses in support of this project, and for providing guidance to me during my first two years of PhD, especially for sharing her expertise in mouse breeding and experimental methods with me. Thank you for your caring about my progress when we still meet at DKFZ from time to time. I also thank you for translating the thesis summary into German for me.

A great thank to **Dr. Giesela Gabernet** for analyzing the RNA-seq data, **Dr. Tanja Poth** for performing histopathological evaluation all the tissue samples, and the members from the pathology lab at the Universitätsklinikum Heidelberg for performing the histology staining. I am thankful to them for bringing their expertise into this study, and I appreciate a lot for their time in going back-and-forth to discuss about the results with me patiently. Their analyses have provided tons of important information to this study – without them, the aims of this project cannot be accomplished.

Thank you **Dr. Anna Saborowski** for hosting me at MHH in Hannover. I am thankful that I could learn the organoid culture technique from her lab members, **Dr. Katharina Wolff** and **Barbara Seller**, during the short visit.

I am extremely grateful to have the technical support from **Melanie Sator-Schmitt**. Thank you for taking care of all mouse breeding, genotyping, logistics, and your continuous support on the experiments. It was indeed a lot of work to deal with large number of animals. I was always amazed by how organized and dedicated you are on this work.

Thank you also **Barbara Böck** for taking care of all the animal licenses as well as the logistics with our collaborative partners, which helps to make the collaborations possible.

I would like to express my heartfelt gratitude to our collaborators – **Dr. Fabian Geisler** and **Dr. Simone Jörs** from TUM, **Prof. Jan Hengstler** and **Dr. Nachiket Vartak** from IfADo, and **Dr. Amruta Damle-Vartak** here in our lab for being important collaborative partners in this project. I am grateful that our scientific interests aligned well with Fabian and Simone, and I appreciate a lot about the interesting discussions over the past two years. Thank you Jan and Nachiket for hosting the mice and performed the important intravital imaging experiments, which have added tremendous values to the on-going project. Thank you Amruta for initiating this collaboration. Without her support in building the links between our labs, this collaboration would not have been possible. I am thankful for her scientific support and suggestions along the way, which has help to broaden my expertise as well over the past two years. I would also like to say a huge thank you to **Georgia Günther**, for her tremendous technical support in this collaboration, including huge workload and work hours on the intravital imaging processes, extra care on the mice, logistics etc. I really enjoy my stays in Dortmund while working with Georgia at IfADo.

Furthermore, I would like to acknowledge to all the people who have contributed to this work or helped me along the way. **Dr. Karin Müller-decker** and her team, with lots of help in hosting the mice with CDE diet in the S2 core. **Dr. Damir Krunic**, for writing the ImageJ macros for my image analyses, and for helping to resolve issues with the microscropes. **Manuela Brom**, for introducing me to various microscopes and opened a new world to me. **Dr. Dominic Helm** and **Martin Schneider**, for the insightful discussions and analysis on the mass spectrometry data. **Marvin Wälsch** and **Lena Postawa**, for sharing their liver perfusion techniques with me. **Angela Funk**, for performing lots of genotyping on the mice in the past. Our animal care taker in Barrier A, **Kitty So**, 無諗過 DKFZ 咁大，香港人咁少，加上你仲係 Barrier A 做野，我地都可以透過電話認識到彼此。我相信依啲係緣份。 好開心有時你會打黎同我吹水同食飯，傾吓香港同埋屋企。多謝你好落力盡責照顧我啲老鼠，令到我地嘅實驗都順利進行到。

Of course, a big THANK YOU to all the existing and past members of the Angel lab, who have always created a positive and fun working environment. **Saskia**, for being a great companion along this journey. I always enjoy our lunch and coffee break. Thank you for sharing ups and downs with me, and for your positive attitude to cheer me up in moving forward. **Meli** and **Jule**, for sharing your career experience with me not only during your PhD but also after leaving the lab. **Jakob** and **Lena**, for being my students, which has allowed me to learn how to be a better mentor, better scientist, or even a better person. When I saw you guys working at the bench, it reminded me of how I started my career and to rethink my passion in science. **Thomas**, **Sören** and **Te**, whom have given me lots of good memories and important mental support during my early phase of my PhD. Thank you **Lena**, **Sabrina** and **Betty**, for answering my stupid questions when I searched for lab wares or placing orders for the reagents. Thank you for the laughter during the breaks, which have given me a lot of positive energy despite lots of frustrations from the experiments.

To all my friends – **Steve**, **Ken**, **Hannah**, **Charles**, **Chloe**, **Mat**, thank you for being my family here in Heidelberg. Words cannot describe how much you guys meant to me. I am extremely grateful to have met you guys in my life. 係緣份令我地幾個聚埋一齊。無論發生咩事，你地總係係我身邊令我 recharge 番，多謝你地依幾年嘅陪伴，無你地我諗我根本捱唔過個 PhD。(And special thanks to **Chloe** for proofreading this dissertation meticulously!) **Dorothy** and **TYY**, thank you for being my first two friends in Heidelberg when I was all alone here in the first place. Your supports have always cheered me up. **The badminton club** – including the abovementioned people, as well as **Yin Hsi**, **Shang Chieh**, **Chieh Yu, Debanjan** and many others – it added so much fun to my life in Heidelberg when I play badminton and hang out with you people every weekend. My childhood friends in Hong Kong, especially **Ruby**, **Jean**, **Sam**, **Jess**, **V.Wong**, I know you guys are always backing me and are always available no matter how. My heartfelt thanks to my former mentor and friend, **LK**, who taught me to be a better scientist with perseverance and enthusiasm. Your guidance still influenced me a lot today.

Last but not least, I would like to express my deepest gratitude to **my family** for their unconditional love and understanding. 多謝你哋無條件嘅愛同包容，比我係人生路上好任性咁追隨我自己鍾意做嘅野。我要講聲對唔住，係過去嘅十幾年，我斷續總共離開左香港足足十年， 無好好咁陪伴你地。感激你地對我嘅不離棄同關懷，無聲地支持我而家終於完成自我追求嘅學業。我愛你哋，爸爸、媽媽、哥哥、仲有係天上守護我嘅公公、婆婆。